GRAIN STRUCTURE EVOLUTION OF TIN-BASED LEAD-FREE SOLDER JOINTS IN ELECTRONIC PACKAGING ASSEMBLY AND ITS IMPACTS ON THE FATIGUE RELIABILITY

by

HUILI XU

Presented to the Faculty of the Graduate School of

The University of Texas at Arlington in Partial Fulfillment

of the Requirements

for the Degree of

DOCTOR OF PHILOSOPHY

THE UNIVERSITY OF TEXAS AT ARLINGTON

December 2013

Copyright © by Huili Xu 2013

All Rights Reserved

ACKNOWLEDGEMENTS

First of all, I would like to express my deepest appreciation and gratitude to my advisor, Prof. Choongun Kim, for guiding me into the areas of electronic packaging and providing instructions and encouragement throughout my research. I am deeply grateful for having the opportunity to work under him. I also acknowledge my committee members for their time and suggestions. I would also like to acknowledge Dr. Jiechao Jiang and David Yan for their efforts to help me using the facilities in CCMB.

I would also like to acknowledge my current and previous group members and friends Dr. Nancy Michael, Dr. Woong Ho Bang, Dr. Liangshan Chen, Dr. Tae-Kyu Lee, Dr. Emil Zin, Tinqing Zhao, Patricia Rodriguez, Swathi Murthi, Yoonki Sa, Pocheng Lu, Huandi Gu, Enmee Kim, for their help, support and friendship.

My special acknowledgement goes to Dr. Liangshan chen. His help and instructions in many aspects are far beyond the scope as group member but my family members in America.

I am always grateful to our department secretaries, firstly to Jennifer Standlee. I appreciate her help and patience during my years of study in UT Arlington. I also acknowledge our previous secretary, Lidia Cuauhtli, and our new sectary, Beth Robinson for their help.

Most importantly, none of this would have been possible without the love and patience of my husband, Xiaofei Han. He has always been supporting me, offered his love with great patience. He helped me a lot on the discussion of my research and revision of paper work. I also want to thank my parents for their patience, understanding, support, and believe in me. Also I want to thank my son, Jonathan Han. His arrival makes my life even more wonderful.

This work is supported by Cisco, Inc.

November 18, 2013

ABSTRACT

GRAIN STRUCTURE EVOLUTION OF TIN-NASED LEAD-FREE SOLDER JOINTS
IN ELECTRONIC PACKAGING ASSEMBLY AND ITS IMPACTS ON
THE FATIGUE RELIABILITY

HUILI XU, PhD

The University of Texas at Arlington, 2013

Supervising Professor: CHOONG-UN KIM

Solder is one of the main joints materials used in the electronics for decades of years. It is not only the mechanical support but also conducts the electric signals in the electronics. However, the regulation of lead content in electronic devices has driven the transition from lead-tin solder to the lead-free solder that requires lots of research to fill the knowledge gap in the lead-free solder property. At the same time, the reliability issues due to solder failure are of great interest as the miniaturization and mobilization trend of the electronic devices continues. A lot of works have been done to understand the fatigue failure mechanism and its affecting factors with some degree of inconsistence. In this research, the grain structure evolution of tin-based lead free solder in electronic packaging and its relation to the fatigue reliability are studied.

First of all, to evaluate the fatigue reliability and understand the fatigue behavior of the tin-based lead-free solder joints in BGA packaging assembly, isothermal shear fatigue tester

was designed. Solder joints under cyclic shear load is found to fail by crack opening mode and crack is fixed at the solder neck area in the package side regardless of the testing conditions.

It is found that the failure of the solder joint under shear follows the Coffin-Manson model and a frequency-modified Coffin-Manson Model was developed for fatigue lifetime prediction. Fatigue property parameters that dictate the fatigue behavior of the solder joints were extracted from this model, namely fatigue ductility coefficient, cyclic strain hardening exponent/cyclic ductility exponent, and frequency exponent. The strain/work hardening rate is found to influence the fatigue resistance of the solder joints more than other parameters.

In the second part of this research, the grain structure evolution on tin-based lead-free solder under one-time thermal exposure (cooling to room temperature) was investigated indicating that recrystallization and mechanical twinning can occur far easier than previously thought. First, it reveals that either the activation energy for recrystallization or the thermal stress in the packaging assembly is higher than expected. Second, it is found that deformation twinning in tin is promoted by hydrostatic pressure stress while dislocation glide is prevented in tin in the packaging assembly. Grain structure sensitivity on the cooling temperature, cooling rate, thermal history, solder composition, and assembly configuration are investigated

Finally, fatigue tests on solder joints with polygrain and twin structure were carried out showing that recrystallization and twinning improve the fatigue resistance of the solder joints by more than 50%. In summary, first, this research is scientifically important that it gives a new understanding on the mechanism of deformation twinning promoted by hydrostatic pressure stress in tin and tin-alloys.

TABLE OF CONTENTS

ACKNOWLEDGEMENTS .... ……………..iii

ABSTRACT iv

LIST OF ILLUSTRATIONS.. x

LIST OF TABLES xv

Chapter Page

1. INTRODUCTION………………………………..………..….. 1

1.1 An Overview of Packaging Assembly, Lead-free Solder and Environmental Compliance 1

1.1.1 IC Assembly 1

1.1.2 Lead-free Solder and Environmental Compliance 4

1.2 Lead-free Solder Alloy Candidates 4

1.2.1 Sn-Ag System 7

1.2.2 Sn-Bi System 8

1.2.3 Sn-Cu System 9

1.2.4 Sn-Ag-Cu System 11

1.2.5 Sn-Ag-Bi System...11

1.3 Lead-free Solder Interconnect Reliability 12

1.3.1 Thermomechanical Fatigue..14

1.3.2 Whisker Growth...15

1.3.3 Electromigration (EM) 16

1.3.4 Isothermal Mechanical Fatigue 16

1.4 Objectives of This Study and Organization of This Dissertation....................17

2. FRACTURE MECHCNICS OF LEAD-FREE SOLDER JOINTS IN BALL GRID ARRAY ASSEMBLY UNDER CYCLIC SHEAR LOAD 19

2.1 Background 19

2.2 Experimental Methods...21

2.2.1 Shear Tester Instrumentation 21

2.2.2 Chip Mode Modification 23

2.2.3 Shear Testing Sample 25

2.3 Results and Discussion 27

2.3.1 Failure Characteristic-Resistance Change 27
2.3.2 Failure Characteristic-Microstructure..27
2.3.3 Mechanism of Crack-tip Opening Mode 30

2.4 Conclusion and Implication...33

3. FATIGUE PROPERTIES AND FATIGUE LIFETIME PREDICTION OF THE LEAD-FREE JOINTS IN BGA ASSEMBLY 34

3.1 Background 34

3.1.1 Strain-based Coffin-Manson Model 36
3.1.2 Total Strain Model 37
3.1.3 Plastic Strain + Creep Strain Model..38
3.1.4 Energy-based Model 39

3.2 Experimental Methods..40

3.3 Results and Discussion 42

3.3.1 Resistance Change With the Number of Cycle to Fail 42
3.3.2 Fatigue Lifetime vs. Plastic Strain Range..44
3.3.3 Fatigue Lifetime vs. Solder Alloy Composition 45
3.3.4 Fatigue Lifetime vs. Thermal Aging 46
3.3.5 Fatigue Lifetime vs. Temperature..53
3.3.6 Fatigue Lifetime vs. Frequency 59
3.3.7 Frequency Modified Coffin-Manson Model..60

3.4 Conclusion and Implication...63

4. GRAIN STRUCTURE EVOLUTION OF SN-AG-CU LEAD-FREE SOLDER IN BGA PACKAGING ASSEMBLY AND ITS MECHANISM 65

4.1 Background 65

4.1.1 *Elastic Anisotropy of Sn* 65
4.1.2 Microstructure of SAC Solder..66
4.1.3 Microstructure Dependence on the Joint Position in the Package...68

4.2 Experimental Methods..70

4.3 Results and Discussion 71

4.3.1 Thermal Aging vs. Microstructure..71
4.3.2 Grain Structure Evolution vs. Cooling Rate 75
4.3.3 Grain Structure Evolution vs. Joint Position 75

4.3.4 Grain Structure Evolution vs. Thermal History and Alloy Composition 78
4.3.5 Recrystallization Mechanism 79

4.4 Implications 87

4.5 Summary 89

5. OABSERVATION OF DEFORMATION TWINNING AND ITS MECHANISM IN TIN-BASED LEAD-FREE SOLDER 90

5.1 Background 90

5.1.1 Deformation Twinning 90
5.1.2 Deformation Twinning in Tin 91

5.2 Samples and Experiments 95

5.3 Results and Discussion 96

5.3.1 Observation of Twins in Tin-based Lead-free SAC Solders 96
5.3.2 Factors Affect the Deformation Twinning Behavior During Cooling 98
5.3.3 Proposed Deformation Twinning Mechanism 99

5.4 Conclusions and Implications 109

6. SENSITIVITY OF FATIGUE RELIABILITY ON GRAIN STRUCTURE 111

6.1 Background 111

6.2 Experiments 111

6.3 Results and Discussion 111

6.3.1 Fatigue Reliability vs. Cooling Rate 111
6.3.2 Crack Path vs. Cooling Rate 117

6.4 Conclusions and Implications 118

7. CONCLUSIONS AND FUTURE WORK 119

7.1 Conclusions 119

7.1.1 Shear Fatigue Mechanism and Mechanics 119
7.1.2 Fatigue Property Parameters and Fatigue Lifetime Prediction 120
7.1.3 Grain Structure Evolution and Its Impact on the Fatigue Reliability 121
7.1.4 Deformation Twinning in Tin-based Solder Alloy 122

7.2 Future Work 123

7.2.1 Fatigue Parameters and Fatigue Reliability of Solder Joints........123
7.2.2 Deformation Twinning in Tin and Its Mechanism 124

REFERENCES..125

BIOGRAPHICAL INFORMATION 142

LIST OF ILLUSTRATIONS

Figure Page

1.1 Overview of IC assembly process. 2

1.2 Cross-section of a flip chip connection 3

1.3 Cross-section of a ball grid array (BGA) microelectronics component. 3

1.4 Cross-section of a pin through hole connection of a microelectronics component on a printed wiring board 3

1.5 Cross-section of a surface mount connection of a microelectronics component with leads on a printed wiring board 4

1.6 Phase diagram of tin-silver 7

1.7 Phase diagram of tin-bismuth 9

1.8 Phase diagram of tin-lead 10

1.9 Phase diagram of tin-copper 10

1.10 Fields that cause damage in solder interconnect and their Interactions 13

1.11 Solder joints subjected to shear strain during thermal cycling due to CTE mismatch between the Die (α_1), the solder (α_2) and the substrate (α_3) 15

2.1 A picture of shear fatigue tester 21

2.2 Picture of shear tester head assembly that is designed to grip and move the chip in a horizontal direction, parallel to PCB, without backlash 22

2.3 Schematic drawing of the shear tester system 23

2.4 A diagram showing the FEM simulation result on the mold deformation field at the condition of 10% shear strain 25

2.5 A plot showing the measured displacement error as a function of the shear displacement distance 25

2.6 Picture showing (a) the PBGA assembly used for shear fatigue testing, (b) solder alloy configuration, and (c) cross-sectional view of the 400mm solder ball 26

2.7 A plot showing the change in the electrical resistance of as-reflowed SAC 305 solder joint during 1Hz shear fatigue testing under ~+/-4% shear strain 27

2.8 The image of the fracture SAC105 solder surface at chip side (a) overview, (b) microstructure of the crack initiates area located at the solder edge,(c) microstructure of the final fracture surface due to over shear located at the center of the solder 29

2.9 Figure 2.9 SEM cross section of the SAC105 solder after shear test (a) overview showing the neck area and solder rotation, (b) enlarged SEM showing the crack opening 29

2.10 SEM images of 150°C 1000 hours aged (a) (d) SnPb, (b) (e) SAC105, and (c) (f) SAC305 30

2.11 FEM analysis result showing the distribution of total plastic strain developed in a solder joint developed by shear strain 31

2.12 A plot displaying the tensile and shear stress developed in a solder joint as a 29function of shear displacement 32

3.1 Total strain versus lifetime equation 38

3.2 The image showing the cut line positions in the BGA solder assembly 42

3.3 1st and 2nd row solder resistances change with the number of cycle to fail under +/-2.4% strain (a) SAC305, 0.5Hz, 25°C, (b) SAC105, 1Hz, 100°C, (c) 150°C/500h thermal aged SAC105, 1Hz, 25°C, (d)SnPb, 1Hz, 25°C 43

3.4 Fatigue lifetime variations with strain range for SnPb, SAC105 and SAC305 (a) 1Hz 25°C, (b) 150°C 500 hour thermal aged samples at 1Hz, 25°C,(c) As received sample at 1Hz, 75°C 45

3.5 Fatigue lifetime versus strain range at 1Hz, 25°C for different thermal aging conditions (a) SAC105, (b) SAC305, and (c) SnPb 48

3.6 Microstructures of solder matrix before and after thermal aging at 150°C 49

3.7 Fatigue parameters variation with thermal aging and solder alloy composition (a) fracture strain, (b) ductility exponent and strain hardening exponent 50

3.8 Fatigue life versus temperature tested at 1Hz, 2.2% plastic strain for SnPb, SAC105 and SAC305 52

3.9 Fatigue lifetime versus strain range at 1Hz for different temperatures (a) SnPb, (b) SAC105, (c) SAC305, (d) 150°C 500h aged SAC305, and (e) 150°C 1000h aged SAC305 52

3.10 Fatigue ductility coefficient, ductility exponent and cyclic strain hardening exponent variations with the environment temperature for SnPb, SAC105 and SAC305 55

3.11 Shear strain distribution in BGA packaged solder joints under 100^oC 56

3.12 The temperature dependency of (a) strain hardening exponent and (b) ductility coefficient for SnPb, SAC105 and SAC305 after thermal strain correction 58

3.13 The relationship between fatigue life and frequency at temperature at 2.44% plastic strain, at the temperature (a) 25^oC and (b) 75^oC 59

3.14 The frequency exponent dependence on the temperature for SnPb, SAC105 and SAC305 solder alloy 62

4.1 Ambient temperature measurements of Young's modulus and the coefficient of thermal expansion for Sn with respect to crystal direction 66

4.2 (a)SEM back scatter composition mode image showing small and large Ag_3Sn intermetallic within Sn-3.0Ag-1.1Cu.(b), (c) Optical polarized light image of (b) Sn–3.0Ag-0.8Cu commercial BGA joint, and (c) a near eutectic SAC solder ball illustrates "Kara's Beach ball" texture, which has six-fold, cyclic twin relationship with 60° rotations about a common [100] axis 68

4.3 SEM images of Sn-3.5wt%Ag solder microstructure for cooling rates of (a) 24^oC/s (water cooling), (b) 0.5^oC/s (air cooling), and (c) 0.08^oC/s (furnace cooling) 68

4.4 Schematic drawing of the sample layout (SAC105 and SAC305) 71

4.5 Schematic temperature profile for solder thermal treatment 71

4.6 Optical Microscope of the solder joints in outmost row Prom position 1 to 14 after reflow 72

4.7 Optical Microscope of the solder joints in outmost row P from position 1 to 14 150^oC for 500 hours 73

4.8 SEM images of the solder joint SAC105 in package side (top) and board side (down) before (left) and after 150^oC 500 thermal aging 74

4.9 Optical and SEM images of 150°C 500 hours thermal aged BGA SAC105 after cooling at (a)(d) fast water quench,(b)(e) medium air cool, and (c)(f)slow furnace cool 75

4.10 Corner, Edge and inner joint microstructure of 150^oC 500 hours thermal aged BGA SAC105 after air cooling and water quenching 77

4.11 Grain structure map with cooling rate, joint position and thermal history 78

4.12 Schematic quarter model for FEM analysis. Chip Size: 1cm x 1cm; Packaging Size: 1.3cm x 1.3cm; BT Substrate Thickness: 400um; Solder joint diameter: 600um; Solder Joint Height: 400um; Pitch Size: 800um 81

4.13 FEM analysis of Total deformation of solder joints in BGA assembly cooled from 150°C to 22.5^{o}C, unit: mm 81

4.14. Stored strain energy variations with solder position and cooling rate 83

4.15. Schematic drawing of BGA assembly showing the solder joint layout 84

4.16 The optical microstructure of the 150°C 500 hours thermal aged joint after (a) fast cool, (b) medium cool showing twins 85

4.17 FEM analysis of Total deformation of solder joints in BGA assembly cooled from 150°C to 22.5^{o}C, unit: um 85

4.18 The optical microstructure of the 150°C 500 hours thermal aged joint after (a) and (b) medium cool from 180°C (c) slow cool from 180°C, and (d) medium cool from 165°C 87

5.1 The four twinning elements. The twinning and the conjugate (or reciprocal) twinning planes are K_1 and K_2, and the twinning and conjugate (or reciprocal) twinning directions are η_1, and η_2, respectively. The directions η_1, η_2 and the normals to K_1, and K_2, are all contained in the plane of shear P 91

5.2 Crystallography of β-Sn structure and its possible slip systems 92

5.3 Optical images of solder joint after aging at 150°C for 24 hours and water quenched 97

5.4 EBSD analysis of the twin (a) optical image of water quenched solder joints after 150°C 500 hour thermal aging; (b) (001) inversed pole figure of the red rectangular area in (a); (c) misorientation angle plot 97

5.5 Simplified configuration of the solder joints in BGA assembly 101

5.6 Change of Critical resolved shear stress for dislocation slip and twinning with hydrostatic pressure stress 102

5.7 The schematic drawing of the solder joints layout in BGA packaging assembly 102

5.8 3-D Quarter model of the BGA assembly 104

5.9 1/8 model showing the hydrostatic pressure distribution in the solder joint in BGA assembly after cooling from 150°C to room temperature 105

5.10 Hydrostatic pressure stress distribution in the solder joint after cooling 105

5.11 The hydrostatic pressure distribution in solder joints in BGA assembly when cooling from 180°C 106

5.12 optical image showing the grain structure of SAC105 solder joint after cooling from (a)150°C, (b)180°C, and (c)and (d)165°C 108

6.1 Fatigue lifetime of 150^oC 500 hour aged SAC105 cooling with fast, medium and slow rate, at strain 2%, 1Hz, room temperature 113

6.2 Resistance change with number of cycle for (a) fast cool, (b) medium cool and (c) slow cool for SAC105 150^oC, 500 hour aged samples, and (d) SAC305 fast cool sample, at strain 2%, 1Hz, room temperature 114

6.3 Fatigue lifetime of 150^oC 500 hour aged SAC305 cooling with fast, medium and slow cooling rate, at strain 8%, 1Hz,room temperature, first row solder joints lifetime 115

6.4 Fatigue lifetime of 150^oC 500 hour aged SAC105 cooling with fast, medium and slow cooling rate after stored in 100$_oC$ for 24 hour. Shear test at strain 8%, 1Hz, room temperature, first row solder joints fatigue life 116

6.5 crack path of the solder joint after shear fatigue test at room temperature, 8% strain, 1Hz for (a)slow cool, (b)medium cool, (c)(d)fast cool 117

LIST OF TABLES

Table Page

1.1 Lead-free solder alloys with melting point between 200°C and 230°C 5

1.2 Major lead-free solder system candidates to replace eutectic Sn-Pb 6

2.1 A list showing the elastic property of component materials used for FEM analysis 30

3.1 Summary of fatigue models 35

3.2 Fatigue ductility coefficient, ductility exponent and strain hardening exponent for as received and thermal aged solder at 25°C extrapolated from Figure 3.5 47

3.3Calculated fatigue constants $\varepsilon_f^{'}$ and C of different solders at various temperatures 54

3.4 Fatigue constants at different temperatures for different solder alloys 62

4.1 Corner, Edge and inner joint microstructure after water quenching and slow cooling 76

4.2 Materials constants for FEM analysis 80

5.1 Reciprocal twinning modes in β-Sn 93

5.2. Material constants for FEM analysis 103

CHAPTER 1

INTRODUCTION

1.1 An Overview of Packaging Assembly, Lead-free Solder and Environmental Compliance

1.1.1 IC Assembly

Solder is very important in decades since the beginning of the electronics industry, especially for the assembly and interconnection in Silicon die, which provides the mechanical, thermal and electrical continuity in the electronic devices. Solder is used in different levels in IC assembly industry as shown in Figure 1.1 [1]. Bonding of the die to a substrate and its encapsulation is referred to Level 1 packaging. As a die bonding material, solder provides electrical and mechanical connection between silicon die and bonding pad and dissipates heat generated by the devices. Conventionally, wire bonding is the major technique for silicon die assembly. However, the use of solder bump in the first level packaging is gaining more acceptances since ball grid array and flip chip technology were developed [2-3]. The cross-section of solder bump used in first level flip chip configuration is shown in Figure 1.2 [1]. Figure 1.3 shows the solder ball in BGA first level assembly [1]. Level 2 assembly is referred to the connection between the component (encapsulated silicon die) and printed wiring board (PWB). Practically all the components are connected to the printed circuit board with solder. Pin through hole (PTH) and surface mount technology (SMT) are two main assembly methods for attaching the components to PWBs. Figure 1.4 and Figure 1.5 show the image of PTH and SMT [2].

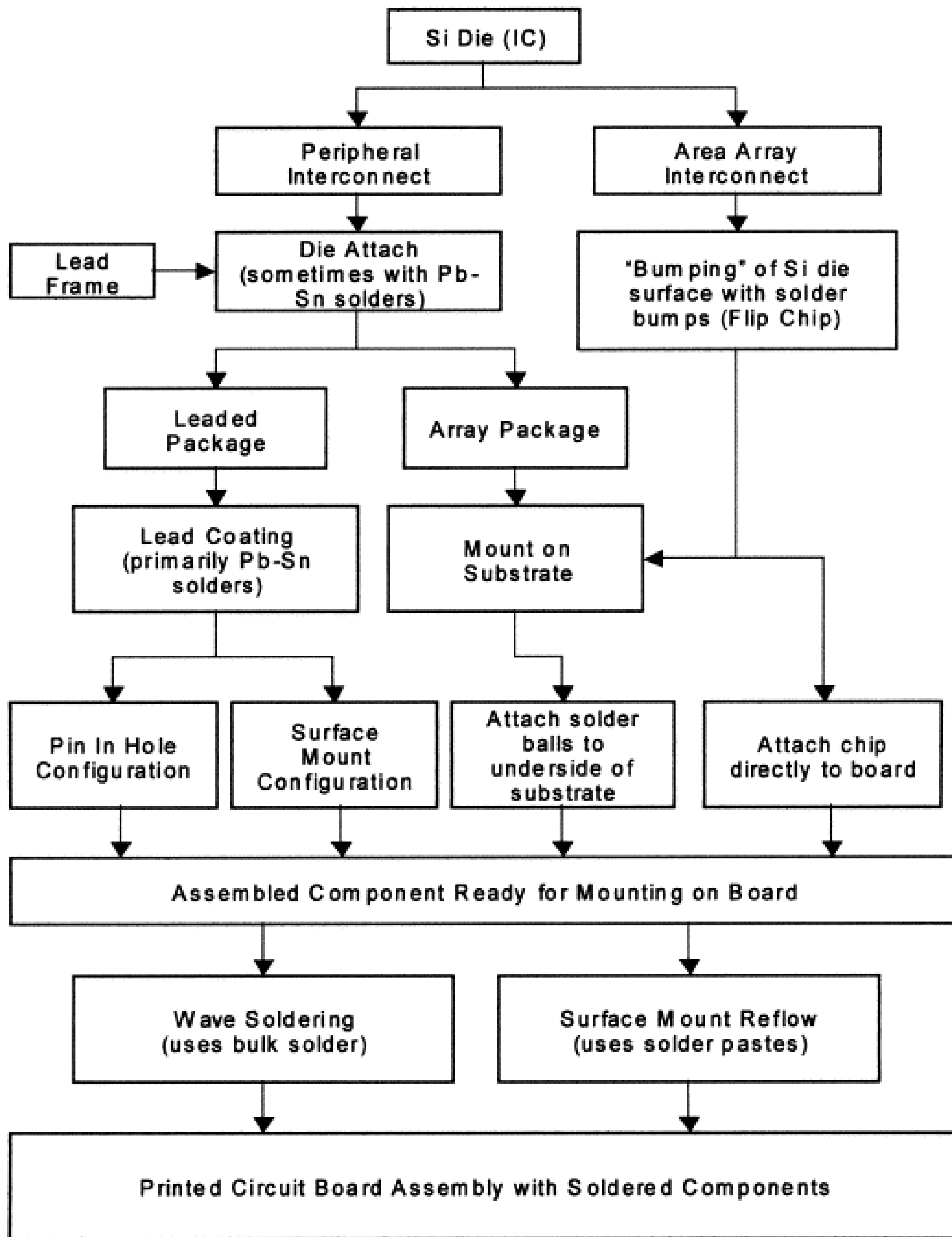

Figure 1.1 Overview of IC assembly process [1].

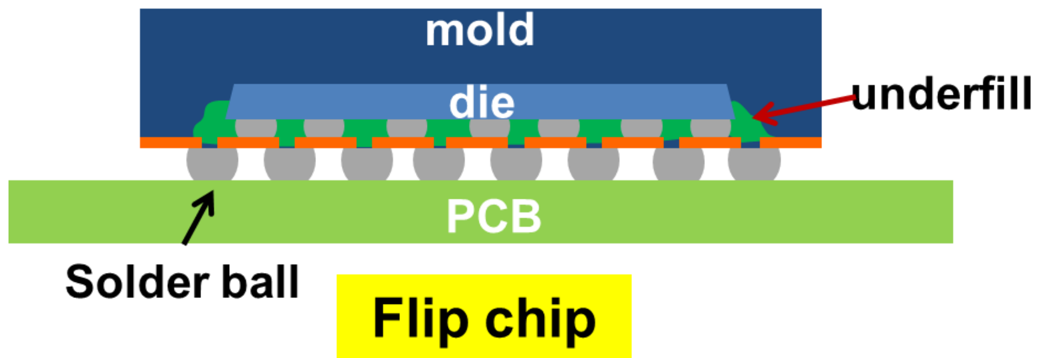

Figure 1.2. Cross-section of a flip chip connection.

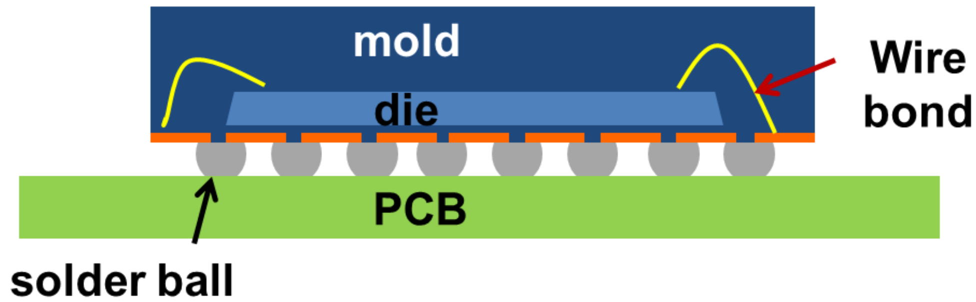

Figure 1.3. Cross-section of a wire bond ball grid array (BGA) microelectronics component.

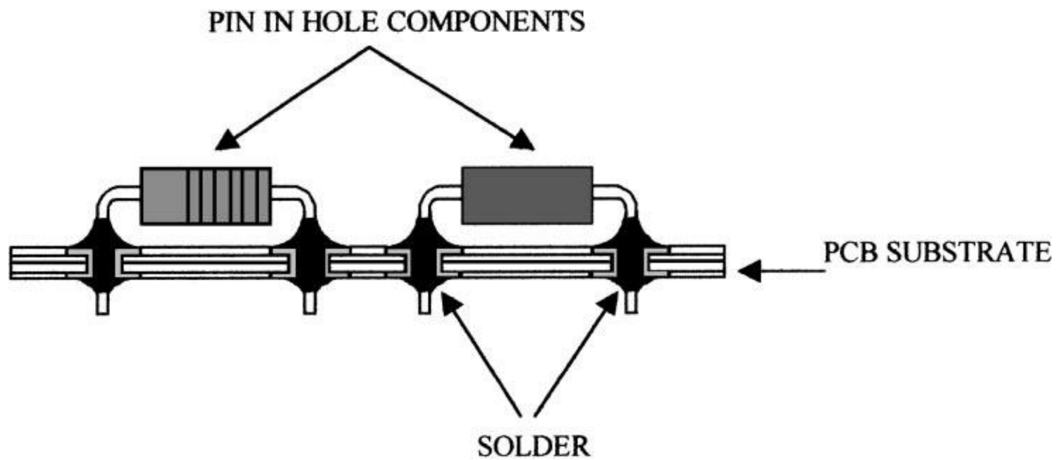

Figure 1.4. Cross-section of a pin through hole connection of a microelectronics component on a printed wiring board [2].

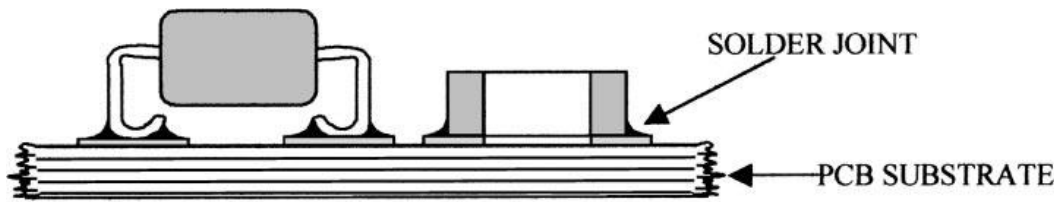

Figure 1.5. Cross-section of a surface mount connection of a microelectronics component with leads on a printed wiring board [2].

1.1.2 Lead-free Solder and Environmental Compliance

Solder material has not been changed much for many years and lead-tin is main solder alloy. Use of lead-tin solder can be dated back to 300 BC by Greeks and Romans [3]. In the early 20th century, soldering was introduced to the electronic industry. The eutectic tin-lead, 63Sn37Pb, and near eutectic 60Sn40Pb are the most popular solder materials due to their unique characteristics, such as relative low temperature (183 $^{\circ}$C), low cost, wide availability, ease of use, and good electrical/thermal/mechanical/chemical properties [1, 4-9].

However, due to the health-related and environmental issues, although lead-tin solder has been successfully used for packaging industry, transition from lead-tin solder to lead-free solder is inevitable. The regulation of lead was firstly initiated by U.S. Congress back to 1991, and the U.S. Senate proposed the Reid Bill to restrict the use of lead and increased the tax for lead containing product. Later, the European Union directived on Waste Electrical and Electronic Equipment (WEEE) dictated that products sold in EU must be lead-free from July 1, 2006. Further in Asia Pacific, many big companies took their steps forward to develop alternative alloys instead of lead tin solder. Nowadays, the replacement of lead-bearing alloying is inevitable and is in action world widely [6-9].

1.2 Lead-free Solder Alloy Candidates

For the past twenty years, the semiconductor industry has studied a wide range of alloys to replace lead-tin solder. The selections are based on variety of considerations, including toxicity, physical properties (melting temperature, surface tension, wettability, thermal and electrical conductivity), mechanical properties, microstructure characteristics, electrochemical

properties (corrosion, oxidation and dross formation, and compatibility with non-clean fluxes), manufacturability, cost, and availability [10-13.] Meanwhile, patents issues associated with lead-free solder selection needs to be considered [14-16]. . Among all the requirements, wettability (bondability) and suitable melting temperature are the two basics. First, solder must be capable to wet and bond which indicates that it should be able to form intermetallic compounds with Cu, Ni, and other metals routinely used in microelectronic packages. Second, the melting temperature should be sufficiently low enough to be reflowed as a paste and high enough to avoid by ill effects due to operating temperatures. To conform with the standard surface mount and wave soldering processes, and to avoid the damage of PCB and components, the alloy melting temperature should be lower than 230 °C and higher than 175 °C [17]. Currently, the replacement alloys candidates include ternary, binary and some quaternary alloys of Sn with Ag, Zn, In, Sb, Bi, and Cu. Table 1.1 lists some of lead-free solder with melting temperature between 200 °C to 230 °C. Table 1.2 lists the major lead-free solder alloys to replace eutectic Sn-Pb with their advantages and disadvantages based on the selection criteria [1, 4-5, 7-9, 14, 16-33].

Table 1.1 Lead-free solder alloys with melting point between 200°C and 230°C

composition	Melting range (°C)	composition	Melting range (°C)
Sn-3.4Ag-4.8Bi	205-210	Sn-4.7Ag-1.7Cu	216-218
Sn-7.5Bi-2.0Ag	207-212	Sn-2.5Ag-0.8Cu-0.5Sb	213-218
Sn-7.5Bi-2.0Ag-0.5Cu	186-212	Sn-3.8Ag-0.7Cu	217-219[a]
Sn-3.5Ag-3.0Bi	206-213[a] 216-220[a]	Sn-2.0Ag-0.8Cu-0.5Sb	213-219[a] 216-222
Sn-3.5Ag-5.0Bi-0.7Cu	210-215	Sn-2.0Ag-0.75Cu	217-219
Sn-2.0Ag-3.0Bi-0.75Cu	210-215	Sn-4.0Ag-0.5Cu	217-219

Table 1.1 – *Continued*

Sn-2.0Ag-4.0Bi-0.5Cu-0.1Ge	216	Sn-4.0Ag-1.0Cu	217-219
Sn-3.4Ag-4.8Bi	208-216[a] 200-216[a]	Sn-3.5Ag-1.0Zn	218-221
Sn-3.5Ag-0.7Cu	217(E)	Sn-3.5Ag	221(E)
Sn-3.0Ag-0.7Cu	217-218	Sn-2.0Ag	221-226
Sn-3.5Sb-2.0Bi-1.5Cu	218(E)	Sn-0.7Cu	227(E)
Sn-3.5Ag-1.5In	218(E)	Sn-2.0Cu-0.8Sb-0.2Ag	226-228
Sn-3.2Ag-0.5Cu	217-218	Sn-5.0Sb	232-240[a] 236-240[a]

E=eutectic composition
[a] Different values reported in the literature

Table 1.2 Major lead-free solder system candidates to replace Eutectic Sn-Pb

Alloy system	Remarks
Binary	
Sn-Ag	Fairly high melt temperature (221°C); Alternative for wave soldering, but cost a reliability issue related to Ag3Sn platelet growth
Sn-Cu	Fairly high melt temperature (227°C); Wave solder candidate; moderate wetting but sufficient for most applications
Sn-Bi	Not applicable as a general assembly solder due to high cost, low melting temperature (138°C), and availability ; good for low temperature end of a solder hierarchy
Sn-Zn	Cheap; Lower melting temperature than most lead-free solders An is highly active, presents potential corrosion and process concerns
Ternary	
Sn-Ag-Cu	Leading candidate system for reflow soldering; Lower melt temperature than Sn-Ag, Sn-Cu binary alloys; Adequate wetting,

Table 1.2 – *Continued*

	mechanical properties; Much reduced Cu scavenger characteristics compared to Sn-Ag
Sn-Ag-Bi	Even lower melt temperature than Sn-Ag-Cu alloys Best fatigue resistance among most popular Pb-fess alloys Poses some reliability and end-of–life reclamation concerns
Other additions	
Ag, Al, Bi, Ga, In, Cu	Reduce melting temperature and enhance mechanical properties
Ni, Sb	Do not reduce melting temperature but added to enhance properties

1.2.1 Sn-Ag System

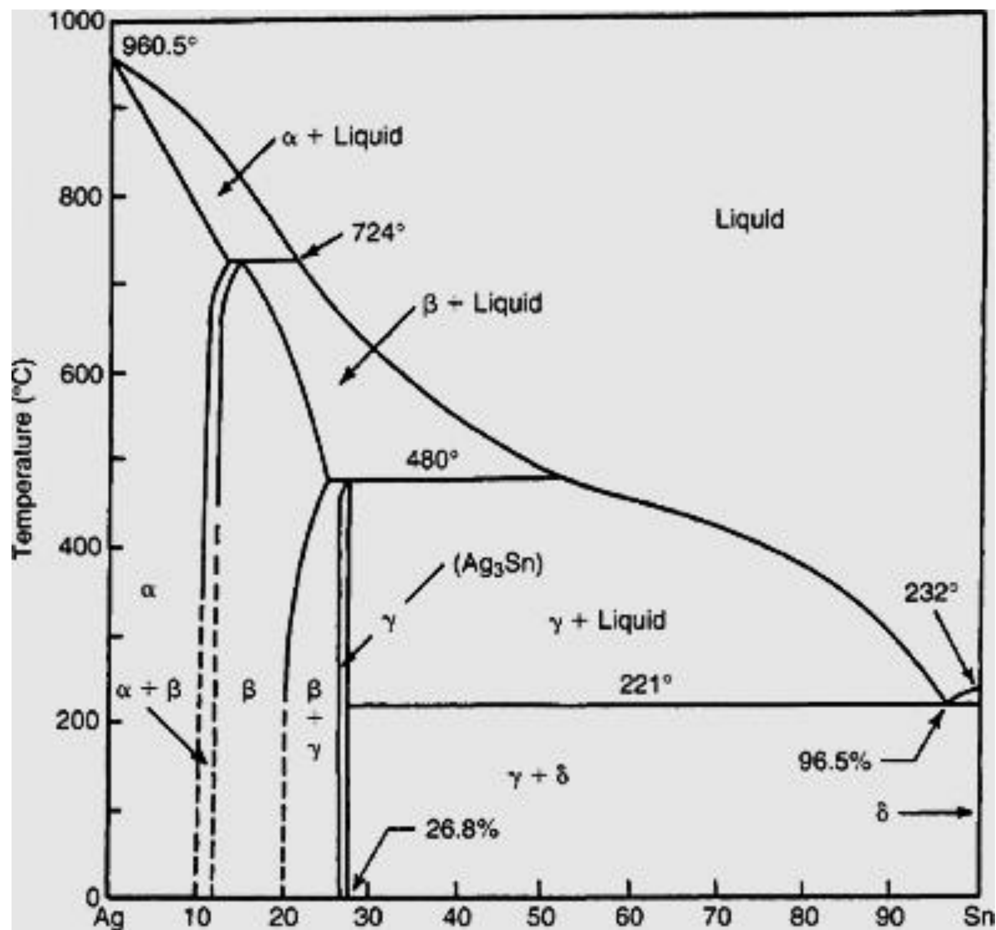

Figure 1.6. Phase diagram of tin-silver

Among all the lead-free solders, Sn-Ag based system with tin content higher than 90% and Ag ranges from 1% to 4% is the most promising alloy chosen by the industry. Figure 1.6 is the phase diagram of the Sn-Ag [3]. The eutectic composition for the Sn-Ag binary system occurs at Sn-3.5%Ag with eutectic temperature 221 °C. The microstructure consists of Sn and the intermetallic Ag_3Sn in the form of thin platelets. McCormack et al. [34] described the solidified microstructure of the binary eutectic Sn-3.5%Ag as consisting of a β-Sn phase with dendritic globules and inter-dendritic regions with a eutectic dispersion of Ag_3Sn precipitates within a β-Sn matrix. However, binary eutectic Sn-3.5Ag or near eutectic Sn-Ag is not adequate due to the high melting temperature, cost and poor wettability. A small addition of Cu, Zn, or Bi to create ternary alloy, or a minor addition of a fourth element, less than 1%, can reduce the melting temperature and cost, enhance wettability, strength and reliability [20-33].

1.2.2 Sn-Bi System

The bismuth–tin binary system is favored when low soldering temperatures are required [35]. According to the phase diagram of tin-bismuth shown in Figure 1.7, the eutectic composition is Sn57wt%Bi and the eutectic temperature is approximately 139 °C. In some ways, the phase diagram and microstructure of tin–bismuth are fairly similar to that of tin–lead shown in Figure 1.8 with eutectic composition at Sn-38.1%Pb and eutectic temperature 183°C. However, the mechanical properties are significantly different. Because bismuth is a very brittle metal, the eutectic suffers from lack of ductility, particularly under conditions of impact and rapid stressing [35]. In addition, tin–bismuth–lead forms a ternary eutectic at even lower temperature (95°C), which can lead to associated process problems during soldering (such as fillet lifting) [36]. To reduce brittleness, increase ductility, and avoid the harmful ternary eutectic, the electronic industry has selected a Sn–3 wt.% Bi alloy through trial and error during the late 1990s and early 2000s [37-38].

1.2.3 Sn-Cu System

The tin–copper binary eutectic forms at 0.7 wt. % Cu and with a eutectic temperature of approximately 227°C. It is noted from the phase diagram that the liquidus line rises steeply to high temperatures if the copper level exceeds 0.7 wt. % so that the copper composition is usually below 0.7%. Due to the abundant availability, tin–copper binary solder is cheaper compared to tin-silver and tin-bismuth and thus favored in low-cost applications within electronics assembly.

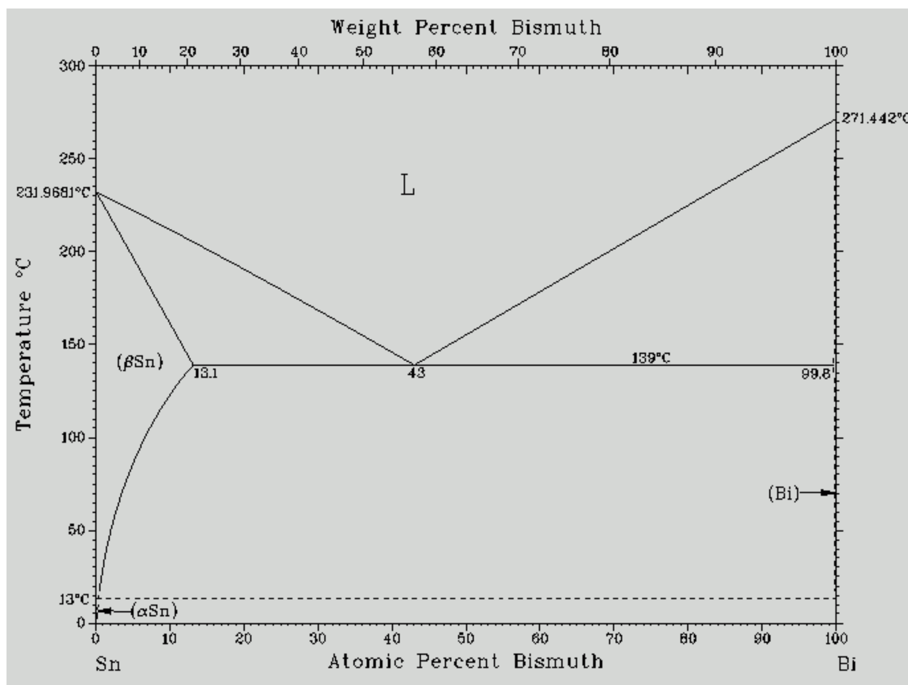

Figure 1.7. Phase diagram of tin-bismuth

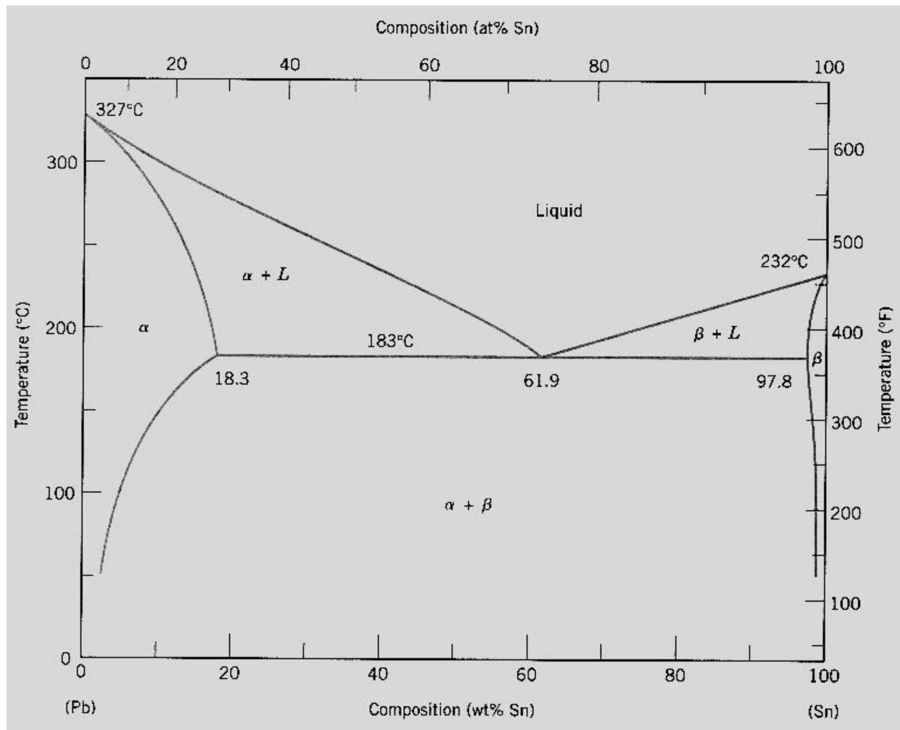

Figure 1.8 Phase diagram of tin-lead

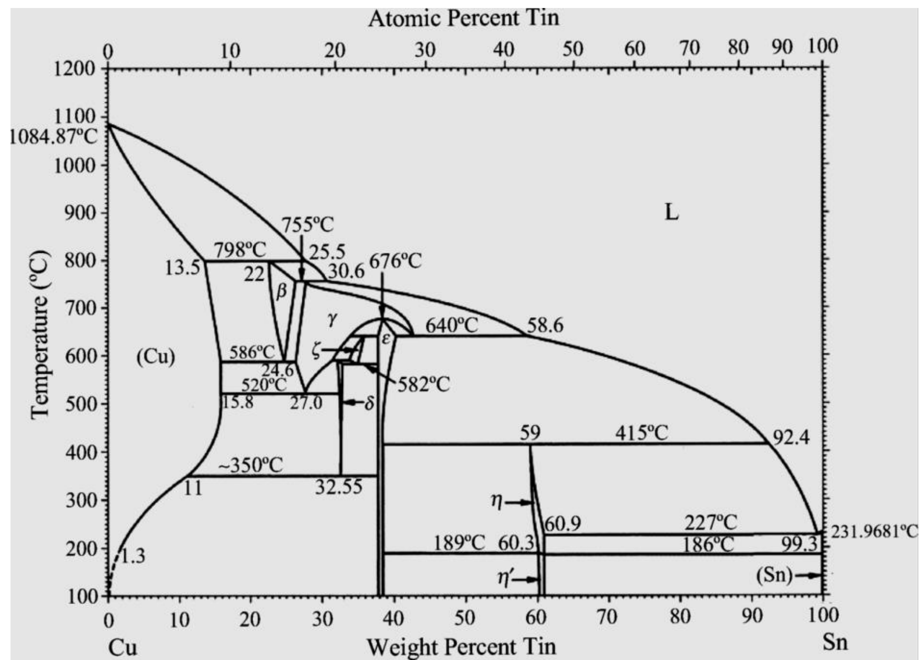

Figure 1.9. Phase diagram of copper-tin.

1.2.4 Sn-Ag-Cu

The ternary eutectic behavior of Sn-Ag-Cu and its application for electronics assembly was discovered (and patented) by a team of researchers from Ames Laboratory, Iowa State University, and Sandia National Laboratories-Albuquerque. The addition of minor Cu, typically in the range of 0.7%, can lower the melting temperature of Sn-Ag to about 217 ˚C slightly higher than that of Sn-Ag-Bi ternary system. The presence of Cu greatly reduces the Cu dissolution rate from the terminal pads [39-41]. The cost of Sn-Ag-Cu is lower than both Sn-Ag and Sn-Ag-Bi. Meanwhile, the reliability and yields of eutectic or near eutectic Sn-Ag-Cu are found to be comparable to that of eutectic Sn-Pb, and the solderability and reliability are reported to be better than that of Sn-Ag and Sn-Cu binary system [42-46]. Sn-Ag-Cu (Tin-Silver-Copper) solders are used by two thirds of Japanese manufacturers for reflow and wave soldering and by about 75% of companies for hand soldering.

Much recent research has focused on selection of 4th element additions to Sn-Ag-Cu to provide compatibility for the reduced cooling rate of solder sphere reflow for assembly of ball grid arrays, e.g. Sn-3.5Ag-0.74Cu-0.21Zn (melting range of 217–220 ˚C) and Sn-3.5Ag-0.85Cu-0.10Mn (melting range of 211–215 ˚C) [47-50].

1.2.5 Sn-Ag-Bi

The melting temperature of Bi is 271 ˚C, much lower than Cu which is 1083 ˚C, so that compared to the Sn-Ag-Cu ternary system, Sn-Ag-Bi, with Bi composition in the range of 5%, melts between 208 ˚C and 215 ˚C. In addition to lowering the melting temperature, Sn-Ag-Bi with Bi less than 5% exhibits the best solderability among all the lead-free solder alloys [51-54]. Besides, the addition of Bi greatly improves the fatigue resistance and strength [55-59]. However, the adverse effects of Bi are also found. First, it is found that Bi will increase the brittleness of the solder [58-59]. Second, fillet lifting when wave-soldered joints cooled down is observed at through hole joints [54]. Moreover, Bi is easy to be oxidized so that fluxes activity at lower temperatures is recommended [37-38].

1.3 Lead-free Solder Interconnect Reliability

This part is meant to provide an overview of the issues affecting the reliability of the lead-free electronic solder joints subjected to service environment. First, it is important to mention that solders used in interconnects are in a joint geometry that the constraints present in the configuration influence the overall response of solder joints to the environment and in-service parameters. The substrate, silicon die, molding and intermetallic compound exist in connection with the solder can affect the reliability of the joints. Besides the geometry consideration, fabrication process of solder and resultant microstructure, service parameters encountered, and response of the solder material to external influences, play significant roles in determining the reliability of solder joints [60]. Moreover, with the decreasing in device size, the service environments impose ever-increasing demands on the solder joints. The solder joint has to be smaller but at the same time maintain the structural integrity, dissipate higher stress and heat, and provide stable electrical pathway. Therefore, the trend of microminiaturization of electronics induces great challenges for solder joints reliability [61-64].

In addition, the reliability issues in solder interconnect are complicated by the application of lead-free solder for several reasons. First, the material properties of lead-free solder differs from lead-tin solder and the database of lead-free solder is far from completion. Different from lead-tin solder, in primary tin-based lead-free solder, thermally induced phase coarsening presents within the solder matrix and at the solder/substrate interface, while lead is usually chemical inert which does not form intermetallic compound. Also, phase diagrams, mechanical properties, chemical reactions between the solder material and its finishes and the substrate, et al. need further investigation. In addition, many researches on lead-free solder property are based on bulk solder, while for solder joints in packaging level, the solder geometry and constrains encounter are different from bulk solder resulting in changing of mechanical properties. Again, the differences in thermomechanical, dynamical, electrochemical and electrical properties create difficulties for developing appropriate acceleration testing methods

and conditions for property and reliability evaluation. The methods and loading conditions commonly used for lead-tin may not be suitable for lead-free solder. Worldwide researchers have undertaken serious efforts to study lead-free solder reliability under different loadings and achieved insightful understandings on the solder joint reliability [59-64].

Failure of the solder interconnect is primary caused by thermal, electrical, mechanical field or the interactions between these fields. Figure 1.10 schematically illustrates damage from those fields and their complex interactions [65-75]. Processes identified in this figure are EM-electromigration, TM-thermalmigration, PF- plastic flow and fracture, JH-joule heating, CS-current stressing and TMF-thermomechanical fatigue. Among these listed factors, the major damage contributors that affect the reliability of the lead-free electronic solders are (i) mechanical integrity, (ii) thermomechanical fatigue, (iii) whisker growth, (iV)electromigration, and (V) thermalmigration. However, the mutual interactions between them are becoming progressively more important with the continued efforts towards microminiaturization of electronic packages, especially whisker growth, electromigration and fatigue processes. In this research, fatigue due to mechanical and thermal load is the main interest and is studied extensively.

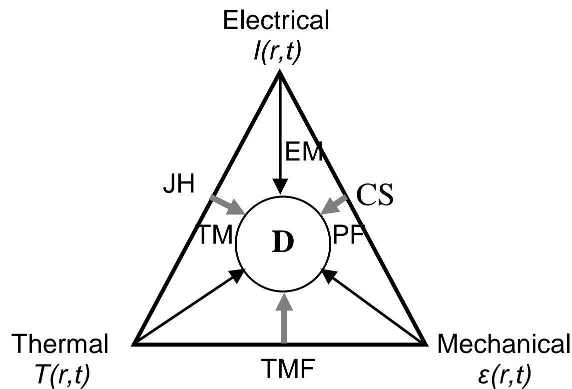

Figure 1.0 Fields that cause damage in solder interconnect and their Interactions

1.3.1 Thermomechanical Fatigue

Thermomechanical fatigue is resulted from the highly inhomogeneous stress distribution due to the differences of thermal expansion coefficient between the solder and surrounding components and also within the body-centered tetragonal beta-tin solder between the a- and c- directions[64-65, 68-69,72]. It is found that the CTE mismatch between the a- and c- directions is twice of the difference between polycrystalline copper and polycrystalline Sn. During service, the device is subjected to temperature fluctuations due to environment change and power change subjecting the solder joints to the stresses and causing damage to the solder joint. Figure 1.11 shows the solder joints under shear stresses due to CTE mismatch during thermal cycling [1]. The accelerated power cycling and thermomechanical testing simulating the solder joints in service condition by many researchers have found that the heating/cooling rate, temperature extremes (high/low temperature), temperature range and dwell times at high/low extremes significantly affect the thermomechanical fatigue behavior of the solder joints [63-64, 66-71]. The failure is usually happens at the solder/substrate interface in the IMC layer. This is probably due to the constraints imposed by the substrate which causes strain localization to interface region. It is also found that coarsening of the intermetallic compound in lead-free solder affects the TMF reliability significantly [66-69]. As a result, methods to prevent the IMC coarsening were investigated extensively. It is found that a small addition of Ni to the Sn-Ag-Cu solder can reduce the IMC formation [23, 26-27, 47, 72]. Besides, nanostructured reinforcements with surface active radicals are proved to be effective in improving the reliability of the solder joints subjected to thermomechanical fatigue during service [73]. However, due to the complexity of the factors affect the TMF, the mechanism and mechanics are not fully understood. It is still a big concern and addresses a lot of research interest in the microelectronic industry.

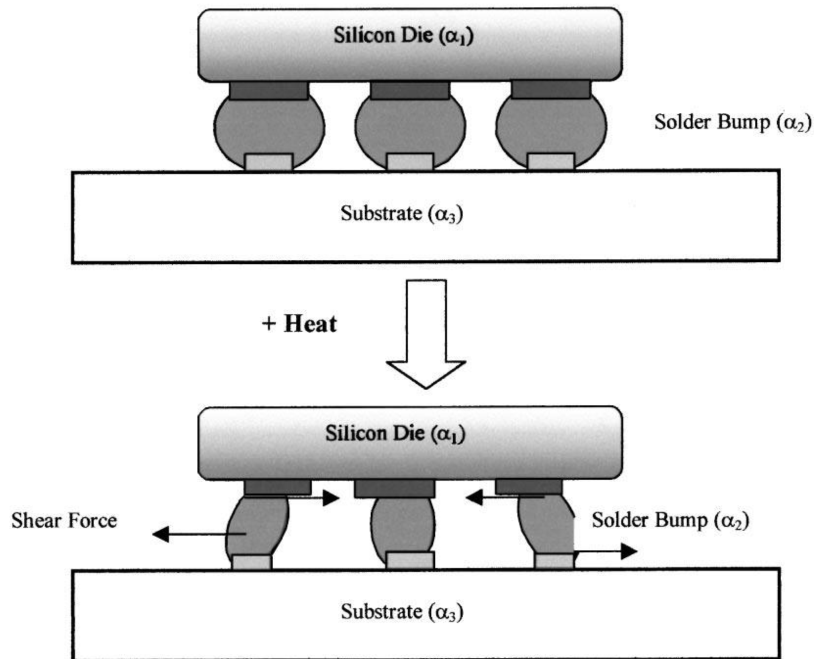

Figure 1.11. Solder joints subjected to shear strain during thermal cycling due to CTE mismatch between the Die (α_1), the solder (α_2) and the substrate (α_3).

1.3.2 Whisker Growth

Although it is well known of Sn exhibits whisker growth, attention is taken till recently because of the microminiaturization of electronic components. The decreasing in solder joint spacing increases the chance of getting electrical short if tin whisker growth occurs. Compressive stress is believed to be the cause of whisker growth. In Sn-based lead-free solder, the compressive stress arises from the Sn-Cu IMC formation at the Sn grain boundaries. This process can be facilitated by copper diffusion from the substrate. In addition, for continuous growth of whisker, continuous compressive stress from the external, or resulting from the volume change with IMC formation, or the stress developed from electromigration, can facilitate tin whisker growth. Since it is difficult to predict when and where whisker grows, the investigation of whisker growth becomes difficult. Therefore, the mechanism investigation and evaluation of mitigation strategies to prevent whisker growth become difficult.

1.3.3 Electromigration (EM)

The enhanced atomic displacement and the accumulated effect of mass transport under the influence of electric field are called electromigration. EM is a result of a combination of electric and thermal effects on mass transport. At low temperature, EM cannot occur because the atomic mobility is too low. When the current density is high, usually above 10^5 A/cm^2, atomic displacement is enhanced in the direction of electron flow. In a very-large-scale-integration in Al or Cu interconnection, the current density is higher than 10^6 A/cm^2 and the device operation temperature is around 100 $^{\circ}$C that EM can occur leading to the voids formation at the cathode and extrusions at the anode. Recently, with the miniaturization of electronic devices and development of flip chip technology, EM in solder joints has gained a lot of interest. As reported, EM can occur in solder joint at the current density of 10^4 A/cm^2 , which is two orders lower than that in Al or Cu interconnect. Many researchers thought EM occurs in solder joint at such low current is due to its low melting temperature and faster lattice diffusion, while K. Tu pointed out it is also due to the higher resistivity and effective charge of lattice diffusion in solder, and lower stress [63]. Based on the Equation 1.1, he calculated the current density needed for EM, which is determined to be 10^4 A/cm^2. Moreover, due to the unique geometry of the solder joint, interfacial reactions between solder and thin film metal interface, EM in solder interconnect is different much more complicated than EM in Al and Cu interconnect. In equation 1.1: J, current density; Δx , critical length; $\Delta\sigma$, hydrostatic stress; Ω , atomic volume; Z*, effective charge number for electromigration; ρ , resistivity.

$$j\Delta x = \frac{\Delta\sigma\Omega}{Z^* e\rho} \qquad 1.1$$

1.3.4 Isothermal Mechanical Fatigue

Unlike early electronic products, the electronic devices nowadays experience a variety of stresses due to their versatility, portability and multiple functionalities. The life cycles of the

electronic tend to be shorter and the environments are becoming increasingly diverse. Thermally induced stresses are not predominant in some cases, especially for consumer products such as cell phone, digital cameras and other portable devices. Mechanical vibration, shock, drop, bending etc. are playing an increasing role in determining the device performance. [74-82] Though a lot of researches on fatigue behavior of lead-free solder under isothermal shock/drop, bending, and vibration load have been carried, conflictions exist within the results due to the complex in assembly configuration, solder geometry, surface finish, solder composition, failure mode, and so on. For example, various reports have shown that the lead-free solders have poorer shock or drop test performance, as compared to the Sn–Pb solder due to the enhanced interfacial reactions; while at the same time, some researchers found that Sn-Ag-Cu lead-free solder show better shock than Sn-Pb [74-82].

1.4 Objectives of This Study and Organization of This Dissertation

As mentioned before, replacement of lead-tin solder with lead-free solder is inevitable and understandings on the properties of lead-free solder are essential. Due to lack of field data on lead-free solder, the transition from lead-tin to lead-free becomes difficult. Therefore, there is a clear need of studying the mechanical properties of lead-free solder and enriching the lead-free database, for example find and include the mechanical fatigue property parameters into the database. At the same time, the fatigue reliability is and will be an ever increasing concern as the devices getting smaller and mobile. The mechanical fatigue behaviors, including thermal cycling and isothermal fatigue, and their affecting factors have to be studied and understood, especially the grain structure of lead-free solder joint and its relation to the fatigue property is crucial for lead-free solder joints application in electronic packaging industry.

In this research, grain structure evolution by one-time thermal exposure and its impact on the fatigue reliability were studied. First, aiming to enrich the database of lead-free solder and understand the fatigue mechanism, shear fatigue test was designed. It is find out that shear

fatigue is an effective and efficient method for extraction fatigue property parameters and studying the fatigue failure mechanism. Coffin-Manson model is found to be applicable for describing the fatigue behavior of solder joint under isothermal shear fatigue. Accordingly, fatigue property parameters, namely, fatigue ductility coefficient, ductility exponent and frequency exponent are extracted from shear test and coffin-Manson model. The strain hardening exponent which is related to the ductility exponent is derived and determined to be the most influential for the fatigue resistance of solder joints in packaging. Second, the grain structure evolution with thermal exposure was investigated to find out the grain structure stability and evolution paths in Tin-based solder joints. Surprisingly, recrystallization and deformation twinning were observed just by simply one time thermal exposure. Their mechanisms were investigated and discussed in this research. These studies posed great scientific and technical importance to the tin-based lead-free solder technology. It indicates that the microstructure of the solder joints in one assembly can be different and is dynamically changing. Moreover, the grain structure evolution in tin-based solder joint in packaging assembly is much easier than in bulk solder due to the constrains from the surrounding components. Finally, using the shear fatigue method, the fatigue reliability of the solder with various grain structure created by one-time thermal exposure were evaluated. It shows that polygrain and twin enhance grain structure can enhance the fatigue resistance of the solder in electronic packaging. In the end, conclusions are made for this research and some future works are planned as well.

CHAPTER TWO

FRACTURE MECHCNICS OF LEAD-FREE SOLDER JOINTS IN BALL GRID ARRAY ASSEMBLY UNDER CYCLIC SHEAR LOAD

2.1 Background

The demand for portable and multifunctional electronic devices is made possible by increasing the density and reducing the size of the electronic components and packaging, as well as decreasing the size of the interconnect such as solder joints. This continuing thrust toward high density and high performance electronic devices has spurred extensive research on the structural stability of solder joints because their mechanical failure is regarded as one of the primary factors limiting the performance of advanced device packaging assemblies. The solder joints in the assembly are more susceptible to failure than any other component in the assembly due to combined mechanical, chemical and electrical loads common at their use conditions. The reliability concern is further exacerbated by the widespread use of mobile and mini electronic products. [80] Decreasing in device size and thus solder joint size significantly reduces the robustness of the solder joint. At the same time, mobilization of the devices subjects device to various unconventional loads such as shock, bending and vibration [71-86]. The failure mechanisms of solder joints at such conditions are not well understood at this moment, resulting in a substantial knowledge gap in assessing their reliability limits. The technical challenges created by such a knowledge gap become even greater with mandated adaptation of Pb-free solder technology.[87-89] Although extensive efforts during the past two decades have provided impressively better understanding on the properties of Pb-free solder alloys, the gap appears to remain large and demands further development.

In many sources of the joint failure, the most concerning and extensively studied is thermal fatigue [42, 66-71, 90-92]. Thermal fatigue occurs because of the mismatch in thermal expansion between the chip and PCB (printed circuit board) subjecting the solder joint to repetitive shear stress with an on/off cycle of the device. The resulting fatigue instigates the

formation of cracks and their subsequent growth until failure of the joint, typically following the interface between the solder and metalized layer either in the chip or in PCB [66-71]. In a typical reliability assessment procedure of any packaging assembly, the failure mechanism is simulated by thermal cycling tests. While thermal cycling test has proven to be very successful in predicting the reliability of the assembly in use condition, it has a few known limitations which have recently become more critical. The first and probably the most troublesome problem is the fact that this test takes an excessively long testing time before gaining meaningful results. It takes at least several months to gain measurable failure rate, resulting in a substantial delay in the development cycle of the assembly. Additionally, the failure risk of the joint under other types of loads such as a shock and vibration may not be directly evaluated from the thermal cycling results.

The limitations of the thermal cycling test, the lack of fatigue property data on Pb-free solders, and the recent emergence of new reliability concerns have resulted in a keen interest in mechanical fatigue methods, for example, cyclic bending and shear fatigue of the solder joint assembly. [69, 74-76, 85, 93-96]. The research interest in these methods is to better assess the reliability of the packaging assembly under pure mechanical fatigue load such as a vibration and gain better understanding on the fatigue mechanism and the contributing fatigue properties. Since these fatigue tests produce well-controlled strain and strain rate at an isothermal condition, the resulting data can yield fundamental knowledge of the fatigue properties of the solder joint at various conditions. Furthermore, since mechanical fatigue can be conducted with high frequency, the reliability evaluation can be shortened to a few days provided that mechanism leading to the fatigue failure shares some mechanistic commonality with the device failure.

In this chapter, the failure mechanism of solder joints in package assemblies under shear fatigue with the specific aim of gaining fundamental understanding of the fracture mechanics and the correlation between the fatigue failure mechanism and solder properties

were investigated. This research reveals that isothermal shear fatigue method is indeed capable of providing data that can be, not only helpful in identifying fatigue-prone assembly structure, but also in collecting fatigue data indicative of solder properties, namely cyclic strain hardening exponent, fatigue ductility coefficient and frequency exponent. With this method, linkages among the solder joint microstructure, fatigue properties and fatigue reliability behavior are able to be identified. This chapter attempts to present comprehensive discussion of the characteristics of shear fatigue method, along with representative examples of the results and understanding gained from Pb-free and Pb-Sn solder joints.

2.2 Experimental Methods

2.2.1 Shear Tester Instrumentation

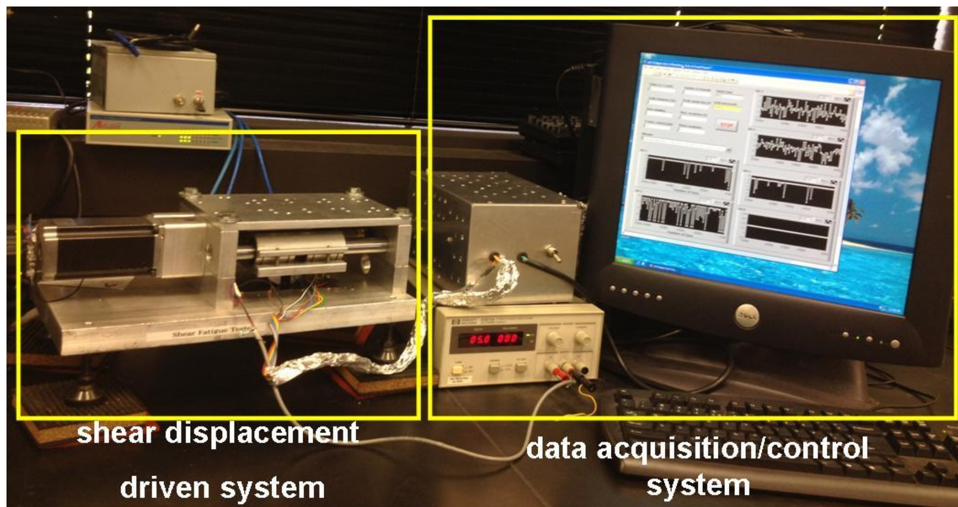

Figure 2.1 A picture of shear fatigue tester

The concept of shear fatigue testing originates from the shear fatigue method of structural materials where the mode II fracture is an important part of material property. For testing of my sample composes a chip bonded to the PCB board, the working principle of the shear fatigue test is extremely simple as it repeatedly displaces the chip with respect to PCB along the direction parallel to PCB. Figure 2.1 is a picture of the shear tester system. It simply consists of two parts: the shear displacement driven system and the data acquisition/control

system. As mentioned above, displacement driven in shear testing is simple in principle because it only requires moving two components of the solder assembly, chip and PCB, against each other. However, it is found that realization of a reliable tester involves careful consideration of many critical factors and the most critical and challenging one is found to be the shear displacement repeatability. Either chip or PCB board has to be displaced by the same distance in each cycle; otherwise, the error in displacement accumulates to result in asymmetrical shear strain between the positive and negative shear direction. In order to overcome this, the shear stage is carefully designed to ensure 1) displacement repeatability (no backlash during shearing) and 2) perfectly parallel displacement with respect to ideal shear direction to suppress solder assembly rotation during shearing. To overcome the backlash, a high power stepping motor and linear actuator with anti-backlash screw and nut are used. To ensure pure shear displacement, two half inch steel rods are installed in the actuator parallel to the chip to eliminate any possibility of chip rotation. Moreover, a very rigid Gig was designed as shown in Figure 2.2. In this picture, two grip blades are designed to make tight contact with the chip on PCB, and this head assembly is fixed to the linear translation mechanism. This translation mechanism is driven by a micro-stepping motor to induce parallel displacement of the chip relative to the PCB surface. As the PCB is firmly fixed to the main body of the stage, the horizontal displacement in the head assembly creates the shear strain.

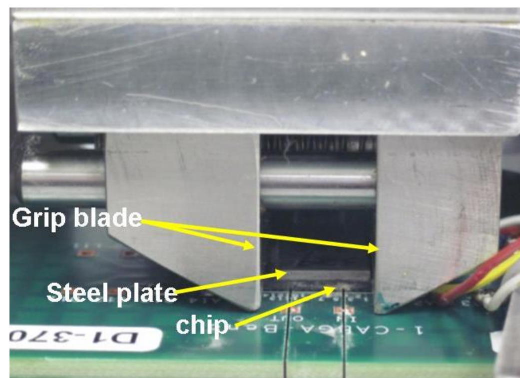

Figure 2.2 Picture of shear tester head assembly that is designed to grip and move the chip in a horizontal direction, parallel to PCB, without backlash.

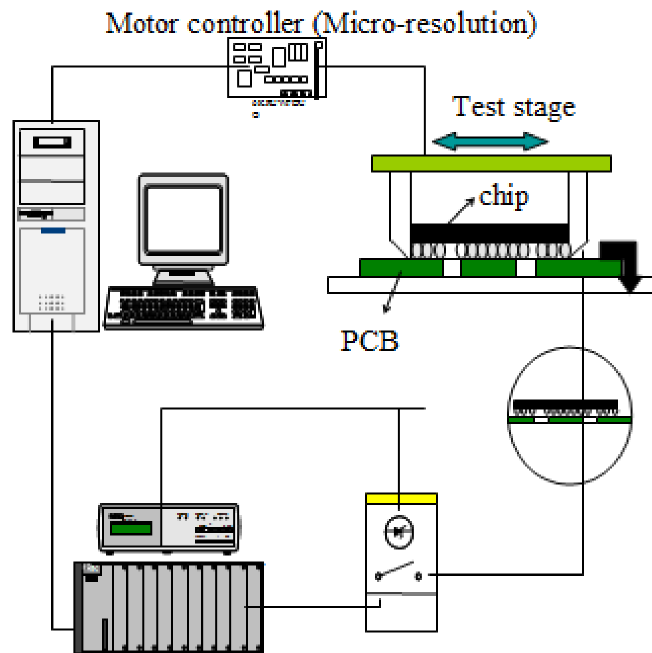

Figure 2.3 Schematic drawing of the shear tester system.

The second component of the system is the data acquisition and control system. Two channel DAC (digital analog converter) PC board is used to generate two pulse trains with designated frequency. The first pulse train is to induce constant displacement of the head assembly and the second is to change the direction as the head assembly reaches the target location. In this way, the solder joint can be subjected to a repeated shear strain with a constant rate. The same PC board contains high speed 8 ADC channels, and they are used for monitoring electrical resistance of the solder joints. Figure 2.3 the schematic illustrates the overall shear tester system. With the head assembly and its motion control using computer, the system is able to test 1x1cm chip assembly with 5 Hz maximum frequency at 5% shear strain condition.

2.2.2 Chip Mode Modification

In ideal shear fatigue testing, the entire amount of applied shear displacement is transferred to solder arrays. However, during the investigation, it is found that a significant error

in displacement can occur by the elastic deformation of the plastic chip mold. The mold is essentially an epoxy which is not mechanically rigid. Since a large number of solder joints exist in a chip (160 in the present case), the solder joint array poses significant mechanical resistance against shear deformation. This subjects the mold to a high load, but due to its low Young's modulus, the mold deforms elastically when displacement is small but viscoplastically when it is large. Either form of deformation is a source of error, as it not only affects the total displacement but also induces chip rotation. The FEM analysis of mold deformation during a typical shear fatigue load condition reveals that the deformation cannot be ignored. An example case of deformation simulated to occur in a chip model is shown in Figure 2.4. This is the case when the load for 10% shear strain of solder joint is applied to the edge of the chip mold assuming that elastic modulus of the mold is 22GPa. It can be seen that the mold edge experiences as high as 6% shear deformation. The experiments also confirmed the fact that a sizable amount of mold deformation occurs. This measurement result is shown in Figure 2.5, where the difference between target displacement and actual displacement is displayed as a function of the target displacement. In this experiment, high resolution camera was used to determine the actual position of the chip while the shear fatigue test system was controlled to the targeted displacement distance. While scatter in data exists, the result clearly demonstrates that a significant amount of shear deformation occurs at the chip mold and that it effectively reduces the actual displacement transmitted to the solder array. In order to prevent or minimize the mold deformation, a 1mm thick steel plate with the same dimension as the chip was cut and glued on top of the chip mold. The steel plate can be seen in Figure 2.2. With its application, the displacement error was significantly reduced, as shown in Figure 2.5. Therefore, all subsequent tests were conducted with steel plate reinforcement. While it is difficult to exactly align the steel plate and the chip continuing to be some scatter in failure data, this application greatly improves the consistency of test results within the test conditions and alloys used in my study.

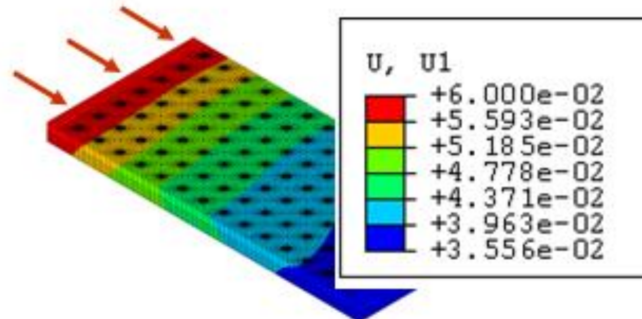

Figure 2.4 A diagram showing the FEM simulation result on the mold deformation field at the condition of 10% shear strain.

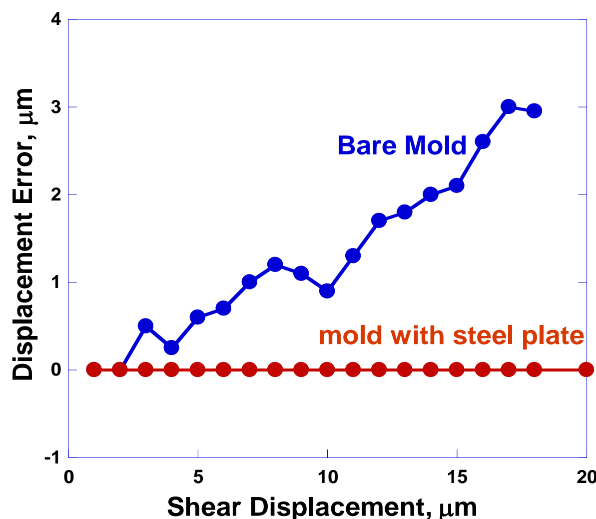

Figure 2.5 A plot showing the measured displacement error as a function of the shear displacement distance.

2.2.3 Shear Testing Sample

Figure 2.6 shows the shear fatigue testing sample configuration and all the samples are provided by Cisco Incorporation. As illustrated in Figure 2.6 (a) and (b), this assembly consists of 14x14 solder arrays with 6x6 array missing in the center so that there are total of 160 solder joints. The diameter of the solder ball is about 600um and pitch size is 800um. The joints are made with an industry standard PBGA chip and PCB metallization structure that consists of Cu UBM/ENiG (Electroless Nickel immersion Gold) at chip side and Cu on PCB side. In this paper, the top side shown in the cross section is the package side, and the bottom side is the PCB side.

Figure 2.6(c) is the cross section of the solder ball. It is worthy to note that there is a neck area or name it solder mask area where the stress/strain is going to develop the most due to the stress singularity. The solder array is daisy chained in several different segments to enable tracking of solder joint resistance in multiple places. The solder alloys tested in my research are three different solder alloys and they are SAC305 (Sn-3%Ag-0.5%Cu), SAC105 (Sn-1%Ag-0.5%Cu), and eutectic Pb-Sn. They were processed by an industry standard reflow process, which involves steady heating up to ~260°C, and slowly cooling to room temperature after a short hold period at the reflow temperature.

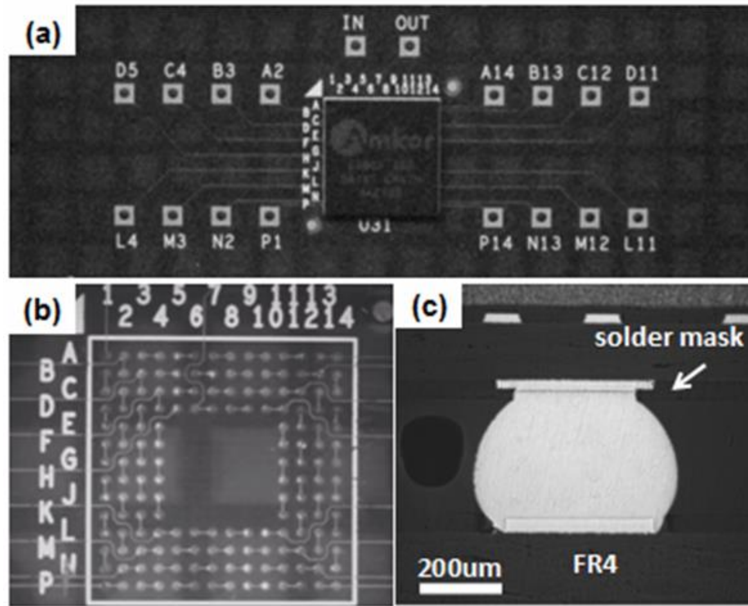

Figure 2.6 Picture showing (a) the PBGA assembly used for shear fatigue testing, (b) solder alloy configuration, and (c) cross-sectional view of the 600um solder ball.

For microstructure analysis, mechanical polishing was carried out for as-received and tested samples. 200, 600, 1500, 2500 grit sandpapers were used in sequence. Then micro-polish with 10 um, 3 um, 1 um Alumina powder and 0.5 um silicate powder were used for final polish. Etching with 2% hydrochloride in ethanol was carried out when it was necessary. Optical Microscope (OM) and Scanning Electron Microscope (SEM)/EDS were used primary for cross section microstructure observation.

2.3 Results and Discussion

2.3.1 Failure Characteristic-Resistance Change

Figure 2.7 shows the fatigue resistance change of the solder joint assembly under shear load. The blue and red lines represent solder joints in two different rows in the same assemble. The sample shown in figure 2.7 was as-received SAC305 and was tested under +/- 4% shear strain and 1Hz. The resistance was keeping consistent until it reached some critical number of cycle after which it increased abruptly with additional cycles. This behavior is typical for all the samples tested regardless of the solder alloy composition. The fast increase of resistance at the final stage indicates a fast failure and crack growth rate. However, it is expected that the crack growth rate under shear mode (mode II) would be slow at least compared to tensile mode (mode I). The fast crack growth rate may indicate a crack tip opening mode failure other than shear mode failure, and this is true and will be explained later.

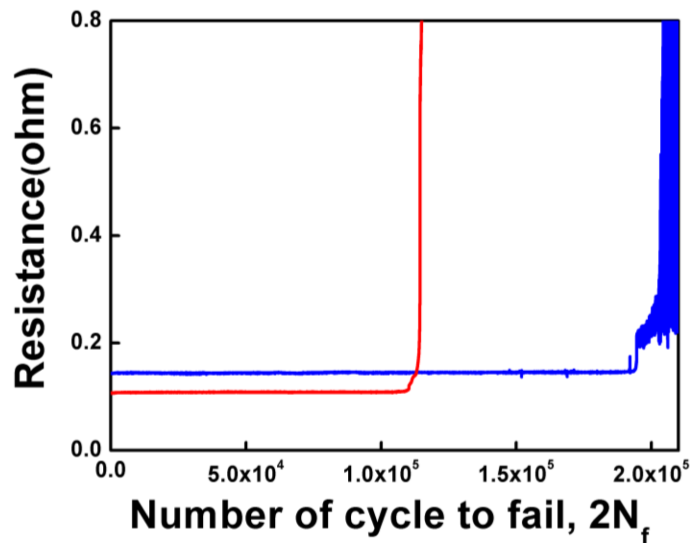

Figure 2.7 A plot showing the change in the electrical resistance of as-reflowed SAC 305 solder joint during 1Hz shear fatigue testing under ~+/-4% shear strain.

2.3.2 Failure Characteristic-Microstructure

Figure 2.8 is an image showing the fractured solder surface after test. Two distinguished microstructures can be seen in Figure 2.8(a): the edge of the solder joint where

the crack initiates shows very rough fatigued feature due to rubbing between the surfaces, while the center of the solder joint shows final fracture surface due to over shear with strikes of shear bands. The two characteristic features are shown in Figure 2.8(b) and (c) more clearly. From these images the fatigue crack initiation, propagation and fracture can be traced.

Figure 2.9 is a cross-section image of the solder joint after shear. Several things need to be marked in this image. First, as displayed in figure 2.9(a), the solder joint shows some degrees of joint rotation toward shear direction. Second, the crack initiates at the solder neck area at chip side and propagates in the solder matrix close to the solder/IMC interface. Third, crack-tip opening is clearly seen in Figure 2.9(b). It is important to point out that the fixation of crack site and rotation of the joint are typical throughout our tests regardless of the joint composition. This is besides my expectation that under pure shear the solder joint should show only shear without rotation and fail by shear mode. However, both microstructure and resistance signal indicate failure by crack opening feature. The source for this will be explained by the stress/strain analysis using ANASYS. Moreover, it is also worthy to mention that besides the chip side solder matrix, cracks are found at the PCB side in solder /IMC interface as well when samples are aged for sufficient time usually 1000 hours and longer at 150 $^{\circ}$C. Cracks at both chip side and PCB side are shown in Figure 2.10 for 1000 hours aged SnPb, SAC105 and SAC305. This is due to the growth of intermetallic compound in the solder/copper interface and weakening of the solder matrix after thermal aging. The IMC formed during aging is very brittle and makes the interface weak for crack initiation.

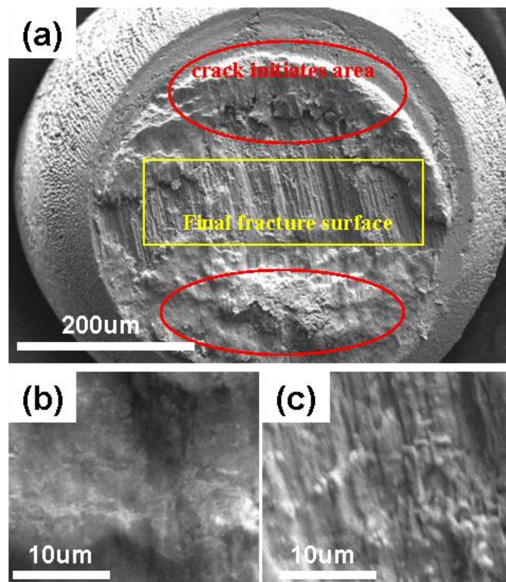

Figure 2.8 The image of the fracture SAC105 solder surface at chip side (a) overview, (b) microstructure of the crack initiates area located at the solder edge, (c) microstructure of the final fracture surface due to over shear located at the center of the solder.

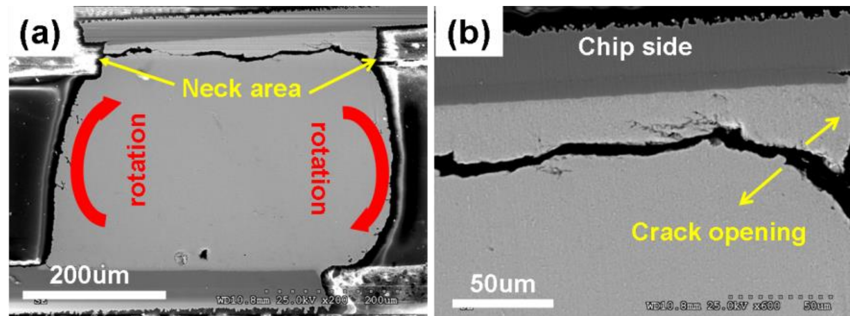

Figure 2.9 SEM cross section of the SAC105 solder after shear test (a) overview showing the neck area and solder rotation, (b) enlarged SEM showing the crack opening.

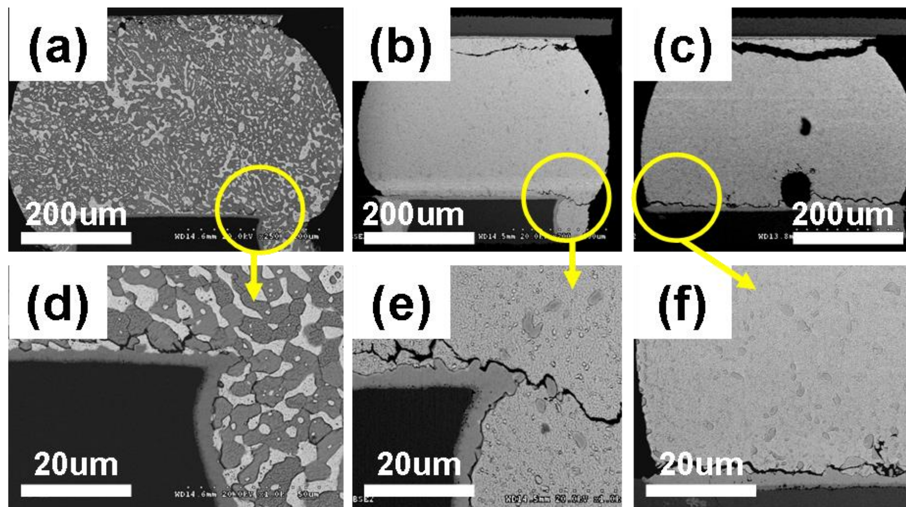

Figure 2.10 SEM images of 150°C 1000 hours aged (a) (d) SnPb, (b) (e) SAC105, and (c) (f) SAC305

The observation of resistance and microstructure give rises of several questions related to the failure mechanics of the solder joint under shear. Although it is expected that solder joints should be under pure shear and will fail by shear mode, the fast crack growth rate revealed by the fast resistance increase, rotation of the solder joint, and shape of the crack-tip suggest a different failure mechanics which is believed to be mode I, crack-tip opening mode. In order to understand this, the finite element analysis of the stress state is carried out.

2.3.3 Mechanism of Crack-tip Opening Mode

Table 2.1 A list showing the elastic property of component materials used for FEM analysis

Material	Elastic modulus (GPa)	Poisson's ratio (ν)
Copper	117	0.35
Cu_6Sn_5	85	0.31
Sn-3.0Ag-0.7Cu	45	0.4
FR4 substrate	22	0.28
BT	22	0.28
Mold	22	0.28

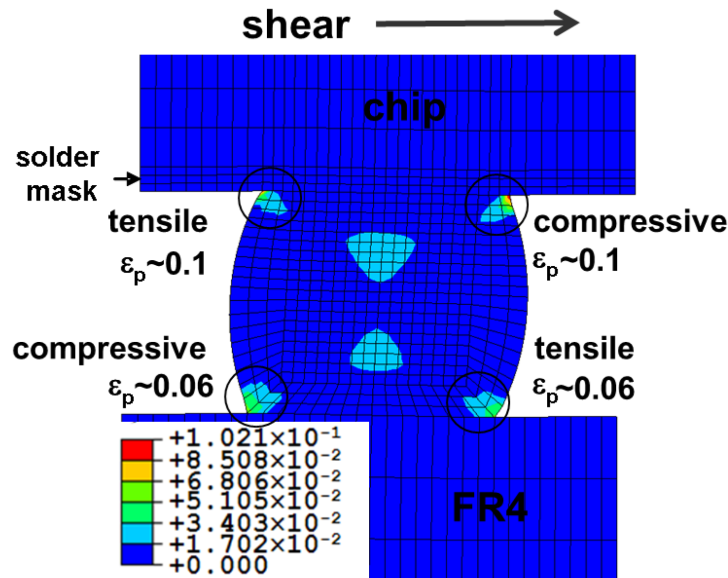

Figure 2.11 FEM analysis result showing the distribution of total plastic strain developed in a solder joint developed by shear strain.

The finite element analysis of the stress/strain state of the solder joints in BGA assembly under shear was calculated with assumption of fully elastic chip and PCB. Table 2.1 lists the material property parameters used for this simulation. The result is shown in Figure 2.11, where the distribution of total plastic strain developed in a solder joint is displayed. There are a few interesting facts to notice from this result. First is that the FEM (Finite Element Method) mesh used for simulation showed rotation toward the shear direction. This means that the solder in the joint was subjected to a non-zero rotational moment and experienced a rotation to the shear direction with rotation axis near to the center of the solder. Since the aspect ratio of solder (ratio between width and height) is close to or less than one, the rotational moment arises with the shear displacement, resulting in a sizable amount of body rotation. A similar body rotation was found to exist in a ball shear test due to the same mechanism in the previous study. [34] As the solder rotates, areas with tensile and compressive stress appear in the solder. As indicated in Figure 2.11, bottom right and top left corner of the joint were under tensile stress while the opposite corners were under compressive stress. When the shear direction reversed,

the opposite stress developed at these corners. Figure 2.12, where maximum tensile and shear stress in the joint is compared as a function of shear displacement, clearly demonstrates the presence of non-shear stress in an overwhelming magnitude. It is therefore reasonable to conclude that the fatigue crack should initiate and propagate by the mode I (crack opening) not by mode II (in-plane shear). The fact that the fatigue failure occurs by the crack opening mode may appear to pose a challenge in quantifying the fatigue property because the true strain at the solder is unknown until simulation. However, it turns out that the total plastic strain at the solder is reasonably proportional to the applied shear displacement. Therefore, it is possible to use the shear displacement as the fatigue parameter and correlate it to the fatigue failure rate.

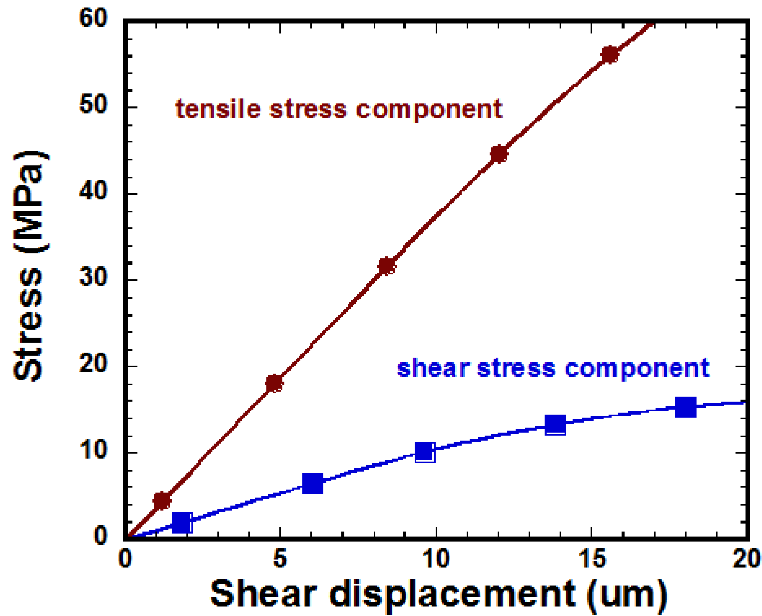

Figure 2.12 A plot displaying the tensile and shear stress developed in a solder joint as a function of shear displacement.

Another important aspect of the shear testing configuration revealed by Figure 2.11 is that the maximum plastic strain area is located at the solder neck created by the solder mask. Such a concentration of plastic strain is a result of the stress singularity created by the steep change in solder geometry. Therefore, fatigue failure should occur at the same place for a given assembly regardless of test condition, package design and solder types. This, fixation of

failure location, allows characterization of fatigue property of solder at various test conditions without losing consistency in measurement due to variation in failure location.

2.4 Conclusion and Implication

Although the mechanics of the shear fatigue testing appears to be simple, my research reveals that the application to the study of solder joint assemblies is not straightforward. The core of the complexity stems from the fact that the actual strain exerted on the solder joint is not pure shear but includes considerable amount of tensile and compressive strains. This is learned from the finite element analysis of the stress-strain of the BGA assembly and experimental results. The experimental and theoretical FEM analysis of the stress/strain of the solder joints under shear reveal that 1) the solder joints are under non-pure shear stress, but tensile/compression as well; 2) solder body-rotation exists due to the solder geometry resulting crack-opening solder joint failure under shear load 3) the highest stress/strain position is located at the solder neck area in the chip side, resulting in fixed crack initiation and failure site within the solder matrix at chip side neck area; 4)The failure by tensile mode dictates the fast crack growth indicated by the resistance variation. The characteristic of the solder joint failure under shear mode may appear to be unfavorable, but it actually has its own beneficial for solder reliability evaluation. The fast failure by crack-opening mode can reduce the testing time and is more efficient in producing useful data. Moreover, the fixation of the failure site within the solder matrix ensures that the data collected are solder property related not interface strength related. Therefore, shear fatigue test is an efficient and effective method for solder fatigue property evaluation.

CHAPTER THREE

FATIGUE PROPERTIES AND FATIGUE LIFETIME PREDICTION OF THE LEAD-FREE JOINTS IN BGA ASSEMBLY

3.1 Background

The electronic industry has successfully transitioned from Sn-Pb to lead –free solder for many consumer electronics, yet there is no single industry-wide standard lead-free solder reliability model available for solder Fatigue lifetime prediction.[97-100] Numerous studies have been done regarding thermal cycling reliability of lead-free solder joints under accelerated testing conditions attempting to achieve a good model for reliability prediction. However, due to the complexity of thermal fatigue and lack understanding of lead-free solder properties, the predictability of the solder joint reliability under thermal cycling is difficulty. At the same time, with the miniaturization and mobilization of microelectronics, the reliability concern is not limited to the failure by traditionally concerned thermo-mechanical (temperature and power cycling) but including emerging sources of fatigue such as vibration and shock, resulting in a growing interest on understanding the fatigue properties of lead-free solder. Several previous studies have made aims to characterize fatigue behavior of Pb-free solder alloys but with limited scope and using bulk alloys. [100-103] The use of bulk alloy may be an inevitable choice because it permits an access to clean data, which is not affected by complex geometry and constraints presented in actual solder package assembly. However, by the same reason, those studies yield data with a limited value as they may not be applicable to the fatigue prediction for solder in package without facing a significant error. In order to have greater merit fatigue data, the fatigue testing needs to be done at the proximity condition to the real solder joint microstructure, this, however, often leads to highly convoluted data. In this study, shear fatigue test is designed to study the fatigue property of the solder joints in packaging with great confidence.

Before discussion the experimental results, some empirical fatigue lifetime prediction models developed for solder in packaging were reviewed first. They can be divided into five

categories based on the fundamental mechanism for inducing damage: (a) stress- based, (b) plastic strain-based, (c) creep strain-based, (d) energy-based, and (e) damage accumulation based, and are tabulated in Table 3.1.

Table 3.1 Summary of fatigue models [97]

Fatigue model		Model class	Applicable package	Required Parameter	Coverage
1	Coffin-Manson	Plastic strain	All	Plastic strain	Low cycle fatigue
2	Total Strain	Plastic +elastic strain	All	Strain range	High and low cycle
3	Soloman	Plastic shear strain	All	Plastic shear strain	Low cycle fatigue
4	Engelmaier	Total shear strain	Leaded and leadless, TSOP	Total shear strain	Low cycle fatigue
5	Miner	Plastic and creep strain	PQFP, FCOB	Plastic failure and creep failures	Plastic shear and matrix creep
6	Knecht and Fox	Matrix creep	All	Matrix creep shear strain	matrix creep only
7	Syed	Creep strain energy	PBGA, SMD, NSMD	Gbs energy and mc energy	Full coverage
8	Akay	Total strain energy	LLCC, TSOP	Energy	Joint geometry accounted for
9	Liang	Stress/strain energy density based	BGA and Leadless joints	Energy	Low cycle fatigue
10	Heinrich	Energy density based	BGA	Energy	Hysteresis curve
11	Pan	Energy density	Leadless,	Damage + energy	Hysteresis

Table 3.1 – *Continued*

12	Darveaux	Strain energy density	LCCC	Strain energy density and plastic energy density	Hysteresis curve
13	Stolkarts	Damage accumulation	All	Damage	Hysteresis curve and damage evolution
14	Norris and Landzberg	Temperature and frequency	All	Temperature and frequency	Test condition versus use conditions

3.1.1 Strain-based Coffin-Manson Model

The Coffin-Manson fatigue model is perhaps the best known and most widely used approach for fatigue life prediction today. [104-105] It assumes that fatigue failure is due to the plastic deformation that the elastic strain only contributes a very small portion of the fatigue failure. It takes the forms that the total number of cycles to failure, N_f, is dependent on the plastic strain amplitude, $\Delta\varepsilon_p$, the fatigue ductility coefficient, $\varepsilon_f^{'}$, and the fatigue ductility exponent, C. as shown in Equation 3.1. The fatigue ductility coefficient is approximately equal to the true fracture ductility. The fatigue ductility exponent varies from -0.5 to -0.7 for most of the materials. Also it is suggested by Morrow that the cyclic ductility exponent can be related to strain-hardening rate of materials as shown in Equation 3.3, where α is the cyclic strain hardening exponent. [106]

$$\frac{\Delta\varepsilon_p}{2} = \varepsilon_f^{'}(2N_f)^C \qquad (3.1)$$

$$\log\frac{\Delta\varepsilon_p}{2} = \log\varepsilon_f^{'} + C\log(2N_f) \qquad (3.2)$$

$$|C| = 1/(1+5\alpha) \qquad (3.3)$$

This model was originally proposed to predict the fatigue life of metals in the aircraft industry, so that a variety of strain life engineering data is available on steels and other metals.

However, not many experimental data are available for solder joints because the actual tests are often time consuming and the results are usually applicable dependent on the geometry of the solder joint and design of packaging assembly. Therefore, for solder joints in the packaging assembly, FEA modeling can be used to determine the plastic strains which are then used to predict the fatigue life. In some cases, such as in the shear fatigue test, because the elastic strain/yield strain constitutes small portion of the total strain that the total displacement applied is transferred to plastic strain only. Therefore, the shear fatigue test in this paper is plastic strain controlled test.

Due to its simplicity and ability to link the fatigue behavior to fundamental material properties, Coffin-Manson model is widely adapted as a standard model for many metallic systems including the solder.

3.1.2 Total Strain Model

Since Coffin-Manson model only consider plastic deformation, to incorporate the elastic deformation, the total strain model is developed by combing the Coffin-Manson equation with the Basquin's equation. [107] This new model is shown in Equation 3.4. $\Delta\varepsilon$ is the total strain, $\sigma_f^{'}$ is the fatigue strength coefficient, E is the elastic modulus, b is the strength exponent, $\varepsilon_f^{'}$ is the fatigue ductility, and c is the ductility exponent.

$$\frac{\Delta\varepsilon}{2} = \varepsilon_f^{'}(2N_f)^C + \frac{\sigma_f^{'}}{E}(2N_f)^b \qquad (3.4)$$

Figure 3.1 is the total strain versus number of cycle to failure plot. As seen in the figure, in the low cycle region to the left, the fatigue lifetime is governed by Coffin-Manson model; while in the high cycle region to the right, fatigue lifetime is governed by the Basquin's equation or elastic strain amplitude.

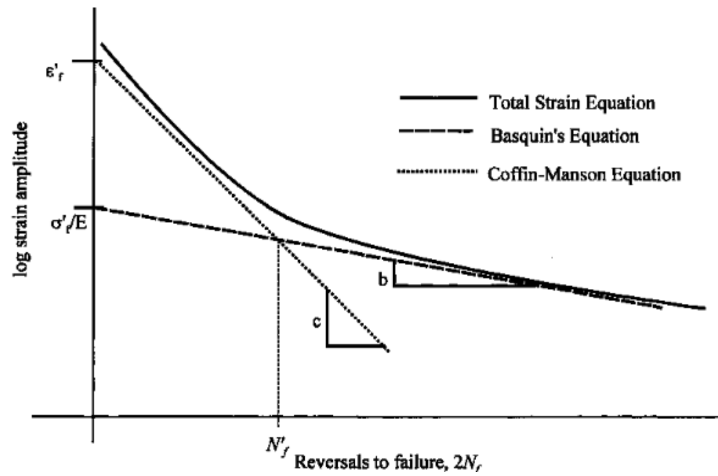

Figure 3.1 Total strain versus lifetime equation.

3.1.3 Plastic strain + Creep Strain Model

To consider both plastic deformation and creep deformation on the fatigue and apply Miner's linear superposition principle [108], the plastic-creep strain-based model can be written in the following Equation 3.5:

$$\frac{1}{N_f} = \frac{1}{N_p} + \frac{1}{N_c} \qquad (3.5)$$

N_p refers to the life cycle due to plastic deformation and N_c is the life cycle due to creep. According to Solomon's fatigue model, the relationship between N_p and plastic shear strain can be expressed in Equation 3.6.

$$\Delta\gamma_p (N_p)^{\alpha} = \theta \qquad (3.6)$$

$\Delta\gamma_p$ is plastic shear strain range, θ is inverse of ductility coefficient, and α is material constant. N_c is depending on the creep mechanism. For solder joints, there are two main creep mechanisms: grain boundary creep and matrix creep. Knecht and Fox proposed a simply matrix creep model relating the solder microstructure and the matrix creep shear strain range as shown in Equation 3.7. $\Delta\gamma_c$ is strain range due to creep, C is the material constant depending on the solder microstructure. [109]

$$\Delta\gamma_c N_c = C \qquad (3.7)$$

Syed proposed another creep fatigue model which incorporates matrix creep and grain boundary creep together. [110] In this model, the fatigue lifetime consists of two parts, as shown in Equation 3.8. D_{gbs} and D_{mc} are accumulated creep strain per cycle for grain boundary sliding and matrix creep.

$$N_c = [0{,}022D_{gbs} + 0.063D_{mc}]^{-1} \qquad (3.8)$$

Inclusion of creep strain into the strain-based fatigue model is more comprehensive for fatigue lifetime prediction, especially for solder joints under thermal-cycling. It is important to determine whether to include elastic damage, plastic damage or creep damage into the fatigue model. The selection of the fatigue model is difficult because it is highly depending on the thermal cycling condition as well as the packaging design, solder joints geometry and solder microstructure. It is strongly recommended to pay attention to three important facts while choosing the fatigue model. The first point refers to solder joint geometry. Data collected from one geometry can lead to erroneous predictions when applied to a different geometry. The engineering material properties of bulk solder are not fully representative of a small solder joint geometry. The second point refers to the importance of solder microstructure, including grain size and shape. Solder joints can have radically varying microstructures, depending on the conditions under which they were formed. The third point refers to small impurities, deliberate or not, which can affect the size or shape of each individual grain, and also strength characteristics.

3.1.4 Energy-based Model

The plastic strain model suggests that the fatigue life is determined by the amount of plastic deformation per cycle, while the energy model suggests that the fatigue life is related to the stored plastic energy, which takes the form,

$$\Delta W_d (2N_f)^m = 2C \qquad (3.9)$$

Where ΔW_d is strain energy damage term and is equal to the area in the cyclic stress-strain hysteresis loop. Since the strain energy includes both stress and strain information, it is thought to be a good indicator of solder joint damage. However, the energy based fatigue models predict the accumulated energy required to initiate a crack; it does not predict when fatigue failure will occur, because the crack propagation is not included in the fatigue model. Nevertheless, the benefit of an energy -based fatigue model, as compared to the strain-based or creep-based fatigue models, has the ability to capture test conditions with more accuracy.

In this paper, the low cycle shear fatigue test was carried out and the fatigue model was determined for the solder joints in the BGA packaging assembly. The experiment results fit into the strain based Coffin-Manson model very well. Furthermore, frequency-modified Coffin-Manson equation was developed by incorporating frequency exponent into the equation since the fatigue lifetime is also sensitive to strain rate. The strain range was determined by the shear displacement by neglecting the elastic strain. The ductility coefficient, frequency exponent, ductility exponent and strain hardening exponent were extrapolated from the fatigue tests and the fatigue model. Their dependence on the temperature, solder alloy, and thermal aging were investigated as well. However, as mentioned before, the fatigue parameters from one test may not be applicable to the other because the results are highly dependent on the solder geometry and assembly. These results will be valuable for lifetime prediction for solder joints within similar BGA packaging assembly.

3.2 Experimental Methods

In the previous chapter shear fatigue test was introduced and the mechanics of solder joint failure under cyclic shear was studied. Based on the characteristics of the shear test, it is believed that shear test system can be used to evaluate the fatigue reliability of the solder joint in BGA packaging assembly with great consistency and accuracy. In this chapter, series of tests are conducted using the shear test system and the results were summarized and analyzed. The shear tester configuration is shown in Figure 2.1. The BGA packaging assembled sample

configuration from Cisco is displayed in Figure 2.6. The tests were carried out under various strain range, temperature, frequency, solder alloy and thermal aging condition. Thermal aging of the samples were conducted in the commercial oven at 100°C and 150°C for 500 hours, 1000 hours, and 1500 hours. After thermal aging, the sample wrapped with ceramic were taken out from the furnace and cooled slowly in the ambient. The samples rested were mostly common used Sn-Ag-Cu lead-free solder, SAC305 and SAC105. As a comparison, 60Sn40Pb solder was also tested under the same condition as lead-free solder. Plastic strain ranges from +/-1% to +/-5%, frequency from 0.1Hz to 5Hz. To introduce testing temperature variable, a cartridge heater inserted inside a small Aluminum block was placed on top of the sample. The size of Aluminum was 1.25"X 0.375" X0.25" and the steel plate size for chip reinforcement is 0.45"X0.45"X0.03125". The temperature for testing was set at 25°C, 50°C, 75°C and 100°C. Before each testing, the heater was turned on first for half hour in order to get uniform temperature distribution in the solder joints. To reduce the force needed for shearing all the solder joints in the assembly, the sample was carefully cut into three sections, and only four rows of solder joints were sheared. The cutting lines are schematically shown in Fig.3.2 and are also visible in Figure 2.2. A slitting saw with thickness 1/32" cut between two rows of solder joints through the PCB board without touching the chip. This has to be conducted extremely careful otherwise it would affect the reliability of the solder joints. As the solder joints are connected in series which enables the checking of resistance. The current was set at 100mA, voltages of the solder joints in the row were red by the data acquisition system and the resistance were calculated and stored in the computer. There are four resistances (R1, R2, R3 and R4) with each test. The tapping points of the resistances are also shown in Figure 3.2. When the final failure was achieved, the resistance increased more than 400%.

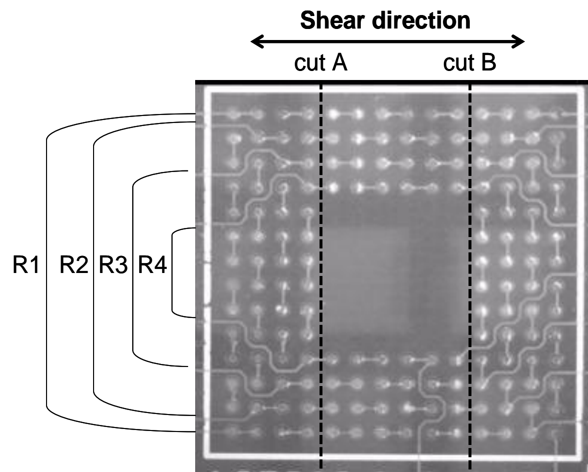

Figure 3.2 The image showing the cut line positions in the BGA solder assembly.

3.3 Results and Discussion

3.3.1 Resistance Change with the Number of Cycle to Fail

Solder joints with different compositions and thermal aging conditions were tested under cyclic shear load with variation in strain range, temperature, and frequency. The resistances of the solder joint in different rows were recorded. Figure 3.3 shows the resistance change with the number of cycle to fail. Figure 3.3(a), (b), (c) and (d) indicate the shear fatigue lifetimes of the solder joints in the first row and second row of SAC305, 150°C 500 hour aged SAC105 and SnPb samples, respectively. Regardless of the solder composition and test conditions, the first row solder joints always fail earlier than the others. It is unexpected because under pure shear, the solder joints are exposed to the same shear strain that if the testing conditions and microstructures are kept the same, they should have the same possibility to fail. In addition, it is a common assumption that the solder joints in the same assembly preserve more or less the same microstructure which contain single or several big grains. However, it is believed that it is the variation in residual thermal stress that results in the fatigue lifetime variation with joint position. The comprehensive explanation will be given in the later chapter.

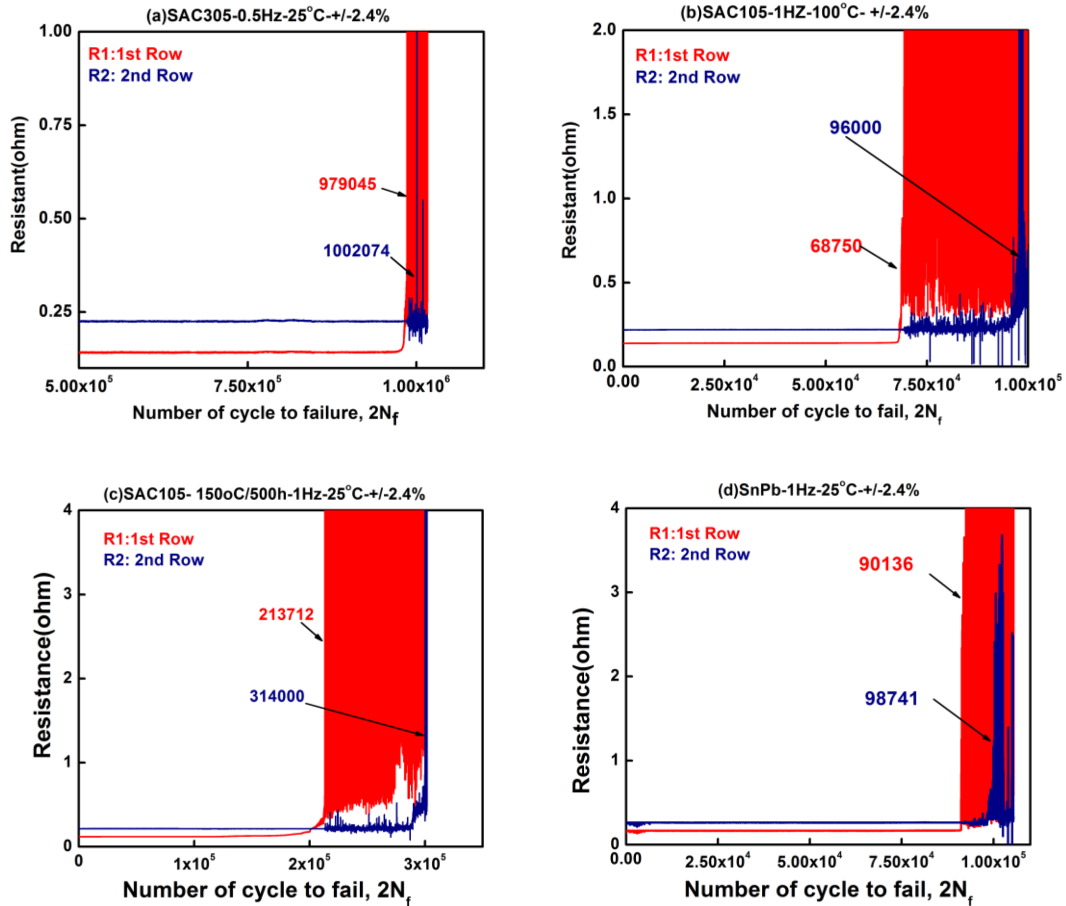

Figure 3.3 1st and 2nd row solder resistance change with the number of cycle to fail under +/-2.4% strain (a) SAC305, 0.5Hz, 25°C, (b)SAC105, 1Hz, 100°C, (c) 150oC/500h thermal aged SAC105, 1Hz, 25°C, (d)SnPb, 1Hz, 25°C.

In addition, it is shown in figure 3.3(c) the increase of resistance approaching the final failure is fast but a bit slower after thermal aging than as received sample. It is well known that thermal aging induces intermetallic compound (An_3Sn and Cu_6Sn_5) growth in the solder matrix as well as in the solder/Cu interface which results in softening of the solder joints matrix. Therefore, the crack growth rate in thermal aged solder joint was slower than that in the as-received sample.

3.3.2 Fatigue Lifetime vs. Plastic Strain Range

A series of tests were carried out using various combinations of testing parameters. In this research, at least six specimens were tested for each test conditions and the average fatigue life was used in the following analysis. Generally, scatter in fatigue life of the solder tested using the same parameters (i.e. the same temperature, frequency and total strain range) was found to be small. Figure 3.4 illustrated the fatigue lifetime variation with displacement/plastic strain range at specific temperature and frequency. Since the elastic strain range is small compared to the plastic strain rage in this case, I assume $\varepsilon_p \approx \varepsilon_T$.

AS shown in Figure 3.4(a) and (b), the relationship between the plastic strain range and the fatigue lifetime is presented in log-log scale. First it is noticed that the fatigue life decreases with increasing plastic strain range. Second, the fatigue life has a good linear relationship with the plastic strain range tested regardless of the solder alloy composition and testing temperature. It indicates that the crack growth is controlled by plastic strain and Coffin-Manson strain model is applicable for the solder joint fatigue life characterization. According to equation 3.2, in the linear $\lg \frac{\Delta\varepsilon_p}{2} \sim \lg(2N_f)$ plot, the slope of the line equals to C and intercept equals to $\lg \varepsilon_f^{'}$. Therefore, the ductility coefficient and ductility exponent can be extrapolated from these plots. For example, at 25°C, ductility coefficient is 0.25, 0.56 and 0.22 for SnPb, SAC105 and SAC305 respectively; the ductility exponent is 0.226, 0.31 and 0.2 for SnPb, SAC105 and SAC305 respectively.

In the following sections, Coffin-Manson model and fatigue life vs strain range graphs are used to analyze the effect of solder alloy composition, thermal aging, testing tempearture, and frequency on the fatigue behavior of the solder joints in the BGA packaging assembly.

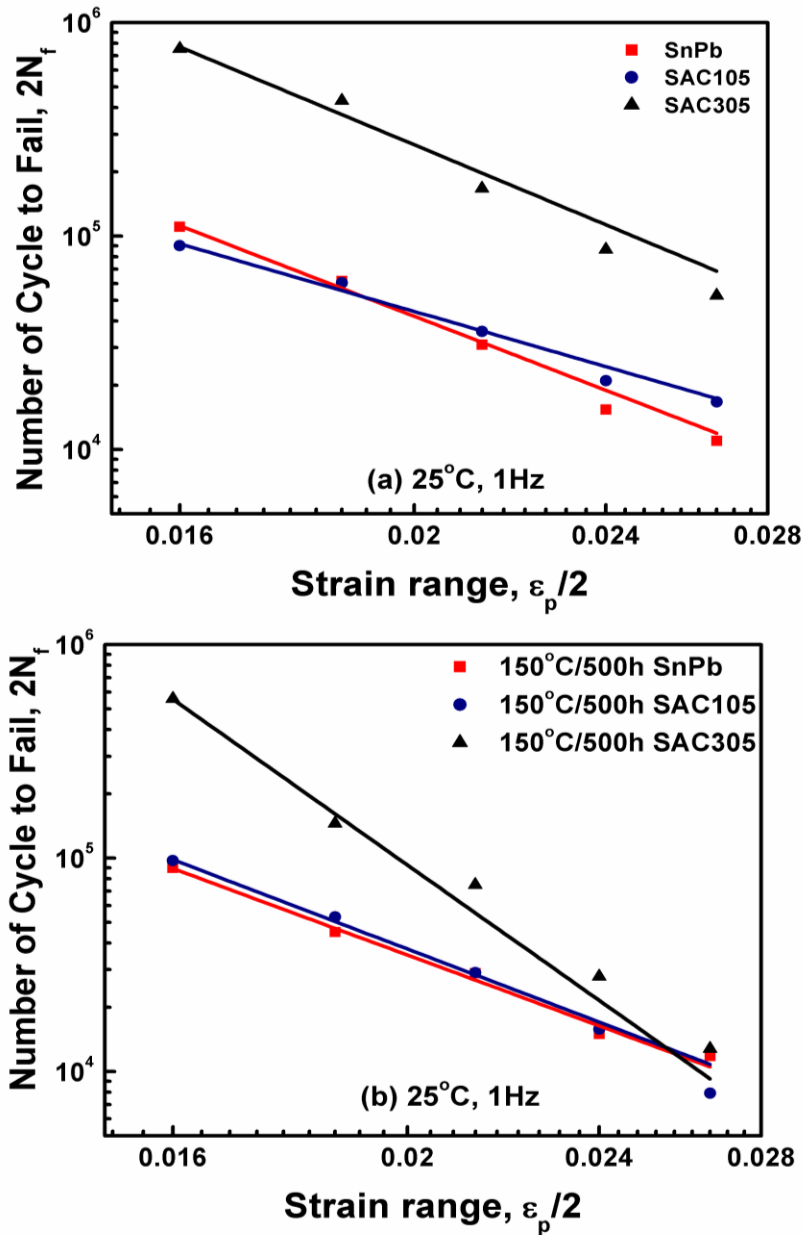

Figure 3.4. Fatigue lifetime variations with strain range for SnPb, SAC105 and SAC305 (a) 1Hz 25°C, (b) 150°C 500 hour thermal aged samples at 1Hz, 25°C.

3.3.3 Fatigue Lifetime vs. Solder Alloy Composition

Another finding from Figure 3.4 is that SAC305 shows superior fatigue resistance than SAC105 and SnPb within the testing strain range. This is consistent with the results from many other research groups. [99-103] According to Equation 3.1, the fatigue lifetime under given

strain range and temperature is determined by the fatigue ductility coefficient ($\varepsilon_f^{'}$) and ductility exponent (C). The higher the fracture strain ($\varepsilon_f^{'}$), the lower the absolute value of ductility exponent ($|C|$) or the higher the strain hardening exponent (α), the longer the fatigue lifetime. Moreover, it can be predicted that the in the high strain range, the fatigue lifetime is more dependent on the fracture strain or ductility, while at the low strain range, it is more dependent on the strain hardening exponent or ductility exponent. From the slope of the plot SAC305 has the highest strain hardening exponent but the lowest ductility coefficient, while SAC105 has the highest ductility coefficient but lowest strain hardening exponent. As a result, SAC305 shows superior fatigue resistance due to its high strain hardening or ductility exponent in the low strain range; while SAC105 shows better fatigue resistance due to its high fracture ductility at the high strain range. The high strain hardening exponent of SAC305 is a result of IMC strengthening in the solder matrix. It is known that due to the higher concentration of Silver content in SAC305, more Ag_3Sn particles exist in the solder matrix which results in higher strength and brittleness. [111-118]

Moreover, as shown in Figure 3.4(b), after thermal aging at 150 $^{\circ}$C for 500 hours, the fatigue life of the SAC105 and SnPb became comparable to each other, while SAC305 still showed the best fatigue resistance. Thermal aging induced IMC growth in SAC solder and phase coarsening in SnPb. Thus, the fatigue resistance reduces for all solders, but the reduction ratio is hard to determine. However, it is believed that after thermal aging for long enough time, the SAC105 and SAC305 fatigue resistance may be similar. More detailed discussion on thermal aging effect on the fatigue resistance will be given further in the following paragraph.

3.3.4 Fatigue Lifetime vs. Thermal Aging

The fatigue life of solder joints after thermal aged for 500 hours and 1000 hours were measured under a series of plastic strain ranges. The fatigue life-plastic strain plots were shown

in Figure 3.5. It was found that the fatigue life decreases with increasing thermal aging time for both SAC solder and SnPb solder. Moreover, the biggest difference in fatigue life before thermal age and after thermal age for SAC305. The three plots in Figure 3.5(b) are furthest apart compared to the plots in Figure 3.5(a). This reveals that thermal aging effect is the biggest for SAC305. After thermal aging, IMC including Ag_3Sn and Cu_6Sn_5 grew bigger and lost the strengthening effect. Since the Ag content is higher in SAC305 than in SAC105, the reduction in solder matrix strength is larger in SAC305. The microstructure of the solder joint matrix before and after thermal aging at 150°C is shown in Figure 3.6. These images clearly show IMC growth in SAC solder and phase coarsening in SnPb solder.

Table 3.2 fatigue ductility coefficient, ductility exponent and strain hardening exponent for as received and thermal aged solder at 25°C extrapolated from Figure 3.5

Fatigue parameters	SnPb			SAC105			SAC305		
	As received	500	1000	As received	500	1000	As received	500	1000
Fracture ductility	0.25	0.09	0.09	0.56	0.18	0.14	0.22	0.1	0.1
Ductility exponent	-0.23	-0.14	-0.15	-0.31	-0.2	-0.19	-0.18	-0.17	-0.16
Strain hardening exponent	0.67	1.23	1.13	0.45	0.8	0.85	0.91	0.98	1.05

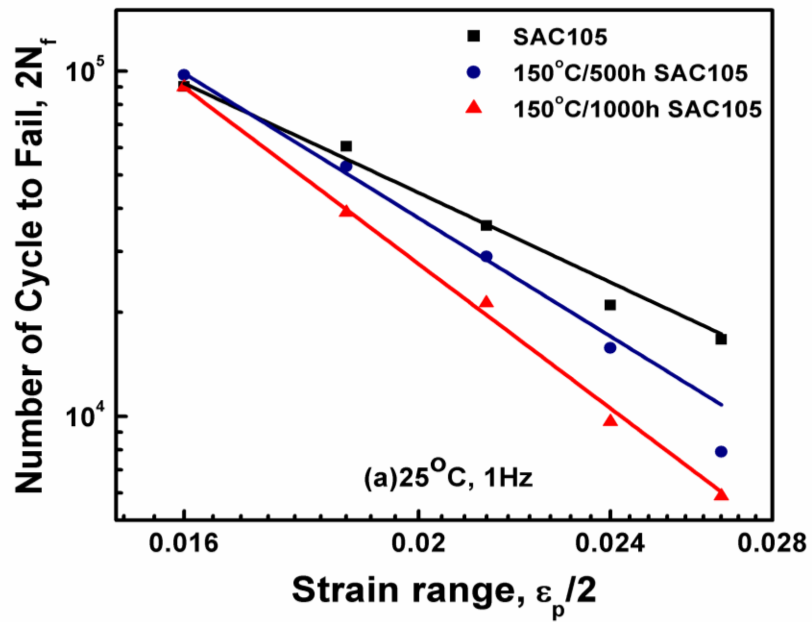

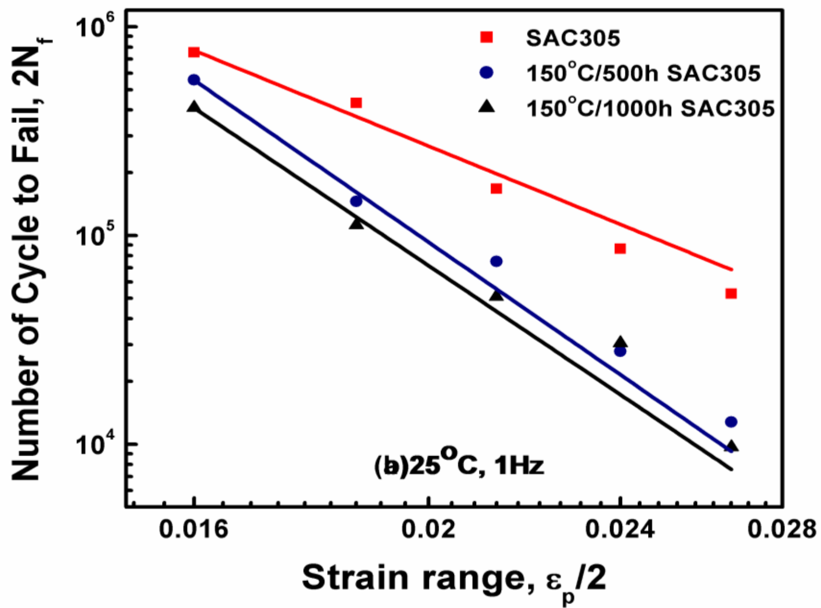

Figure 3.5 Fatigue lifetime versus strain range at 1Hz, 25°C for different thermal aging conditions (a) SAC105, (b) SAC305..

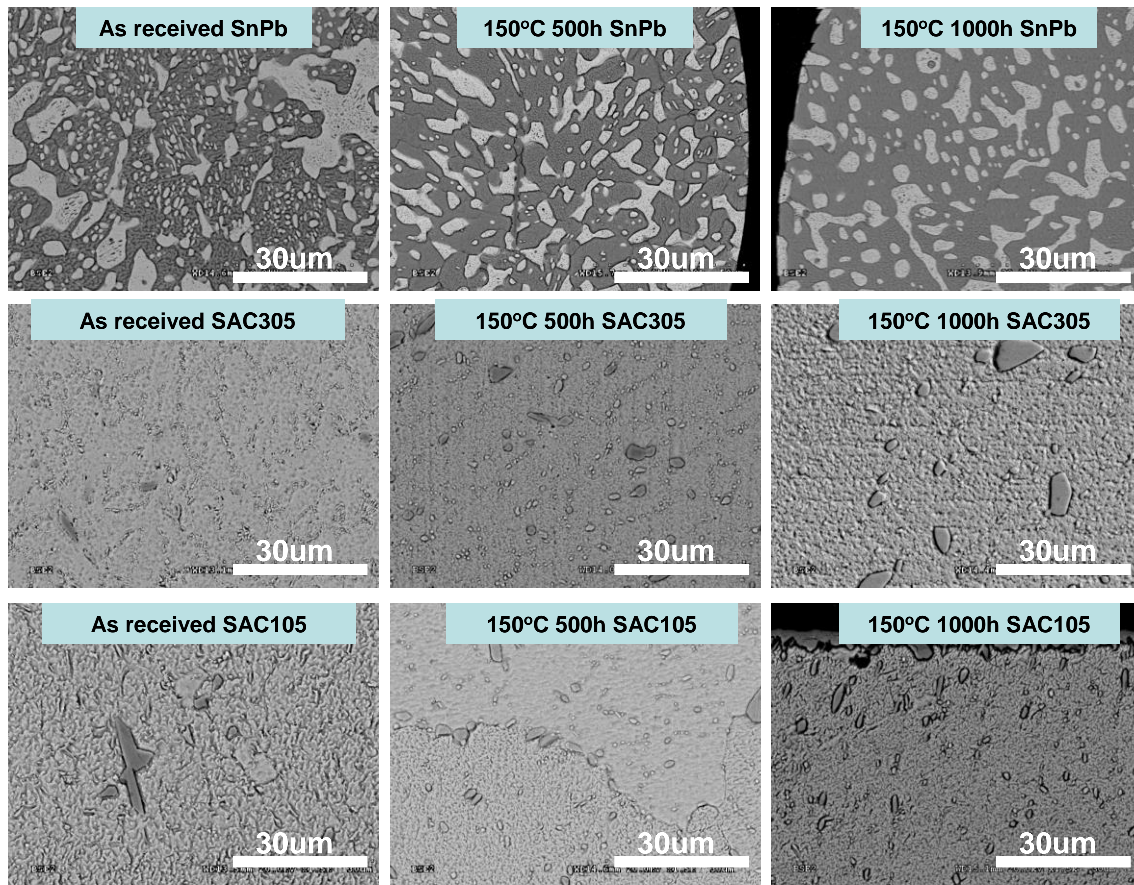

Figure 3.6 Microstructures of solder matrix before and after thermal aging at 150°C.

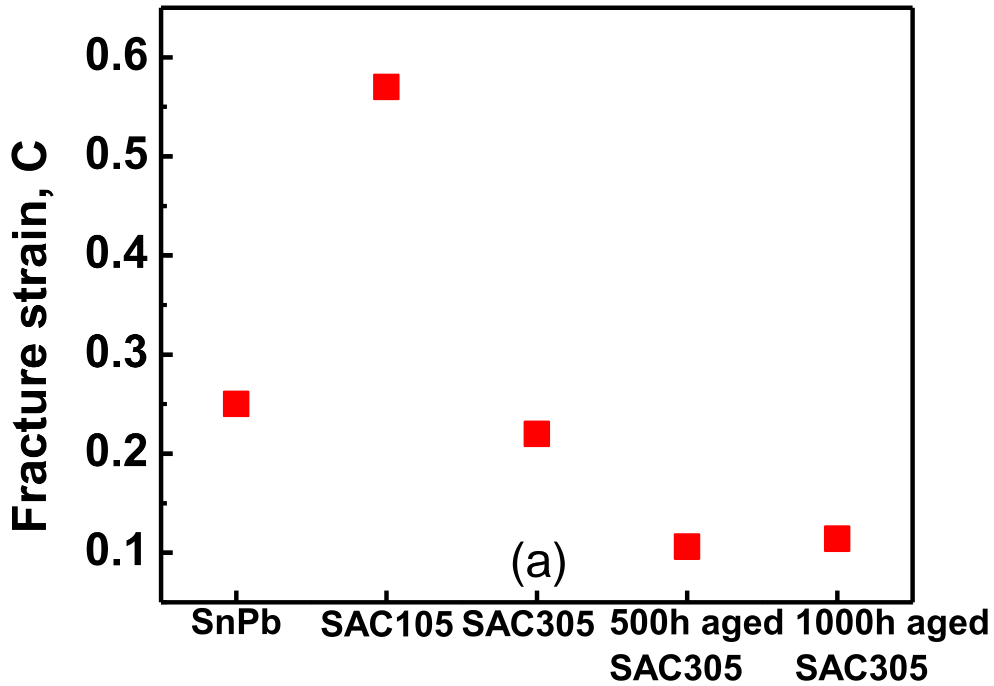

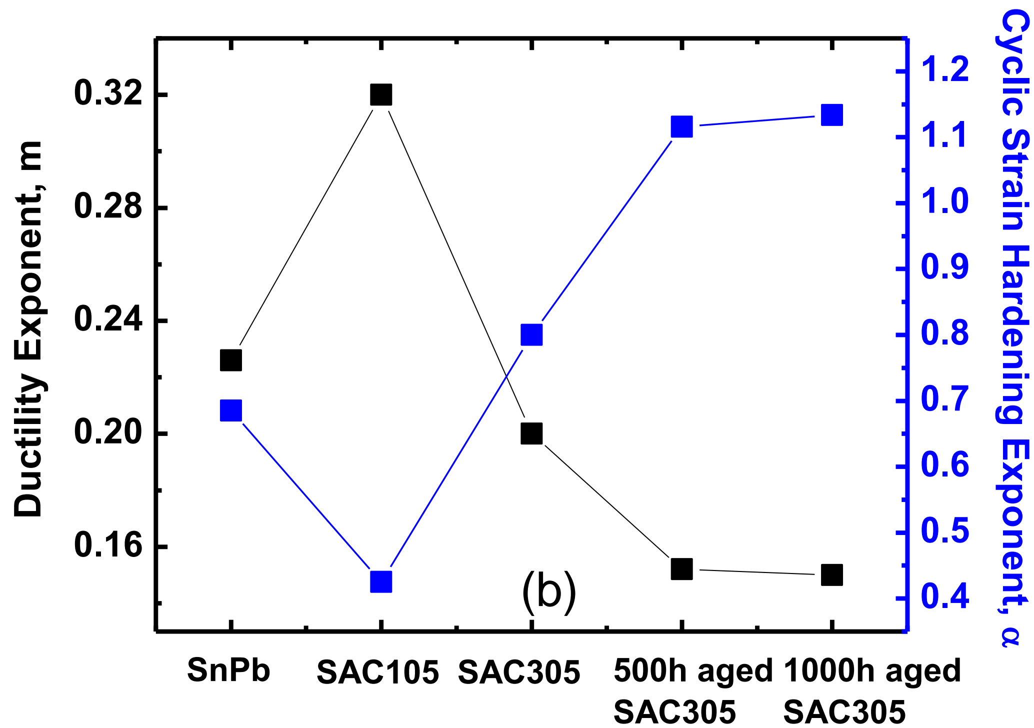

Figure 3.7 fatigue parameters variation with thermal aging and solder alloy composition (a) fracture strain, (b) ductility exponent and strain hardening exponent.

However, the effect of thermal aging is more complicate than expected. The fatigue ductility coefficient and ductility exponent for as-received and thermal aged samples at 25 °C extrapolated from Figure 3.5 using the Coffin-Manson is listed in table 3.2. The variation of fatigue constants with the thermal aging and solder joints alloy composition are shown in Figure 3.7. As seen in Table 3.2 and Figure 3.7, the fracture strain and ductility exponent decreases with thermal aging, and the strain hardening exponent increases with thermal aging. As mentioned in chapter two, due to the fixation of the crack site at the solder matrix in chip side, the fatigue parameters extrapolated from Coffin-Equation is characteristic for solder joint fatigue property itself not the interface property. Therefore, after thermal aging, due to the IMC growth and phase coarsening, the fracture strain and ductility exponent should increase, and the strain hardening exponent should decrease. Yet the trend is opposite as shown in table 3.2 and Figure 3.7. This does not mean the test is wrong but because the mixture of failure site. It is found that the crack is also observed in the solder/IMC interface at chip and PCB side for samples after thermal aging. Therefore, the fatigue parameter is related to the solder joint, interface, IMC property, or their combination depending on the failure site. Because of the growth of IMC in the solder interface and decrease of solder matrix strength, the crack is more possible to propagate in the IMC/solder interface. Thus, the fatigue parameters from the testing are actually more related to the interface and IMC property.

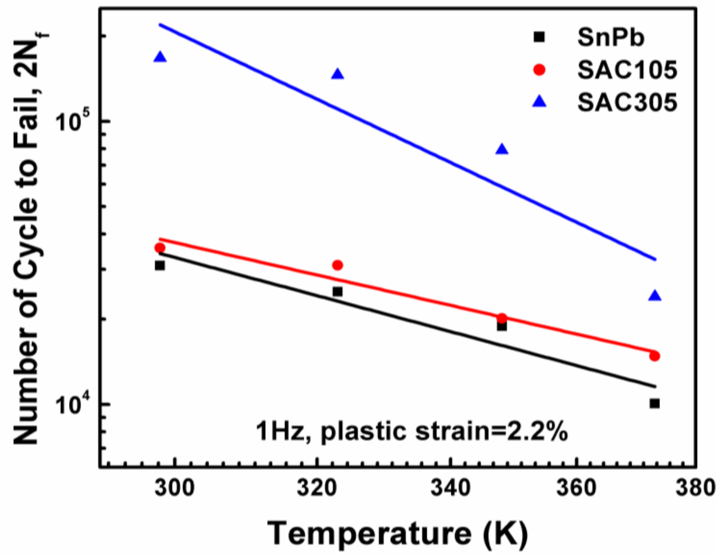

Figure 3.8 Fatigue life versus temperature tested at 1Hz, 2.2% plastic strain for SnPb, SAC105 and SAC305

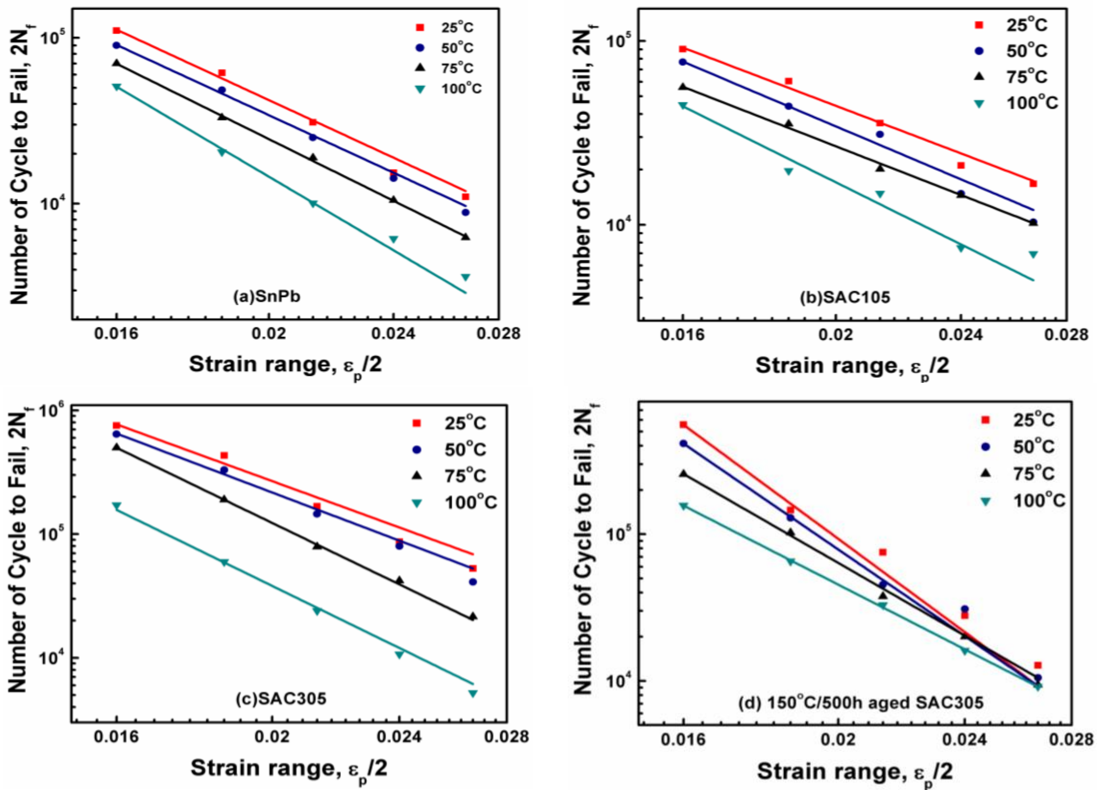

Figure 3.9 Fatigue lifetime versus strain range at 1Hz for different temperatures (a) SnPb, (b) SAC105, (c) SAC305, (d) 150°C 500h aged SAC305.

3.3.5 Fatigue Lifetime vs. Temperature

A series of repeated tests at the same frequency, various strains and at different environmental temperatures (25, 50, 75 and 100 °C) were conducted. The fatigue life was found to decrease with increasing temperature for a test frequency of 1 Hz, as shown in Figure 3.8. The relationship between the mean fatigue life and plastic strain obtained from tests at four different temperatures is presented in Figure 3.9. The fatigue lives for all the as received solder alloys decrease with increasing temperature and fit into Coffin-Manson equation. Discrepancies exist for thermal aged solder alloys as shown in Figure 3.9(d). This may be due to the mixture of failure sites as mentioned in the previous section.

At a first glance, it is not a surprising result because fatigue resistance of many metallic alloys is known to decrease with increasing temperature for various reasons, for example, decreased strain-hardening rate at higher temperature leading to more plasticity and thus faster failure rate [119], or increased creep due to grain boundary sliding at elevated temperature leading to the decrease of fatigue lifetime [120]. However, closer inspection of the data indicates that the mechanism may not be related to the material property and grain boundary sliding but more related to the mechanical constraints unique to the PBGA shear fatigue. First, the lead-free solder joints in this tests consist of only several grains if not single grain, so that creep due to grain boundary sliding may not be the reason. Moreover, notice the fact that the slope of data does not change much with temperature. Since the slope is related to strain-hardening exponent, it is our anticipation that the slope increases with temperature, that is the alloy strain-hardens less at higher temperature. However, in both cases, the result is not consistent with our expectation. Rather, it is found that m does not change much with temperature. This indicates that these alloys do not exhibit significant change in strain-hardening behavior with temperature, at least within the temperature ranges used in our investigation. Rather, the data suggest that the decrease in the fatigue life with increasing temperature stems more from the

decrease in ductility coefficient. This is somewhat opposite to what is expected from the known metallurgical properties of the solder. [121]

From Figure 3.9, the values of constants *C* and $\varepsilon_f^{'}$ for the Coffin–Manson model can be determined for different temperatures by taking the slope and the intercept on the plastic strain axis. The constants $\varepsilon_f^{'}$ and C of different solders at different temperatures are summarized in Table 3.3. According to equation 3.3, the cyclic strain hardening exponent inversely proportional to the ductility exponent and can be calculated. The relationship of fracture strain, ductility exponent and strain hardening exponent are presented in Figure 3.10.

Table 3.3 calculated fatigue constants $\varepsilon_f^{'}$ and C of different solders at various temperatures

Solder Alloy	ε_f'=				C=			
	25ºC	**50ºC**	**75ºC**	**100ºC**	**25ºC**	**50ºC**	**75ºC**	**100ºC**
As receive SnPb	0.25	0.212	0.17	0.168	-0.226	-0.218	-0.205	-0.211
500h aged SnPb	0.09	0.085	0.068	0.06	-0.143	-0.13	-0.12	-0.105
1000h aged SnPb	0.0908	0.0808	0.0708	0.0608	-0.149	-0.144	-0.139	-0.134
As receive SAC105	0.56	0.49	0.43	0.363	-0.31	-0.306	-0.297	-0.295
500h aged SAC105	0.176	0.16	0.125	0.11	-0.2	-0.19	-0.19	-0.175
1000h aged SAC105	0.14	0.15	1.08	0.17	-0.19	-0.20	-0.218	-0.236
As receive SAC305	0.22	0.18	0.135	0.104	-0.2	-0.18	-0.16	-0.146
500h aged SAC305	0.106	0.132	0.15	0.19	-0.152	-0.17	-0.196	-0.22
1000h aged SAC305	0.114	0.118	0.16	0.21	-0.15	-0.16	-0.18	-0.188

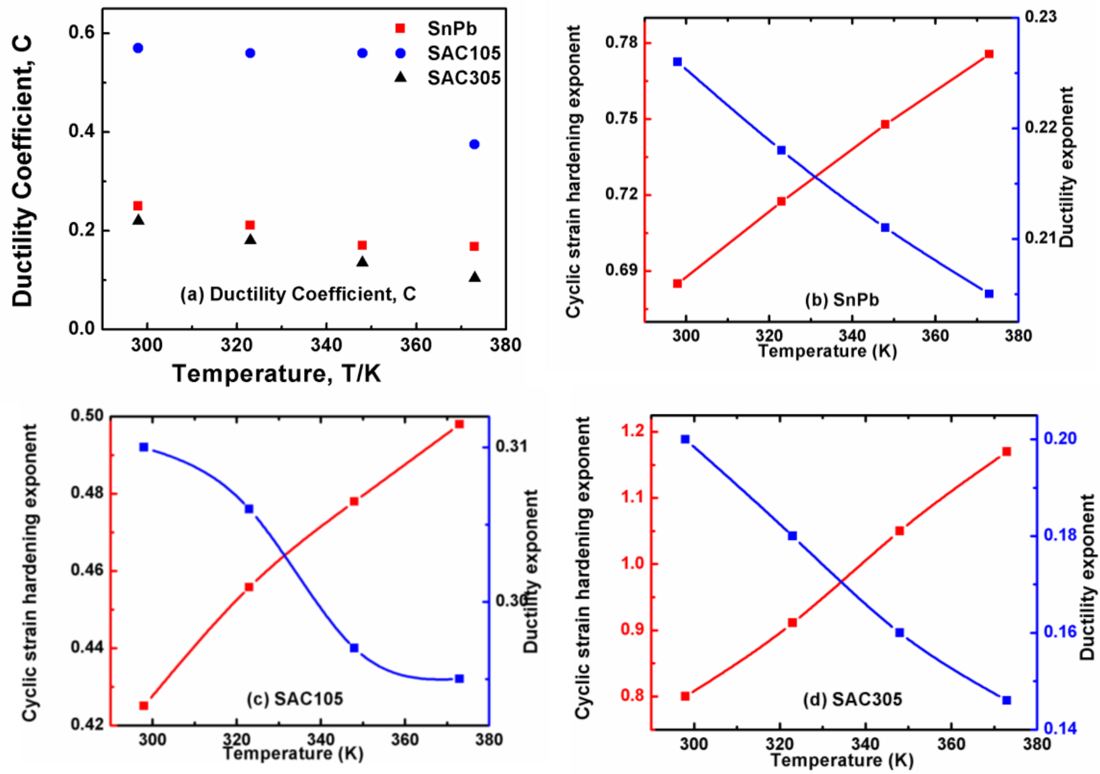

Figure 3.10. Fatigue ductility coefficient, ductility exponent and cyclic strain hardening exponent variations with the environment temperature for SnPb, SAC105 and SAC305.

3.3.4.1 Effect of Temperature on the Fatigue Ductility Coefficient, Ductility Exponent and Cyclic Strain Hardening Exponent

As shown in Figure 10(a), the fatigue ductility coefficient (fracture strain) decreases with increasing environment temperature for SnPb, SAC105 and SAC305. As seen in Figure 10(b) (c) and (d), the fatigue ductility exponent decreases with temperature, and strain hardening exponent increases with increasing temperature. These results are opposite from what is expected. At higher temperature the solder matrix got softer because besides dislocation glide, more plastic deformation modes were activated, such as grain boundary slide and creep. Therefore, the fracture strain should increase and strain hardening exponent should decrease. The source of the odd results needs to be understood.

3.3.4.2 Thermal strain effect on the fatigue life under cyclic shear load at elevated temperature

One thing that neglected from the test at high temperature is that thermal strain may exist in the solder. Therefore besides applied shear strain, the total plastic strain should include the thermal shear strain. Accordingly, the Coffin-Manson equation should be modified as shown in Equation 3.10. $\Delta\varepsilon_T$ is the thermal shear strain. As a result, the fatigue constants will be changed as well.

$$\frac{\Delta\varepsilon_p + \Delta\varepsilon_T}{2} = \varepsilon_f^{'}(2N_f)^C \qquad (3.10)$$

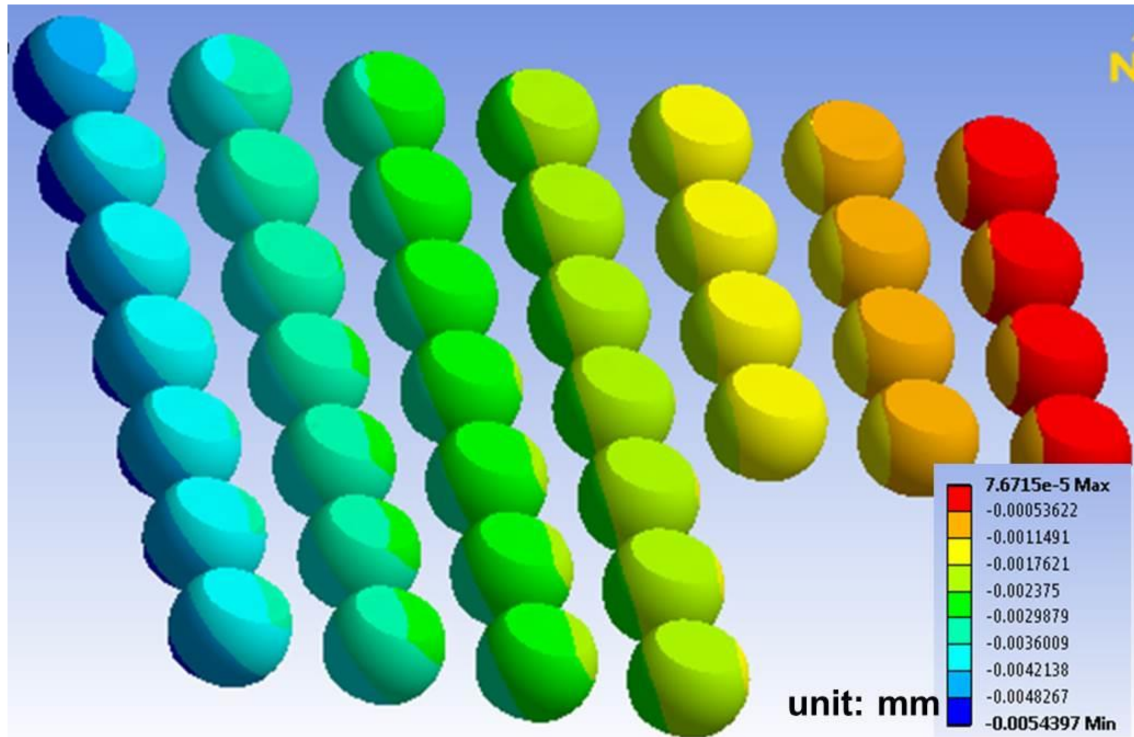

Figure 3.11 Shear strain distribution in BGA packaged solder joints under 100°C.

The thermal shear strain at different environment temperature was simulated using ANSYS. Due to the symmetry of the solder, the quarter model was used for the thermal strain

simulation. It is assumed that at 25 °C, the solder joints are thermal stress free. The thermal shear strain distribution is presented in Figure 3.11. It is shown that the shear strain is not the same in each solder joints but reduces from the corner to the center. For simplicity, the shear strain at the corner solder joint was used for thermal strain correction and fatigue constants calculation. This is also reasonable because the solder joint at the corner usually fails first. The maximum shear displacement is 5.4um, 3.7um, and 2um at 50 °C, 75 °C and 100 °C, respectively. Using thermal strain modified Coffin-Manson equation shown in Equation 3.10, the relationship between the fatigue constants and temperature is reconsidered and the data for SnPb, SAC105 and SAC305 are shown in Figure 3.12. It is found that after correction, the ductility coefficient increases with temperature, while the strain hardening exponent decreases with increasing temperature. This result is consistent with what is expected. Therefore, it is important to consider thermal strain effect on the fatigue behavior at elevated temperature. For other isothermal fatigue tests, such as vibration, bending, and shock tests, it is necessary to incorporate thermal strain/stress into the total stress/strain.

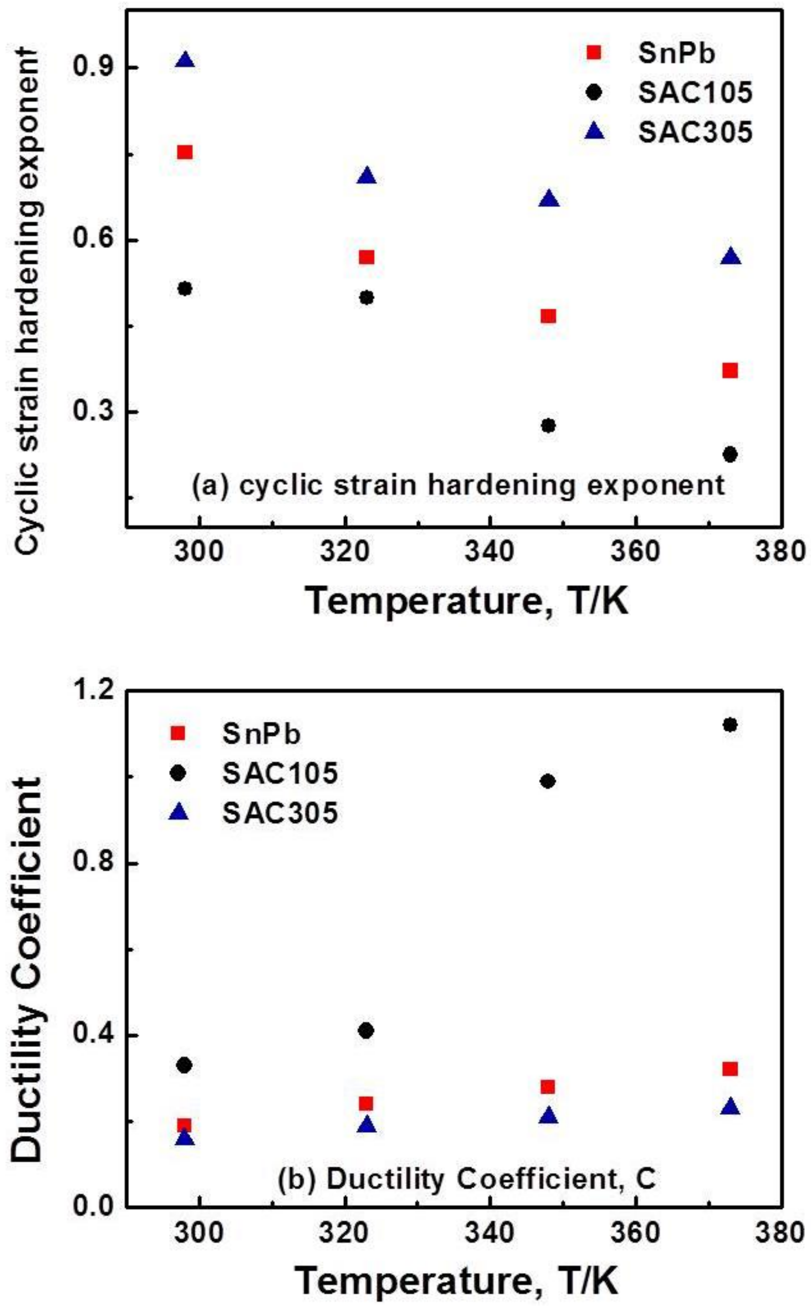

Figure 3.12 The temperature dependency of (a) strain hardening exponent and (b) ductility coefficient for SnPb, SAC105 and SAC305 after thermal strain correction.

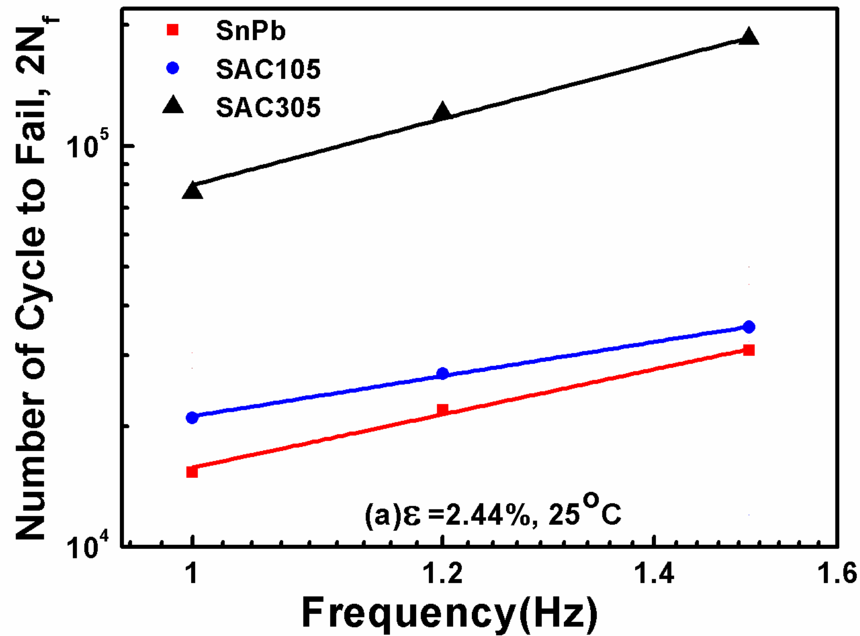

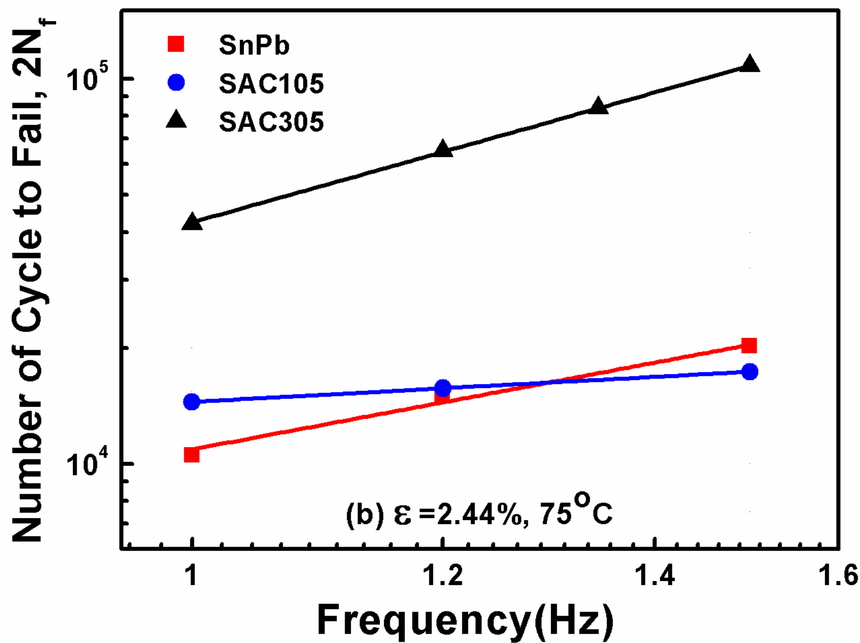

Figure 3.13 The relationship between fatigue life and frequency at temperature at 2.44% plastic strain, at the temperature (a) 25°C and (b) 75°C.

3.3.6 Fatigue Lifetime vs. Frequency

The fatigue behavior of the BGA packaged solder joints at different frequencies (1Hz to 3Hz) was analyzed. It is found that if the frequency is too high, the backslash of the

displacement occurs which induces early failure of the sample. Therefore, the data tested at higher frequency is not used, but the data tested from 0.5Hz to 2Hz are used for the later frequency-modified Coffin-Manson equation deduction. Figure 3.12 shows the fatigue life tested at different frequencies (1Hz, 1.2Hz and 1.5Hz) at the same 2.44% plastic strain and different temperatures. The fatigue life increases linearly with frequency regardless of the solder alloy composition and testing temperature. Moreover, the fatigue life frequency dependency is higher lower temperature and in SAC305. It is clear that the slope in Figure 3.12(a) and SAC305 is higher.

The frequency dependency can be understood by considering the deformation behavior of the solder. X.Q. Shi drew the stress-strain hysteresis loop for solder at different temperature and frequencies. [102] It is found that area of the hysteresis loop which represents the energy dissipation decreases with increasing temperature and increases with increasing frequency. Therefore, the fatigue life decreases with temperature, while increases with frequency.

3.3.7 Frequency modified Coffin-Manson Model

The conventional Coffin-Manson equation does not include frequency effect to the deformation behavior. In order to incorporate frequency into the Coffin-Manson model and consider creep and fatigue interaction frequency-modified Coffin-Manson equation is developed, as shown in equation 3.11, where k is frequency exponent.

$$\frac{\Delta\varepsilon_p}{2} = \varepsilon_f'(2N_f v^{k-1})^C \qquad (3.11)$$

According to the plastic flow law, the applied stress range, plastic strain range, and the plastic strain rate can be defined as follows:

$$\Delta\sigma = A\Delta\varepsilon_p^{\alpha}\,\dot{\varepsilon}_p^{\beta} \qquad (3.12)$$

Where A, α and β are numerical constants. For fatigue carried out at constant cycling frequency v, Equation 3.12 becomes

$$\Delta\sigma = A'\Delta\varepsilon_p^{\alpha}\,v^{\beta} \qquad (3.13)$$

Where A’ is a numerical constant. When frequency is constant, equation 3.13 can be written as

$$\alpha = (\frac{\Delta log\Delta\sigma}{\Delta log\Delta\varepsilon_p})_v \quad (3.14)$$

α is the strain hardening exponent. When $\Delta\varepsilon_p$constant, equation 3.14 becomes

$$\beta = (\frac{\Delta log\Delta\sigma}{\Delta log v})_{\Delta\varepsilon_p} \quad (3.15)$$

β is related to the frequency and represents the viscous property of solder deformation; a higher β means more stress relaxation and creep. The constant strain range but different frequencies, it can be assumed that the fatigue life is dominated by the applied stress range.

$$N_f \propto \Delta\sigma \quad (3.16)$$

Substituting Equation 3.11 and Equation 3.13 in to Equation 3.16, we can get that

$$(1 - k) \propto \beta \quad (3.17)$$

Therefore, k is also related to the viscosity of the material and it is independent of the strain range. A smaller k means more stress relaxation and creep, and thus better fatigue resistance.

In Equation 3.11, the term $(2N_f v^{k-1})$ can be defined as the frequency modified fatigue life. When the plastic strain range is plotted against frequency modified fatigue life, the fatigue life at different frequencies should merge into one single curve.

Similar to the ductility exponent, the frequency exponent under certain temperature can be extrapolated from the fatigue life-frequency plot at different temperature when the plastic strain range is fixed. As presented in equation 3.18, the slope of the plot in Figure 3.12 is equal to (1-k). Figure 3.13 presents the frequency exponent and temperature relationship, and k decreasing with temperature. This is consistent with the expectation that at higher temperature, the stress relaxation is easier and creep is more active. Furthermore, the β value, which is proportional to (1-k), is the highest for SAC305, and it also shows the highest temperature dependence. This means that creep behavior of SAC305 is highly related to the temperature more than other solder alloy tested here.

$$\log(2N_f) = (1-k)\log v + \log(\frac{\Delta\varepsilon_p}{2} * \varepsilon_f^{'})/C \qquad (3.18)$$

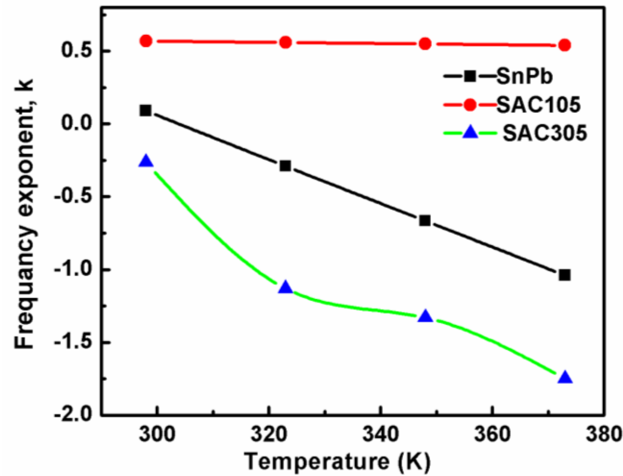

Figure 3.14 The frequency exponent dependence on the temperature for SnPb, SAC105 and SAC305 solder alloy.

Table 3.4 Fatigue constants at different temperatures for different solder alloys

Solder Alloy	ε_f'				C				k			
	25ºC	50ºC	75ºC	100ºC	25ºC	50ºC	75ºC	100ºC	25ºC	50ºC	75ºC	100ºC
As receive SnPb	0.19	0.24	0.28	0.32	-0.21	-0.26	-0.3	-0.35	0.09	-0.29	-0.665	-1.04
500h aged SnPb	0.26	0.095	0.066	0.076	-0.245	-0.181	-0.171	-0.226	-0.72	-1.38	-2.04	-2.7
1000h aged SnPb	0.09	0.082	0.082	0.07	-0.149	-0.163	-0.197	-0.22	-0.14	-0.956	-1.77	-2.585
As receive SAC105	0.41	0.33	0.99	1.12	-0.28	-0.286	-0.42	-0.47	0.57	0.56	0.56	0.54
500h aged SAC105	0.159	0.177	0.158	0.209	-0.198	-0.23	-0.248	-0.308	-1.13	-1.15	-1.16	-1.19
1000h aged SAC105	0.14	0.31	0.96	1.11	-0.19	-0.28	-0.42	-0.47	-2.5	-2.0	-1.5	-1.04
As receive SAC305	0.19	0.23	0.21	0.16	-0.18	-0.22	-0.23	-0.26	-0.263	-1.13	-1.33	-1.75
500h aged SAC305	0.098	0.11	0.15	0.31	-0.137	-0.169	-0.218	-0.314	-0.78	-0.94	-0.98	-1.2
1000h aged SAC305	0.099	0.139	0.184	0.66	-0.15	-0.19	-0.24	-0.4	-0.29	-0.18	-0.07	0.04

With all the results and discussions made above, the frequency-thermal strain-modified Coffin-Manson Equation can be developed for BGA packaged SAC and SnPb solder fatigue life modeling. The Equation is shown below.

$$\frac{\Delta\varepsilon_p + \Delta\varepsilon_T}{2} = \varepsilon_f^{'}(2N_f \nu^{k-1})^C \qquad (3.19)$$

Where $\varepsilon_f^{'}$, k and C are ductility coefficient, frequency exponent and ductility exponent. They are temperature dependent and the values can be achieved by conducting shear fatigue tests at various temperatures and strain ranges. Table 3.4 lists the constants at different temperatures for different solder alloys. The mathematic relationship between the constants and the temperature can be derived from the data in table 3.4 by fitting them into linear or powered line. The more temperatures tested, the more accurate the fit will be. Therefore, knowing the fatigue constants, environment temperature, and plastic strain range and thermal strain range, the fatigue life of the solder joint in BGA packaging can be predicted using the frequency-thermal strain modified Coffin-Manson model shown in Equation 3.19.

3.4 Conclusion and Implication

Shear fatigue tester was used to evaluate the fatigue behavior of lead-free solder joints in BGA package assembly. The fatigue lives of SAC305, SAC105 and SnPb at different aging condition, plastic strain range, frequency, temperature were tested. It is found that the fatigue life decreases with increasing plastic strain range, temperature, but increases with increasing frequency. The Coffin-Manson model is applicable to predict the fatigue life of the solder joint. However, to describe the fatigue behavior precisely, creep and thermal strain effect should be included into the basic Coffin-Manson model. Therefore, frequency-thermal strain modified Coffin-Manson equation is developed by incorporating the frequency and thermal strain into the Coffin-Manson equation. The fatigue constants, namely the fatigue ductility coefficient, ductility exponent, cyclic strain hardening, and frequency exponent are extrapolated from the Coffin-Manson Equation. These constants are determined to dominate the fatigue property of the solder materials. The fracture ductility coefficient represents the ductility of the material, strain hardening exponent is related to the strength, and the frequency exponent is related to the viscoplasticity of the material. Thus, ductility, strength and viscoplasticity determine the material

fatigue behavior. At high strain fatigue, the fatigue resistance is dominated by the ductility, while at low strain region, it is dictated by the strength. Therefore, it is predicted that SAC105 may perform better under shock (high strain test) because of the high fracture ductility; at the same time, SAC305 may perform better under vibration (low strain test). Furthermore, the fatigue constants are temperature dependent. The fracture ductility coefficient increases with increasing temperature, the strain hardening exponent decreases with increasing temperature, and the frequency exponent decreases/the viscoplasticity increases with increasing temperature. At higher temperature, the material softens but the plasticity increases due to more activated and easier dislocation glide and creep process.

One surprising but important finding during the shear fatigue is the thermal strain effect on the fatigue behavior. During elevated isothermal fatigue test, the thermal strain is always ignored, but the shear fatigue indicates that the thermal strain should be included to the total strain at elevated temperature. At high temperature, it is not necessary the material property which causes the worse fatigue resistance, but the thermal strain effect. At higher temperatures, the fracture ductility increases, viscoplasticity increases, but the strain hardening decreases. Therefore, at elevated temperature, the fatigue behavior is more complex than expected and it is a total effect of material property change and thermal strain effect. It is important to consider thermal strain effect when evaluate the fatigue behavior of solder under isothermal fatigue condition such as shock, vibration, bending, and so on.

CHAPTER FOUR

GRAIN STRUCTURE EVOLUTION OF SN-AG-CU LEAD-FREE SOLDER IN BGA PACKAGING ASSEMBLY AND ITS MECHANISM

4.1 Background

As mentioned in the other chapters, the reliability of solder joints is of great interest that it is the major factor which determines the performance of electronic devices. And with the trend of miniaturization of electronic devices and thus the decreasing in solder joints' size, the reliability of solder joint is becoming more problematic. Lots of studies have been carried out by accelerated thermal cycling, vibration, bending, impact, and other mechanical tests aiming to understand the failure mechanism and contribution factors. With numerous investigations on microstructure and its evolution with thermal exposure, processing and fatigue conditions, it has revealed that the microstructure of the solder has a great impact on the reliability.[122-134] As the most popular lead-free solder candidate, Sn-Ag-Cu solder, its microstructure especially the Sn grain structure and orientation are found to dominant the properties of the solder. [122-127] The thermomechanical properties of Sn exhibit large anisotropy that the thermomechanical response depends greatly on the size and crystal orientations of the Sn grains. T.Bieler et al. has found that the variation in microstructure and large anisotropic thermomechanical response of Sn can results in cracking and joint failure in SAC solder balls far from the point of maximum shear stress under thermal cycling. [122, 128-130] Therefore, it is important to examine and understand the grain structure evolution and the consequent properties in order to anticipate and predict the reliability of Pb-free solders.

4.1.1 Elastic Anisotropy of Sn

The elastic modulus and the coefficient of thermal expansion (CTE) are plotted in Fig.4.1 as a function of crystal direction. [129] The solid line shows the variation on the (100) plane, and the dashed line shows the variation on a (110) plane. Red line is for elastic modulus and the black line is for CTE. The length of the line from the origin to the plotted line represents the

magnitude in that direction. The insert image shows the unit cell structure of β-Tin. It is body centered tetrahedral structure with additional atoms located at (0.5, 0, and 0.25) and (0, 0.5, 0.75). It can be seen that the CTE and E increase by a factor of 2-3 from a to c direction, and the elastic modulus varies by a factor of 3 on the (001) plane (between the [100] and [110] directions).

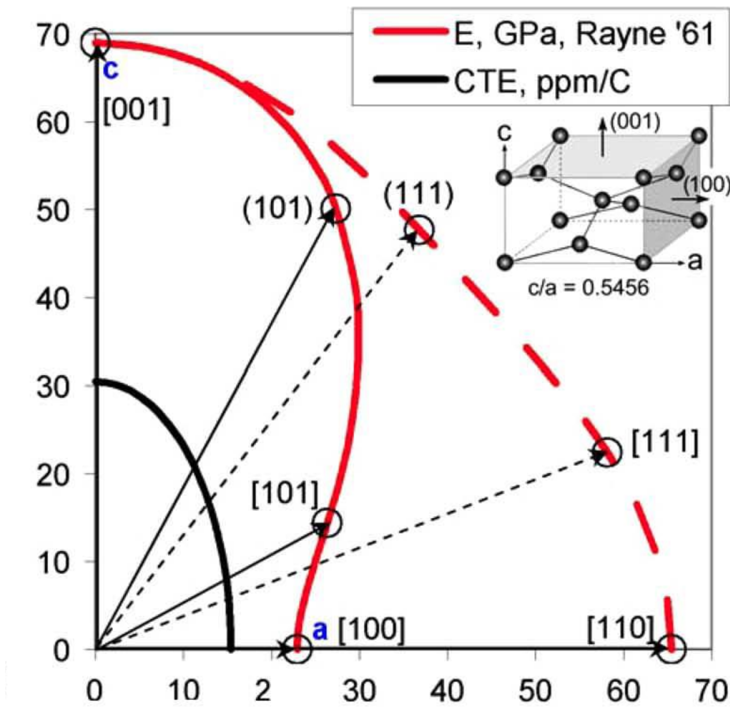

Figure 4.1 Ambient temperature measurements of Young's modulus and the coefficient of thermal expansion for Sn with respect to crystal direction.

4.1.2 Microstructure of SAC Solder

The solidification of SAC solder is similar to Sn, and it shows pronounced undercooling (>100 ˚C) especially in small samples.[135-139] Depending on the diameter, the undercooling in SAC solder at cooling rate near 1 ˚C/s is between 20 ˚C to 80 ˚C.[140-143] The high undercooling results in high growth rate of the Sn. Thus large grains are seen in Sn and Sn-based solders. Typically SAC solder joints consist of large Sn grains with one or at most a few Sn grains with only one orientation. The large Sn grains exhibit β-Sn dendrites surrounded by

an enriched interdendritic eutectic microstituents, which are shown in Figure 4.2(a) and (b). Also, the microstructure analysis using optical microscope, OIM and X-ray texture methods have shown that the grain misorientations present in SAC solder are mostly solidification twins with nominally 60 °C rotations about [100] axis. As seen in Figure 4.2(c), the microstructure of the solder joint shows "Kara's beach ball" structure with six sections, which is a result of cyclic twinning during solidification. Cyclic twinning happens very often within SAC solder which induces typically two morphologies: Kara's beach ball structure or highly interpenetrating structure with a fine grained polycrystalline appearance. Although they look different, both of them consist of cyclic twin structure developed from either 57.2° twin boundaries on (101) planes or 62.8° twin boundaries on (301) planes. [136]

Moreover, the Sn-Ag-Cu solder joint consists of three phases: β-Sn phase, Ag_3Sn and Cu_6Sn_5. The space between β-Sn dendrites and the size of the Tin dendrite are found to be greatly dependent on the cooling rate. [142-143] The space and size decrease with increasing cooling rate. Moreover, the IMC phases get finer and distribution more uniformly within the solder matrix with increasing cooling rate. Figure 4.3 shows the microstructure of Sn-3.5wt%Ag after cooling with different cooling rates. [143] According to the phase diagram of Sn-Ag system, at the eutectic composition under equilibrium solidification condition, the microstructure composes of Tin and Ag_3Sn. With high cooling rate, it is under non-equilibrium solidification condition which results in fine Tin-rich dendrites with fine eutectic mixture of spherical Ag_3Sn in the Tin-rich matrix, as seen Figure 4.3(a). As the cooling rate decreases, shown in Figure 4.3 (b) and (c), the microstructure consists of relatively coarse Tin-rich dendrites surrounded by coarse eutectic mixture of Ag_3Sn.

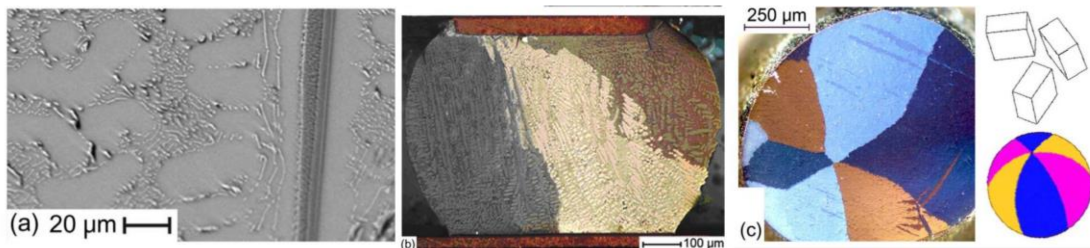

Figure 4.2 (a) SEM Back Scatter composition mode image showing small and large Ag_3Sn intermetallic within Sn-3.0Ag-1.1Cu. (b), (c) Optical polarized light image of (b) Sn–3.0Ag-0.8Cu commercial BGA joint, and (c) a near eutectic SAC solder ball illustrates “Kara’s Beach ball” texture, which has six-fold, cyclic twin relationship with 60° rotations about a common [100] axis.

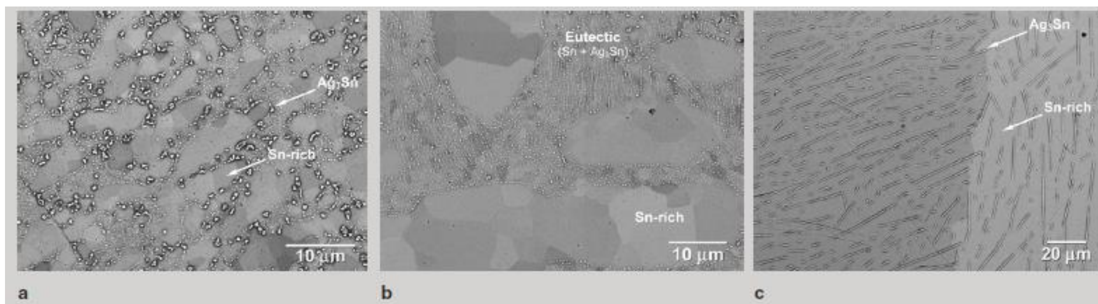

Figure 4.3 SEM images of Sn-3.5wt%Ag solder microstructure for cooling rates of (a) 24 °C/s (water cooling), (b) 0.5 °C/s (air cooling), and (c) 0.08 °C/s (furnace cooling).

4.1.3 Microstructure Dependence on the Joint Position in the Package

It is a common assumption that the solder joints in the same packaging assembly consist of the same microstructure as shown in Figure 4.2 and thus the mechanical properties of one solder joint represents the properties of the others at different locations within the same package. Consequently, it is believed that the solder joints in the same assembly should have the same reliability behavior. However, it is a common observation that during accelerated reliability evaluation, there exists a position in the assembly that is most prone to the failure. The shear fatigue results shown in chapter two and chapter three reveal that solder joints in the first row always fail earlier than the second row of solder joints, although all the solder joints are subjected to equal amount of shear stress and strain under cyclic shear that they should have equal possibility of failure. This result indicates that variation in grain structure or constrain with solder joint position may exist within the package. In the other hand, Telang et al. showed that

the dominant orientations of about 20 separate solder joints were all different, suggesting that it is possible that every solder joint in a package may has different crystal orientation and thus mechanical properties may be different. [122] Therefore, more investigation is needed in order to verify and understand the position dependent solder microstructure and reliability behavior in the same package.

In this chapter, the microstructure evolution of each individual solder with response to the thermal strain within the same package was investigated by series of cooling experiments. Some of the important findings are listed below. First, by controlling the cooling rate, cooling temperature range, and the thermal history, grain structure can be altered within the same assembly. In some positions, more often, the corner joints go through recrystallization and compose of fine polygrain structure; while in the inner side of the assembly, joints consist of single/multiple big grains. First indication of this result is that the grain structure of the solder joint can vary with position and the common assumption on the structure similarity in the assembly is not necessary correct. Second, although recrystallization is usually seen at localized cracking area where stress concentration and plastic deformation accumulation are high enough under mechanical fatigue or thermal cycling [90, 129, 132, 133, 144], this study indicates that the plastic deformation induced by thermal stress by one thermal exposure (cooling once) is enough to trigger recrystallization. Furthermore, the position dependency of recrystallization means that the plastic deformation is joint position related. As a result, the built-in residual thermal stress in any process involving cooling/heating is different in each solder joints within the same assembly. This variation in residual thermal stress and grain structure may be sources for the position dependent reliability seen in many reliability assessments. In the other hand, twins found in the solder joints are believed to form by deformation twinning although it is hard to believe. Deformation twinning rarely occurs unless the strain rate is extremely high or temperature is below cryogenic temperature in tin or tin-based alloys due to the high stacking fault energy and relative low melting temperature [145-158]. However, my

result suggests that deformation twining can occur in tin simply by cooling and the mechanism will be discussed in the coming paper. Nevertheless, all the results reveal that various microstructure evolution paths can occur just by simple cooling in solder joints and result in different grain structures within the same assembly. This provides a good way to create different grain structures and evaluate how they can influence the reliability of the solder joints.

All in all, with the hope of understanding the grain structure and reliability of individual solder joint in the same assembly, careful investigations along with scientific discussions about the microstructure evolution and its contribution factors are given in this chapter. It is the first time an insightful understanding is given on how position dependent plastic deformations develop and affect the microstructure evolution in the packaging assembly by cooling. It also suggests that such position dependency should be included in the reliability evaluation of a solder packaging assembly.

4.2 Experiment Procedure

The samples under investigation are based on Ball Grid Array configuration and can be described schematically in Figure 4.4. In this layout, 160 solder joints with 600μm diameter are arranged with a pitch spacing of 800μm in 14x14 arrays at the outermost area with the absence of inner 6x6 arrays. In Figure 4.3, the solder joints are indexed as column 1 to 14 and row A to P. These solder balls are placed underneath 1 cm by 1 cm Si chip covered with molding compound. With an industry standard reflow process, the assembly was heated up to ~260 °C with a steady heating rate, and then slowly cooled to room temperature after a short hold period at the reflow temperature. The solder alloy investigated here is Sn-based lead-free solder primary SAC105 (98.5%Sn-1%Ag-0.5%Cu) and SAC305 (96.5%Sn-3%Ag-0.5%Cu). Samples are thermal aged at 100 °C and 150 °C for 500 hours and 1000 hours. Subsequently, they were cooled to room temperature in water (50 °C/s), air (0.3 °C/s) or in the furnace (0.01 °C /S) with various cooling rates. The schematic temperature profile is shown in figure 4.5. For microstructure observation, cross-sections of the samples was made by modeling in epoxy,

following with sandpaper polishing, micro-polishing with Alumina powder and 5% HCl etching. Microstructure of the solder joint is investigated by Optical Microscope and Scanning Electron Microscope (SEM).

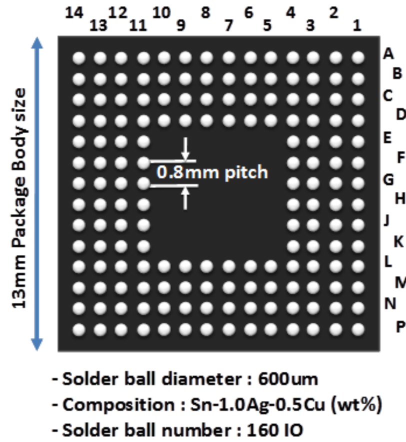

Figure 4.4 Schematic drawing of the sample layout (SAC105 and SAC305)

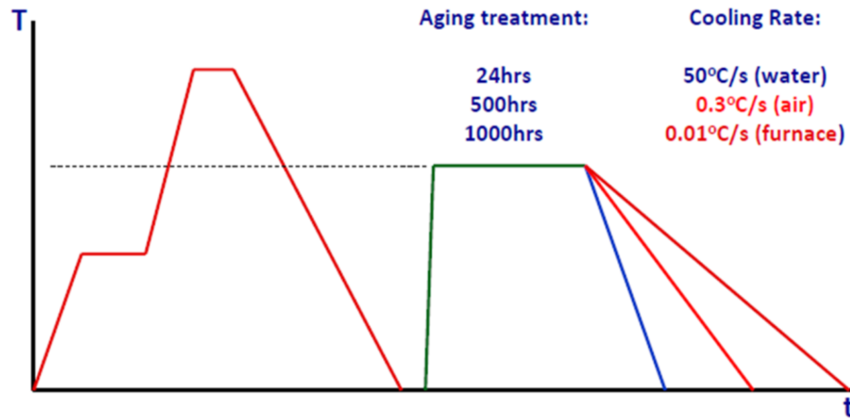

Figure 4.5 Schematic temperature profiles for solder thermal treatment.

4.3 Results and Discussion

4.3.1 Thermal Aging vs. Microstructure

Figure 4.6 shows the microstructure of the SAC105 solder joints in row P after reflow taken by optical microscope. All the solder joints, regardless of the location, show more or less the same microstructures which consist of several large Tin grains with finely distributed Ag_3Sn

particles and some Cu_6Sn_5 particles in the Sn matrix. Figure 4.7 reveals the microstructure of the solder joints which were slowly cooled in the furnace from 150 °C to room temperature after aging for 500 hours. Similar to Figure 4.6, the solder joints at different locations still show similar microstructure without position dependent. The optical microstructure of the solder joint after reflowing and slow cooling are similar and consistent with the assumption that in the same assembly the grain structure of the solder joint is the same. Figure 4.8 shows microstructure of solder joints before and after thermal aging taken by Scanning Electron Microscope (SEM). Two obvious changes induced by thermal aging can be seen. First, IMCs, both Ag_3Sn and Cu_6Sn_5, in the Sn matrix were coarsened. Second, $(Ni_xCu_{1-x})_6Sn_5$ layer in the packaging side and Cu_6Sn_5 layer in the board side grow thicker after thermal aging. For SAC105, the IMCs in the package side interface grow from 1.5um to 3um after thermal aging at 150 °C for 1000 hours, while in the board side it grows from 2.5um to 6um. In case of SAC305, the IMC in package side increases from 1um to about 4um, in board side, from 3um to 13um.

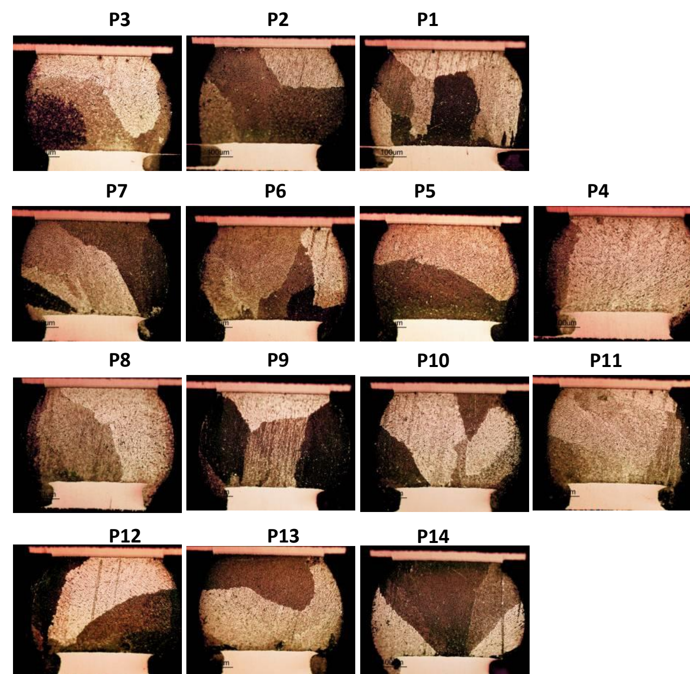

Figure 4.6 Optical Microscope of the solder joints in outmost row P from position 1 to 14 after reflow.

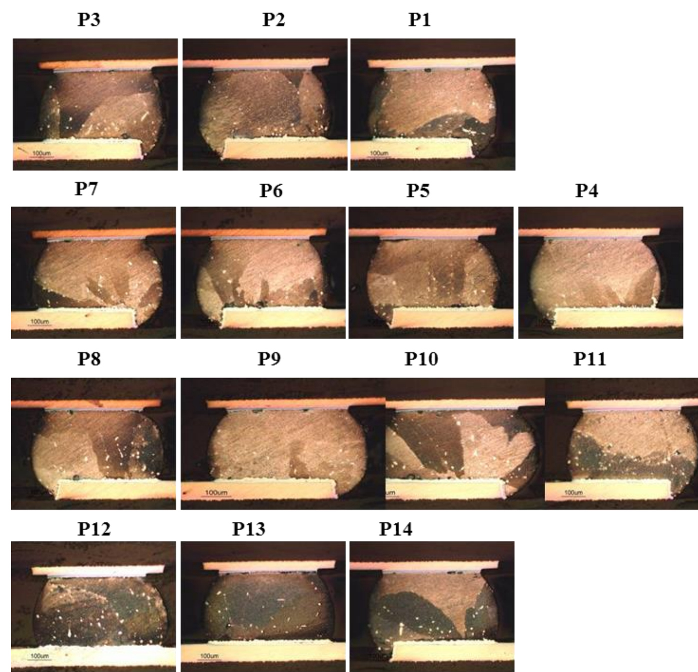

Figure 4.7. Optical Microscope of the solder joints in outmost row P from position 1 to 14 150 °C for 500 hours.

Coarsening of the IMC in the solder matrix and growth of IMC at the solder/Cu interfaces are common observations and are well documented in other papers. It is reported that interfacial reactions among solder material, surface finish layer and copper conductor and their reaction products are very important to the mechanical strength of the package. To prevent the reaction between the copper conductor and solder, various surface finishes are developed, such as ENiG, OSP, DIG, Immersion Silver or Pd, and so on. In this research, electroless nickel immersion gold surface finish (ENiG) was used in the package side, while in the board side, it was bare copper in direct contact with the solder. Therefore, interface IMC growth in the package side was much slower than in the board side. Also, the IMC in the board side is much thicker than the package side. Growth of the intermetallic compound made the solder/Cu interface to be weaker due to the brittleness of the IMC layer. The evidence can be seen from Figure 2.10 that the instead of initiating crack in the package side neck area the crack is found in the board side interface. Moreover, the solder matrix strength decreases because of IMC

coarsening. The finely distributed Ag_3Sn has precipitates strengthening effect, while after thermal aging, the cohesion between the large Ag_3Sn/Cu_6Sn_5 particle and Sn solder matrix is bad that decreases the strength of the solder matrix. Thermal aging effect on the fatigue resistance of the solder joint in BGA package is described in chapter 3. It is found that the fatigue life decreases with increasing thermal aging time for all the solders under test (SAC105, SAC305 and SnPb). However, compared to the growth rate of interface IMC, the coarsen rate in the solder matrix is relatively slow because the Ag_3Sn and Cu_6Sn_5 particles are covalently bonded. It requires high activation energy to break the covalent bond in the particles and diffuse toward the growing particles. Therefore, the degradation of mechanical strength in the solder matrix is not as much as in the interface that instead of crack in the solder matrix the crack is found to be at the solder/IMC interface at the board side.

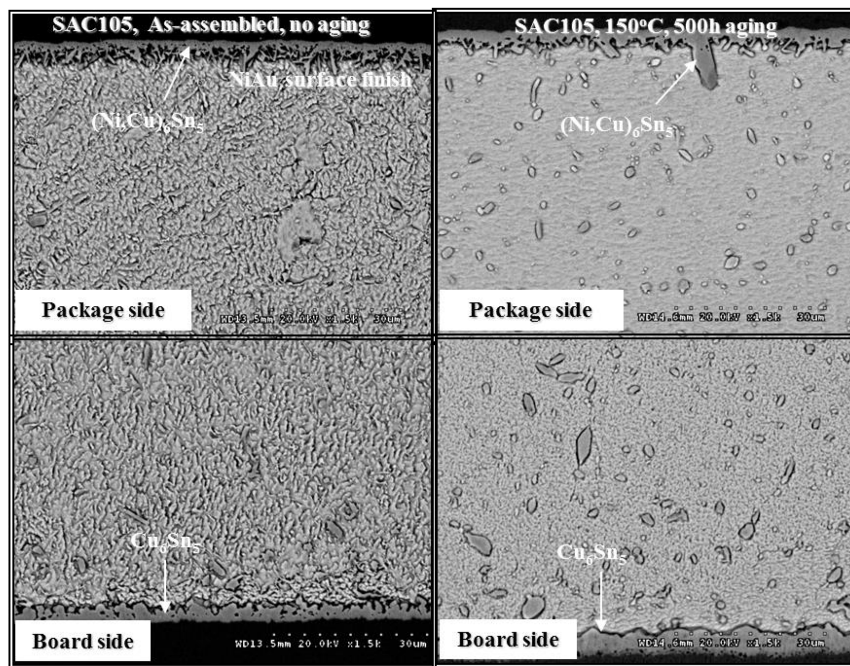

Figure 4.8. SEM images of the solder joint SAC105 in package side (top) and board side (down) before (left) and after 150 °C 500 thermal aging.

4.3.2 Grain Structure Evolution vs. Cooling Rate

The microstructure of the solder joint after cooling with various cooling rate was observed by optical microscope as well as SEM, as shown in Figure 4.9. The color contrast seen from the optical microscope is due to the different grain orientation thus different color represents different grain. All the joints seen in Figure 4.9 are located at the corner of the BGA assembly. It is found that cooling rate has a significant effect on the microstructure. A cooling rate of 50 °C/s results in poly-grain structure with grain size about 10um and smaller. Grain boundaries can also be seen clearly from figure 4.9(d). A cooling rate of 0.3 °C/s results in a similar microstructure as the reflowed. However, a closer inspection of the joint reveals that these grains contains a number of parallel grains as evidenced in figure 4.9(b) and (e). The EBSD analysis as well as other analysis reveals that they are twins. In case of slow cool in the furnace, the grain structure is essentially the same as as-reflowed.

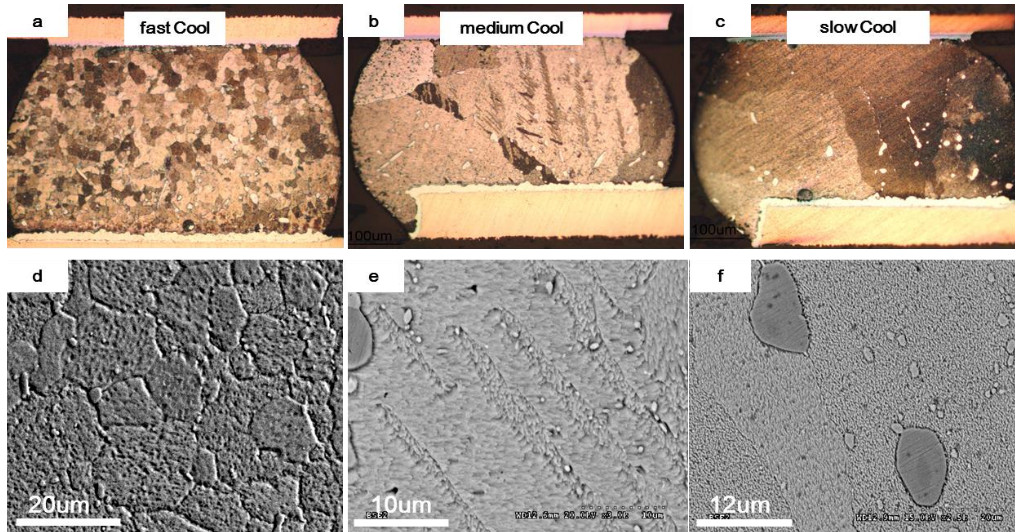

Figure 4.9. Optical and SEM images of 150 °C 500 hours thermal aged BGA SAC105 after cooling at (a)(d) fast water quench, (b)(e) medium air cool, and (c)(f)slow furnace cool.

4.3.3 Grain Structure Evolution vs. Joint Position

Figure 4.9 shows the grain structure of the solder joint at the corner of the assembly because it is the place where cooling rate sensitivity is the most pronounced. Figure 4.10 shows

the grain structure of the joint at various positions after fast and medium cooling. Due to the symmetry of the assembly, quarter model is used. The first column in figure 4.10 is the schematic drawing of the solder joint position in the assembly, and it is grouped into three divisions according to the joint grain structure: corner, edge and inner. The second and third columns are the joints structure after medium cool; the fourth and fifth are the joints after fast water quench. Besides cooling rate, figure 4.10 also reveals that grain structure after cooling is highly sensitive to the joint position. It can be seen that medium rate cooling from 150 °C to room temperature results in the grain structure that is not fundamentally different from the as-reflowed except for the fact that the grains at the corner and edge show mechanical twins. Inner joints do not show any mechanical twins. On the other hand, fast cooled assembly shows mixture of all possible grain structures, namely polygranular, grains with mechanical twin and the beach ball. The corner joints clearly show polygranular structure, the joints in the edge contain the beach ball grains filled with mechanical twins, and the inner joints show no change in grain structure from the reflowed. In case when the same assembly is slowly cooled, there is no position dependence on the grain structure. All joints show the same grain structure and they are all beach ball type after slow cool. Table 4.1 describes the grain structure sensitivity to cooling rate and joint position.

Table 4.1 Corner, edge and inner joint microstructure after water quenching and slow cooling

position / cooling	corner	edge	inner
fast	poly-grain	twin	classical
medium	twin	twin	classical
slow	classical	classical	classical

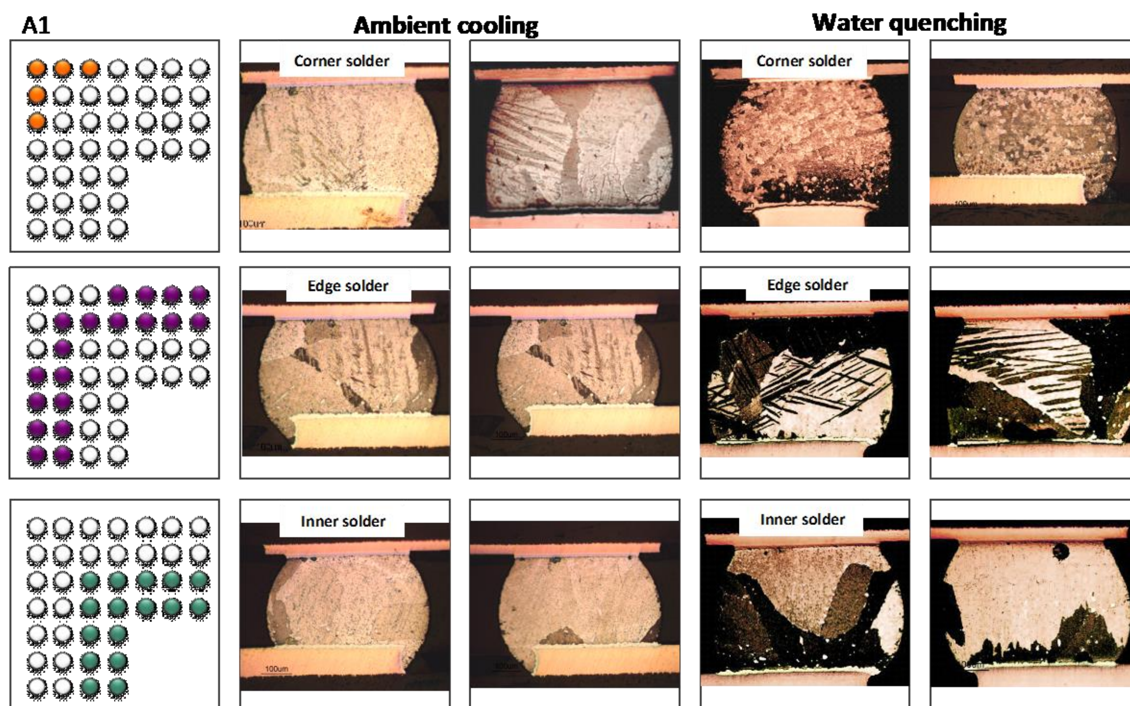

Figure 4.10. Corner, edge and inner joint microstructure of 150 °C 500 hours thermal aged BGA SAC105 after air cooling and water quenching.

The dependence of joint grain structure on the position in the assembly and cooling rate is somewhat surprising and contradicts a conventional wisdom known in this field. First, it is common assumption that cooling rate after thermal exposure should not affect the grain structure. Second assumption is that the grain structure in the same assembly should be more or less the same. However, our results indicate that (1) the plastic deformation after one time thermal exposure is enough to induce grain structure change by dislocation glide and deformation twinning, and (2) the grain structure within one assembly is not necessary the same but position dependent.

The polygrain structure is conventionally formed by recrystallization.[133] It is seen during thermal cycling with hundreds of cycles and is highly localized at the places where crack propagates.[90, 129, 132, 144] However, in this case, macroscopic recrystallization is resulted by one time thermal exposure. This means that dislocation glide and its multiplication is far

easier in Sn grains than previous thought. Alternatively, nucleation energy for grain formation is much lower than expected.

The formation of mechanical twinning is another surprising but interesting observation in this research and will be discussed in the later chapter.

4.3.4 Grain Structure Evolution vs. Thermal History and Alloy Composition

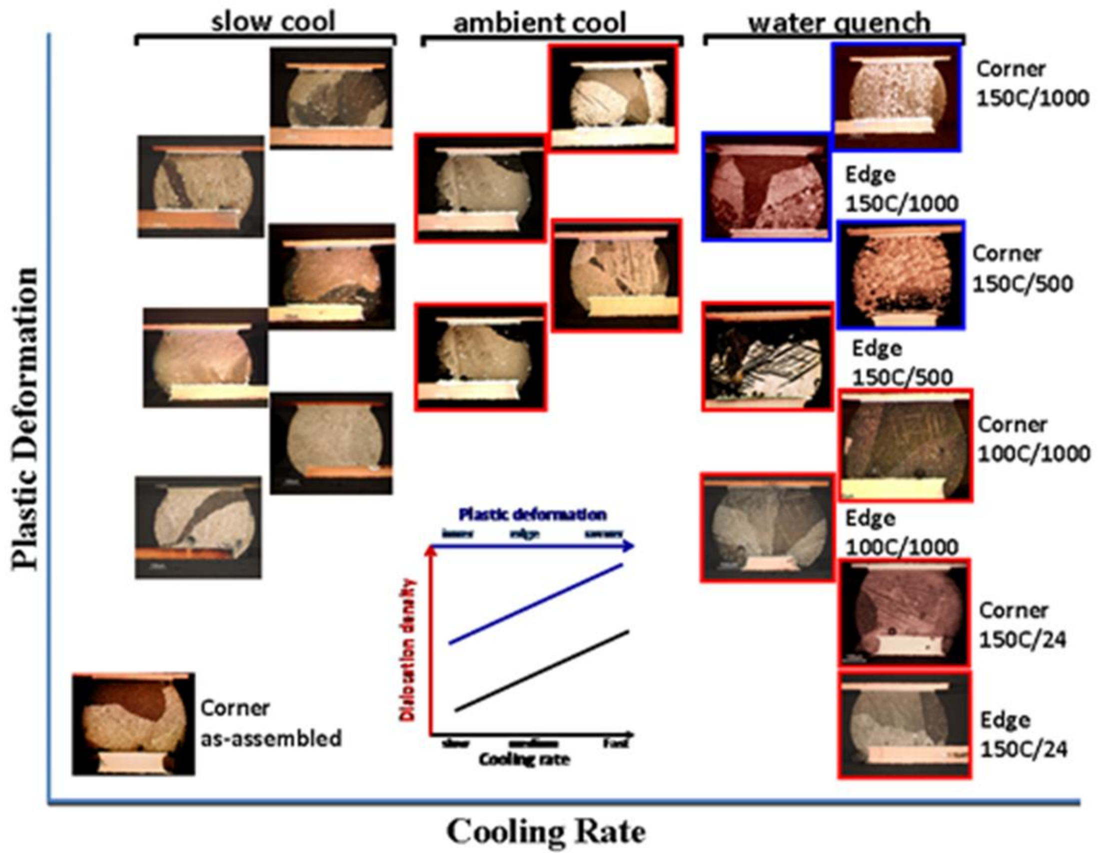

Figure 4.11 Grain structure map with cooling rate, joint position and thermal history.

Figure 4.11 shows the grain structure map showing the grain structure with respect to the cooling rate, joint position and thermal history (aging temperature and time). In case of SAC105 thermal aged at 150 °C for 1000 hours, after water quench, not only the joint in the corner but also in the edge position show polygrain structure. In case of aging at 100 °C, after cooling from 150 °C to room temperature, recrystallization does not occur in any position, but

only deformation twinning is observed. These results indicate that recrystallization and thus polygrain formation is also sensitive to the thermal history of the solder joint.

Furthermore, when the SAC305 (with or without thermal aging) was cooled from 150°C to room temperature, the grain structure does not change but keeps the classical beach ball structure. Even SAC305 was thermal aged at 150 °C for 1500 hours, recrystallization does not occur after water quench.

The sensitivity of grain structure evolution to thermal aging and solder alloy composition share some similarity that is the dependency of grain structure on the solder joint strength and ductility. Compare SAC105 to SAC305, the former one is softer than the latter one. While compared thermal aged SAC105 at higher temperature and longer time, the solder is getting softer. Therefore, it is concluded that recrystallization is easier to occur in softer solder.

4.3.5 Recrystallization Mechanism

4.3.5.1 Driving Force for Grain Structure Change

Considering the driving force for grain structure change which is the accumulation of the stored strain energy due to plastic deformation, the sensitivity of grain structure to the joint location and cooling rate suggests that there exists a close kinetic interplay between the accumulation rate of stored energy and its dynamic release during cooling. In one hand, if the relaxation of stored energy is completely suppressed and stored strain energy in the solder joint is high, such as fast cooling, recrystallization is expected to occur. In the other hand, if the stored energy (as a result of dislocation glide and its multiplication) is fully released, such as slow cooling, the stored energy will be not enough for recrystallization. This is the reason why recrystallization occurs when cooling rate is fast while it is suppressed when cooling rate is excessively slow. Furthermore, in order to explain why this kinetic interplay only works only for the corner (or edge in some cases) joints, the finite element analysis (FEM) of stress state of solder joint for the given assembly is carried out using ANASYS.

Table 4.2 lists the materials constants (young's modulus, CTE and Poisson's ratio) used for the computation. Figure 4.12 shows the quarter model drawing of the assembly for the FEM analysis. The dimension of each component is also listed. The focus of the computation is to determine how much deformation should occur by thermal expansion mismatch between the chip and PCB. Since the inclusion of yield is not relevant in terms of understanding the driving force for the grain structure change, it is assumed that the deformation is completely elastic. Also it is assumed that the solder joint is strain free at 150 °C, which is reasonable because of aging for long time that the residual stress should be completely released by the time of cooling. The total deformation induced by cooling from 150 °C to room temperature is computed and the result is shown in Figure 4.13. It can be seen that corner joint is subjected to the maximum total deformation field. The edge joint is subjected to the next level followed by the inner joint. This is an expected result because the symmetry center of the deformation is located at the center of the chip. The longer the distance from the center, the higher the total deformation field. Therefore, the corner joints are likely to experience the most deformation while the inner joints the least.

Table 4.2 materials constants for FEM analysis

Materials	E(σPa)	CTE(ppm/°C)	ν
Silicon	131	2.8	0.28
Copper	129	17	0.34
Substrate	16.8	16	0.3
PCB	26.2	18	0.3
EMC	20	9	0.3
solder	96.9	15.8	0.42

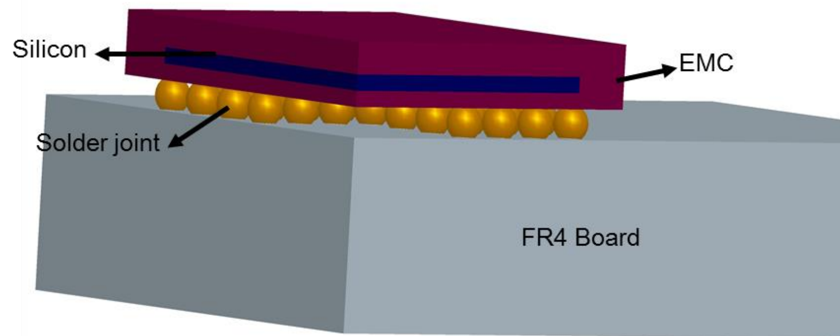

Figure 4.12. Schematic quarter model for FEM analysis. Chip Size: 1cm x 1cm; Packaging Size: 1.3cm x 1.3cm; BT Substrate Thickness: 400um; Solder joint diameter: 600um; Solder Joint Height: 400um; Pitch Size: 800um.

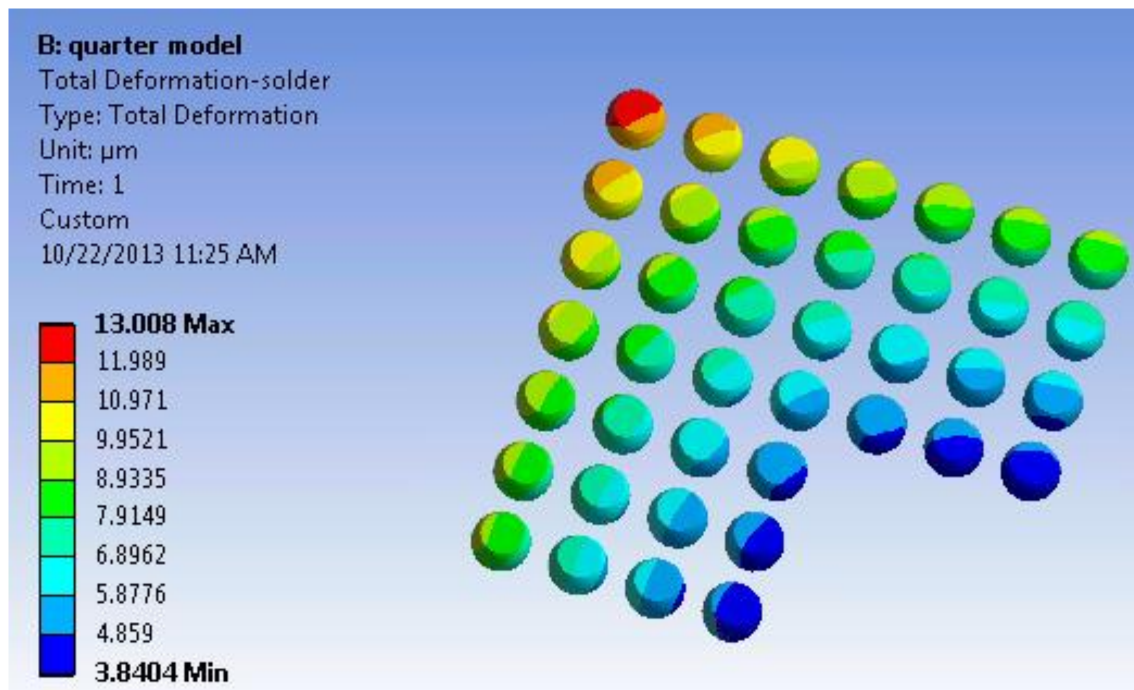

Figure 4.13. FEM analysis of Total deformation of solder joints in BGA assembly cooled from 150°C to 22.5°C, unit: mm.

Because all samples were aged at and cooled to the same temperature, they were subjected to the identical deformation field as shown in Figure 4.13 irrespective of cooling rate. Cooling rate plays a role in the grain structure evolution because it determines the strain rate (deformation rate) and the stress relaxation rate. Recrystallization is a process of reducing the

stored strain energy by removing the dislocation with new dislocation free grains. It is a thermally activated process and occurs when the stored strain energy reaches a critical value for the material to recrystallize. However, besides recrystallization, dynamic recovery by either creep process or polygonization process can occur to reduce the stored strain energy as well. Dynamic recovery competes with recrystallization because both are driven by the stored energy. The difference between recrystallization and recovery is that the latter one does not involve migration and formation of high angle grain boundary. Increasing in the plastic deformation rate increases the net amount of stored strain energy needed for recrystallization because dynamic recovery does not have enough time to release the stored strain energy. This will trigger recrystallization process as seen in the fast cooled corner joint. The edge joint in the same assembly may not develop enough stored energy with less amount of plastic deformation although clearly they deform by another competing process, mechanical twinning. In case when deformation amount is small, as in the case of inner joint of fast or medium cooling rate, or dynamic recovery successfully outcompetes the strain energy storage rate, as in the case of all joint in slow cooled, recrystallization does not occur. Figure 4.14, where a schematic representation of variation in deformation and stored energy with position and cooling rate is shown, may present a simply summary of the mechanism that explains position and cooling rate sensitivity of recrystallization. The stored strain energy for recrystallization increases with increasing cooling rate from the inner position to the corner position.

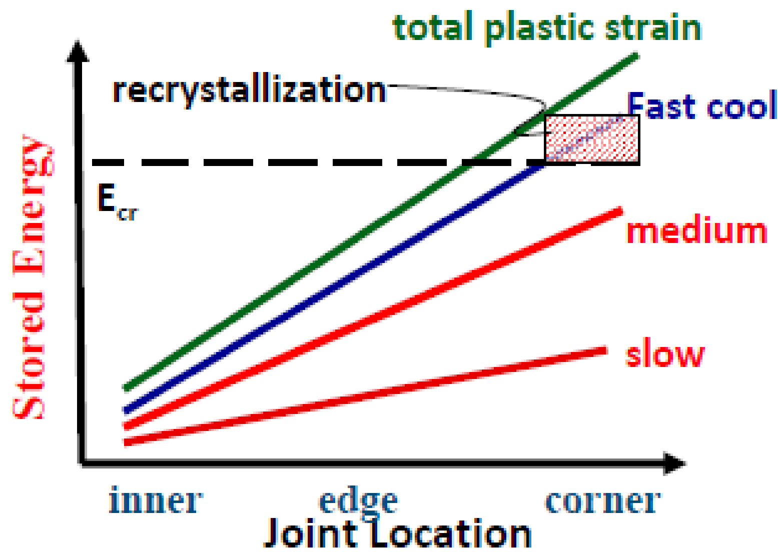

Figure 4.14.Stored strain energy variations with solder position and cooling rate.

Moreover, in addition to joint position, the plastic deformation also varies with the solder joint mechanical property, such as yield strength. The amount of plastic deformation decreases with increasing yield strength because high yield strength means that the solder is more resistant to plastic formation. This can explain why recrystallization only occurs in SAC105 thermal aged at high enough temperature and time.

According to the mechanism explained here, it is predictable that controlling the amount of the plastic deformation may be able to control the grain structure, for example, the cooling temperature or assembly parameter (joint geometry, diameter, pitch size and so on).

4.3.5.2 Grain Structure Change vs. BGA Assembly Geometry

Figure 4.15 shows the other geometry of the BGA assembly under observation. Compared to the previous one shown in figure 4.4, the number of joint, diameter, and pitch size are different. In this assembly, after fast cooling from 150 °C to room temperature, no recrystallized poly-grain structure is seen but only deformation twinning is observed in the solder joints at the corner and edge position. In the case of medium cooling, the result is the same. The grain structure of the joint after fast and medium cooling is shown in Figure 4.16. To

understand why recrystallization does not activate in the case of fast cooling, the estimated plastic deformation was computed by ANASYS, and the result is shown in Figure 4.17. Compared with the total deformation result shown in Figure 4.13 for assembly in Figure 4.4, the total deformation in each solder joint is less. Although the reduction in the total plastic deformation is not that much, the maximum deformation value decreasing from 13um to 12um, the stored strain energy difference can be large because energy (E) $=A\varepsilon^2$. As a result, in this assembly configuration, the stored strain energy is not enough to trigger recrystallization process.

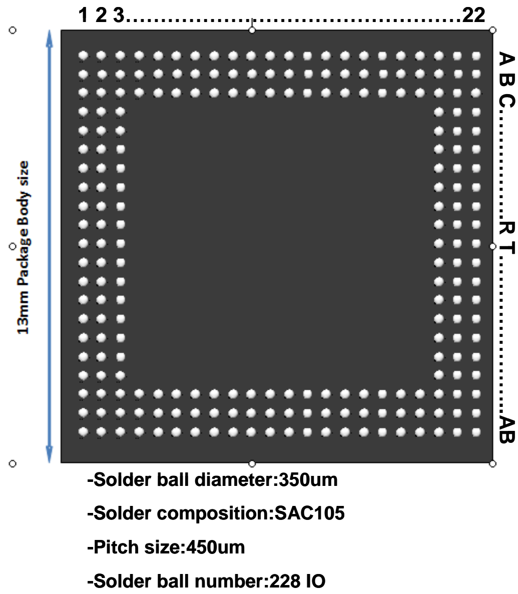

Figure 4.15. schematic drawing of BGA assembly showing the solder joint layout.

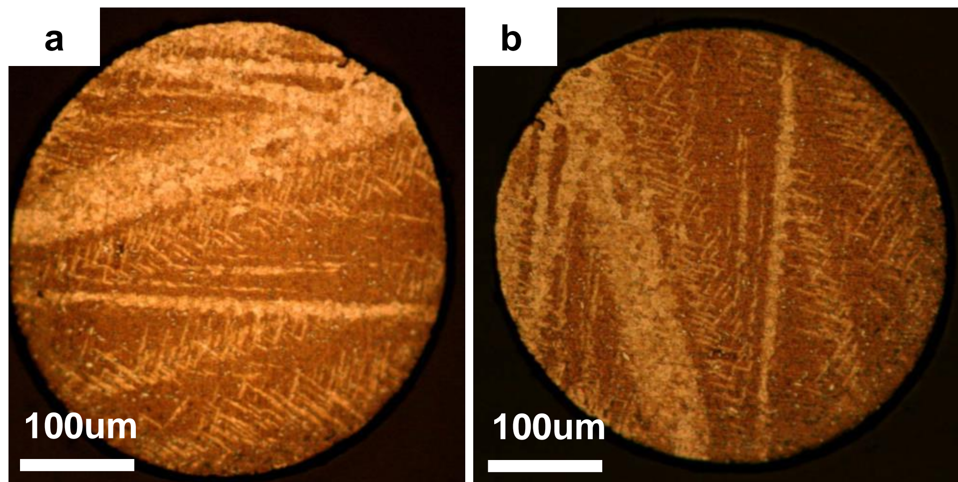

Figure 4.16. The optical microstructure of the 150 °C 500 hours thermal aged joint after (a) fast cool, (b) medium cool showing twins.

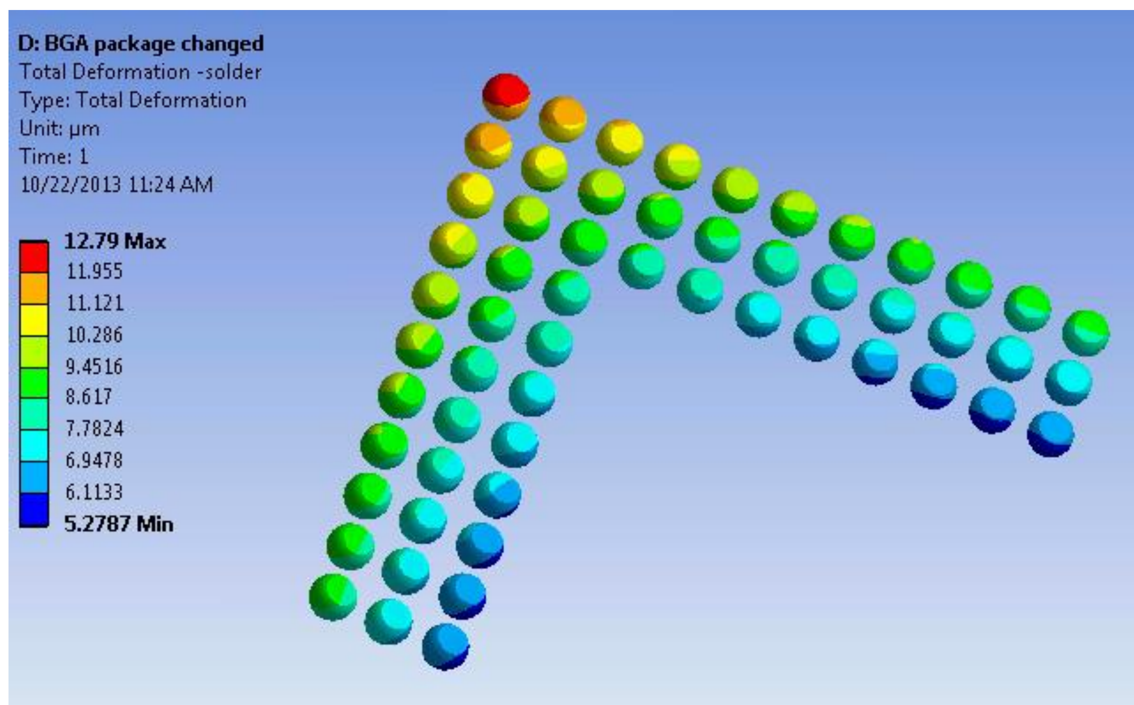

Figure 4.17. FEM analysis of Total deformation of solder joints in BGA assembly cooled from 150 °C to 22.5 °C, unit:um.

4.3.5.2 Grain Structure Change vs. Cooling Temperature

According to the mechanism, if other factors are fixed, increase the cooling temperature will increase the amount of plastic deformation and thus increases the possibility of

recrystallization in the BGA assembly. The assembly as described in Figure 4.15 was cooled from 180 °C and 165 °C with various cooling rate. All the samples are thermal aged at 150 °C for 500 hours before cooling. The grain structures were analyzed using the optical microstructure and shown in Figure 4.18. In case of medium cooling from 180 °C, all the solder joints in the assembly recrystallized and showed polygrain structure due to the high plastic formation. In the case of slow cool from 180°C, twins were formed in all the solder joints. With medium cooling from 165°C, all the solder joints recrystallized as well. Moreover, the FEM analysis of the deformation for assembly shown in Figure 4.17 indicates that the maximum deformation increases to 16um when cooled from 180 °C compared to 13um when cooled from 150 °C. All these results confirm that the mechanism suggested for recrystallization and grain structure evolution is reasonable. Moreover, it suggests that the grain structure of the solder can be tuned by one time thermal exposure and recrystallization and Sn-based solder can be triggered by the stored strain energy resulted from simply cooling.

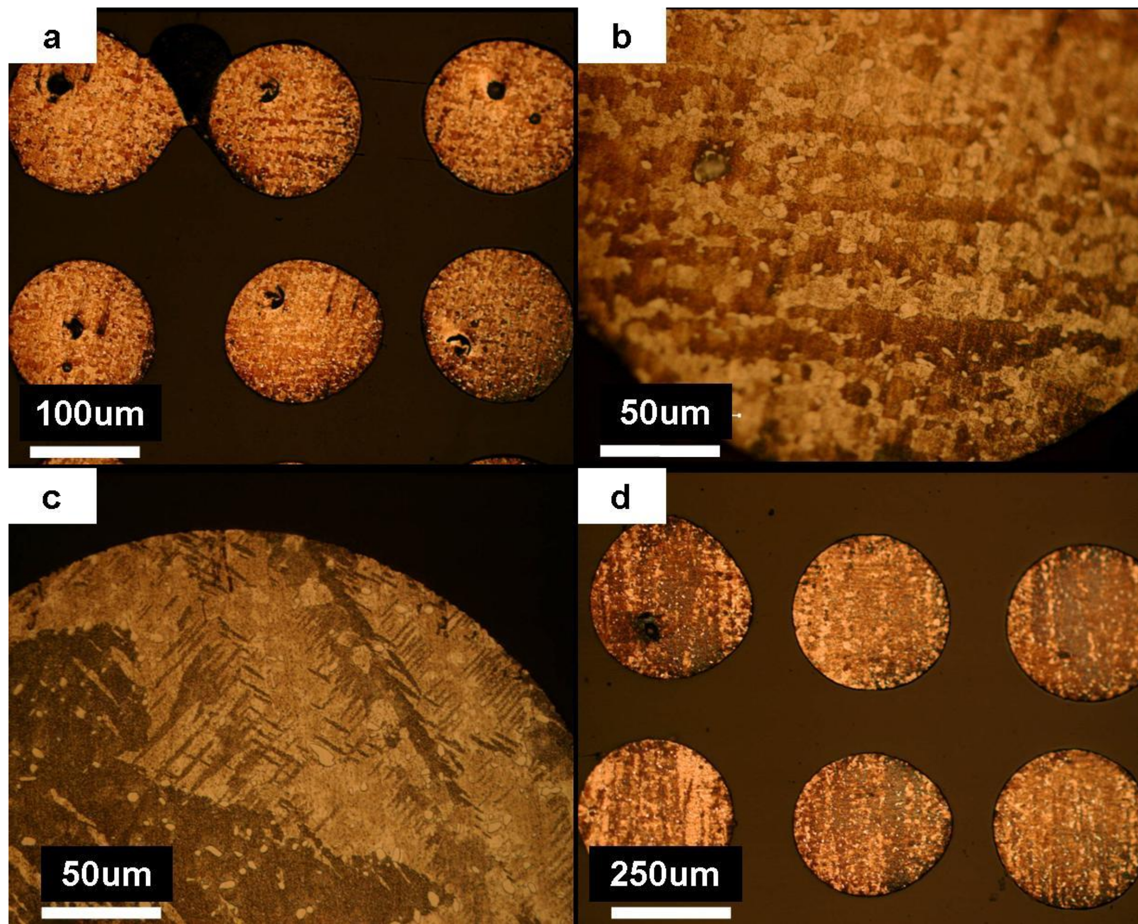

Figure 4.18. The optical microstructure of the 150 °C 500 hours thermal aged joint after (a) and (b) medium cool from 180 °C (c) slow cool from 180 °C, and (d) medium cool from 165 °C.

4.4 Implications

The grain structure evolution by recrystallization and mechanical twinning by one time thermal exposure indicate that tin-based solder alloys are much more susceptible to microstructure change. The stress/strain required for microstructure change is probably much lower than what is known. It suggests that the existing knowledge on tin and tin-alloys is so limited that more investigations are needed to fully understand the tin behavior under deformation, the mechanism of recrystallization and mechanical twinning. At the same time, the distinguish grain structure evolution from the results reveals a simple but effective way of altering the grain structure of tin-based lead-free solder which is very helpful to understand the

linkage between the microstructure and reliability. By conducting reliability tests for samples with different cooling rate, the reliability of solder joints with poly-grain, twin-grain and single grain can be evaluated.

Furthermore, the sensitivity of grain structure to cooling rate suggests that the processes involving cooling/heating, such as thermal cycling and reflow process, can cause huge microstructure evolution if cooling/heating rate is not well controlled. Moreover, the influence of the heating/cooling rate will be more pronounced as thermal cycling continues due to coarsening of IMCs which reduces the yield strength and thus the amount of plastic deformation. Therefore, it is more than necessary to track the microstructure evolution during heating/cooling when the assembly is subjected to thermal cycling, which may be ignored before.

Moreover, the dependency of grain structure on joint's position is very important in many aspects. First, it breaks the common assumption that the solder joints in the same assembly are the same. It shows that the solder joints can consist of different grain structures depending on the position after thermal exposure due to the variation on plastic deformation at different locations. Therefore, the solder joints at different locations preserve unique mechanical properties and thus the reliability behavior will be different. Second, since the plastic deformation varies with the joint's position and is highest at the corner where the residual thermal stress is the highest as well. Consequently, although the grain structure of the solder joint after reflow is more or less the same, as shown in Figure 4, due to the highest built-in residual stress, the corner joints will show inferior shear fatigue reliability as depicted in Figure 2. As a result, in addition to the external stress/strain added to the solder joints when conducting the reliability tests, such as shock, vibration, shear, et al. built-in residual thermal stress should be taken into account in order to evaluate the real reliability behavior of the solder joint in the assembly. Moreover, the impact of residual stress on the reliability will be more pronounced in solder alloys with high yield strength, such as SAC305. With higher yield strength, plastic deformation is more difficult to occur resulting in higher residual stress. In this sense, it is better

to use solder joints with low yield strength but there is a trade off with respect to fatigue resistance. In order to enhance the reliability of the assembly, methods to release the residual stress will be helpful. Also since the corner position is inherently weak, change the packaging design or simply store the packaging assembly at relative relatively high temperature for built-in stress relaxation will be useful. Overall, it will be very meaningful to find an effective way to reduce the residual stress influence on the reliability behavior of the solder joints in the electronic packaging assembly.

4.5 Summary

A series of cooling experiments are carried out to understand the grain structure evolution of Sn-based lead-free solder joint, mainly SAC105. The results show that recrystallization and deformation twinning of can occur by simply one-time thermal exposure. Polygrain structure induced by recrystallization is observed in SAC105. Moreover, the grain structure of the solder joint is found to be very sensitive to the joint location, cooling rate, cooling temperature, thermal history, joint composition and geometry of the assembly. The mechanism of the recrystallization is investigated. The driving force for recrystallization is to release the stored strain energy resulted from the plastic deformation during cooling after one-time thermal exposure. It indicates that the strain energy for recrystallization in Sn-based solder is far less than initial thought. The FEM analysis of the deformation during cooling indicates that the plastic deformation increased from the inner joint to the corner joint. Therefore, recrystallization is more susceptible at the corner joint, while the grain structure of inner joints is the most stable. While the cooling rate sensitivity suggests that there exists a competition between the recrystallization and dynamic recovery process. The recrystallization increases with cooling rate due to the suppressed dynamic recovery process. Furthermore, it is found that any change in plastic deformation, which can be induced by changing of yield strength, assembly structure and temperature of cooling, can induce different grain structure in the solder joint in BGA assembly.

CHAPTER FIVE

OABSERVATION OF DEFORMATION TWINNING AND ITS MECHANISM IN TIN-BASED LEAD-FREE SOLDER

5.1 Background

5.1.1 Deformation Twinning

Dislocation slip and deformation twinning are two fundamental plastic deformation modes in metals and alloys which allow materials to change shape under applied stresses. It is believed that in crystals with high symmetry having more than five independent slip systems dislocation slip is the major plastic deformation mode, while for those crystals with lower symmetry deformation Twinning is especially important. [145] For example, it was observed long time ago in B.C.C. and H.C.P. materials with low symmetry and a few slip systems. However, deformation twinning was also identified recently in some f.c.c metals and alloys when appreciable dislocation slip was recorded. Twinning is found to be very sensitive to temperature of deformation and to strain rate, the relative contribution of twinning to the overall plastic deformation increases as the temperature is lowered or the strain rate is increased. Very high strain rates, e.g. in shock-loaded or explosively deformed materials, often lead to twinning, and under such conditions, twins have been observed even in f.c.c. aluminum-magnesium alloys, which, according to conventional theory, should not twin because the stacking fault energy of aluminum is too high. Therefore, it is a common observation that deformation twinning operates preferable in materials with low symmetry, a few (less than five) independent slip systems, low temperature, and low stacking faults under high strain rates.

Deformation twins are formed, in principle, by a homogeneous simple shear of the parent lattice, and this implies highly coordinated individual atom displacements, in contrast to the apparently chaotic processes of generation and growth of slip bands during dislocation slip

deformation. It usually forms as individual thin plates embedded in the matrix or in contact with the free surface or a grain boundary. In the classical theory of deformation twinning, the original (parent) lattice is re-orientated by atom displacements which are equivalent to a simple shear of the lattice points, or of some integral fraction of these points. To describe the twin, four elements K_1, K_2, η_1, and η_2 are used, as shown in figure 5.1. K_1 is the first invariant plane under twin shear, η_1 is the shear direction, K_2 is the second undistorted (or conjugate) plane, P is the plane of shear which contains η_1 and the normals to K_1 and K_2, and η_2 is conjugate shear direction which is the intersection of K_2 and P. In some cases, the amount of shear, s is also used to describe the twin.

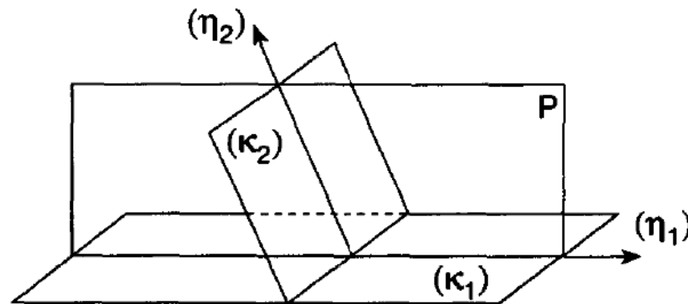

Figure 5.1.The four twinning elements. The twinning and the conjugate (or reciprocal) twinning planes are K_1 and K_2, and the twinning and conjugate (or reciprocal) twinning directions are η_1, and η_2, respectively. The directions η_1, η_2 and the normals to K_1, and K_2, are all contained in the plane of shear P. [145]

5.1.2 Deformation Twinning in Tin

Most of the lead-free solder is tin-based that tin consists more than 90% of the solder matrix. Different from lead-tin solder in which lead phase withstand the primary load, in lead-fee sold, the soft tin phase has to withstand the major load. Therefore, the microstructure of Tin and its plastic deformation behavior under thermo-mechanical load are very important for the integrity of the packaging assembly.

Tin has three allotropic forms, α or grey Tin, β or white Tin and γ Tin. The transformation of white Tin to grey Tin upon cooling occurs at 13.2 °C which is called Tin -cry or Tin-pest; while the transition from white Tin to γ tin happens upon heating at 202.8 °C. For the

applications with lead-free solder, β Tin is the most important one. Figure 2 shows the unit cell of body-centered-tetragonal (BCT) Tin and some common slip systems [128]. The crystal lattice parameters are a=0.58194 nm and c=0.31753 nm, thus c/a=0.54564. In this unit cell, there are eight atoms in the corners, one atom at the center, and four more atoms at locations such as [0, 1/2, 3/4] and [1/2, 0, 1/4]. The possible slip systems are: (110) [-111], (100) [001], (100) [010], (101) [-101], (121) [-101], et al. It has more than five independent slip systems so that plastic deformation by dislocation slip should be easier than twinning. However, deformation twinning is also identified in Tin crystal. It is found that the most common twinning plane is (301) with twinning direction [10-3], and twinning plane (10-1) with direction in [101] [11-12]. Table 5.1 describes the possible twins in Tin crystal using the four elements (K_1, K_2, η_1, and η_2) and twin shear (s). [146]

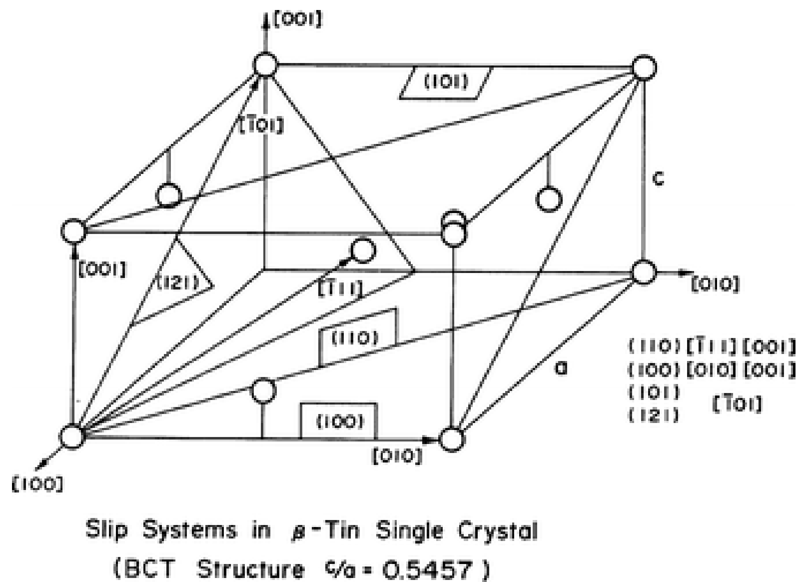

Figure 5.2 Crystallography of β-Sn structure and its possible slip systems. [128]

Table 5.1 Reciprocal twinning modes in β-Sn [146]

Structure	Twinning plane, K1	Twinning direction η_1	Second undistorted plane, K2	direction η_1	Plane of shear, p	Amount of shear, s
B.C.T a=5.8315, c=3.1814	{301}	<10-3>	{10-1}	<101>	(010)	0.0978
	{10-1}	<101>	{301}	<10-3>	(010)	0.0978

Although there are many observation and research on deformation twinning in Tin crystals dated back to 1950s, deformation twinning is believed to be very difficult in normal circumstance due to the high stacking fault energy, low melting temperature and easiness of dislocation slip during plastic deformation. There is no exact value of stacking fault energy found in the references, but it is believed to be higher than that of copper (80 ergs/cm^2). [147] the melting temperature of Tin is 230 $^{\circ}$C, which is low compared to most of the metals. The homologous temperature of Tin at room temperature is 0.6 such that dislocation should be easy to move. Consequently, due to the high stacking fault energy and low melting temperature, as mentioned before, plastic deformation by dislocation slip is much easier compared to deformation twinning in Tin and Tin alloys.

However, in the other hand, it is found that Tin is particularly susceptible to twinning by shock or impact loading with super high strain rate at temperature that is close to or lower than cryogenic temperature [149, 151-155]. It is found that mechanical twinning of Tin takes place in three stages: nucleation of small twin under local stress, propagation of twin and thickening of the twin by twin boundary migration in the direction normal to the twin plane. Two criteria are used to explain the requirements for twin nucleation in deformation twinning: critical resolved shear stress criteria and energy criteria. In the first case, it believes that deformation twinning

only occurs when the applied shear stress exceeds a critical resolved shear stress value or plastic deformation by dislocation slip will be preferred. There are many observations on critical resolved shear stress for deformation twinning in Tin, but with some discrepancy. Ishii et al used the Impact loading on Tin single crystal and found the critical stress for initiation twinning scattered between 7 MPa and 25 MPa. [151-152] Maruyama et al. carried out the compression at temperature between -80°C to 20°C and found that the shear stress needed for twinning initiation is about 5-10 MPa with strain rate ranging from 0.025 /s to 2.5 /s.[153] Overcash et al, found the shear stress needed for Sn single crystal whiskers is around 74 MPa.[150] All these investigations indicate that the critical resolved shear stress criteria is not well defined that many factors contribute to the value of critical resolved shear stress for Tin twinning such as defects in the crystal, temperature, geometry of the sample, accompaniment of dislocation slip with twinning, and discontinuity of twinning. In the other hand the energy criteria is more reasonable when strain rate effect is considered during twinning. It is common observation that twinning is favored during impact, shock, and ultrasonic loading with high strain rate. Dislocation slip causes small amount of shear but in a large number of adjacent lattice sites which require diffusion of dislocations in the lattice and thus it necessitates a critical period of time; while during twinning, it occurs over a stack of planes but in less number of sites which need less time. These considerations lead to the postulation that the energy change is the driving force for twinning deformation.[156] Although this criterion appears to be more reasonable, few experimental works were conducted to confirm the validity. The former critical resolved shear stress criterion has received the most attention although the critical value for the twinning in Tin single crystal is not consistent and determined. Overall, the mechanism of deformation twinning in Tin or Tin-base alloys is an extremely complex process and further investigation is needed.

Based on all the observations, one consistent conclusion with regarding to the deformation twinning in Tin is that it occurs only when the strain rate is super high or the temperature is low. However, surprisingly, it is found that deformation twinning of SAC105

solder joints in the assembly can occur simply by cooling after one time thermal exposure in this study on Lead-free SAC solder joints in BGA assembly. In this chapter, the possible mechanism of deformation twinning in BGA assembled SAC105 solder joints is proposed along with further experimental studies on the deformation twinning supporting the proposed mechanism. It is believed that the hydrostatic pressure stress plays an important role in activating the deformation twinning which promotes the plastic deformation by twinning while prevents dislocation sliding. In addition, the potential impact of such mechanism and twin formation to the reliability of solder joint in the packaging assembly is discussed.

5.2 Samples and Experiments

The samples under investigation are the same as in the previous chapter for grain structure investigation, which are shown in figure 4.4 and figure 4.15. The BGA assembly is processed using an industry standard reflow process, which involves steady heating up to ~260 °C and slow cooling to room temperature after a short holding period at the reflow temperature. Samples were thermal aged at 100 °C or 150 °C for 24 hours, 500 hours and 1000 hours, and subsequently cooled to room temperature in water, air or in the oven with various cooling rate. The cooling rate was determined to be 50 °C/s, 0.3 °C/s, and 0.01 °C/s, respectively. For microstructure observation, cross-sections of the samples were made by modeling in epoxy, following with sandpaper polishing, micro-polishing with Alumina powder and 5% HCl etching. Microstructure of the solder joint is investigated by Optical Microscope, Scanning Electron Microscope (SEM) and Electron Back Scatter Diffraction Microscope (EBSD).

The stress and strain analysis after cooling is carried out by ANASYS using quarter or 1/8 model. The material constants related to the simulation and the structure parameters for the model are listed in table 4.1 and table 4.2.

5.3 Results and Discussion

5.3.1 Observation of Twins in Tin-based Lead-free SAC Solder

As seen in figure 4.9 and figure 4.10, twins exist in solder joints after thermal aging at 150 °C for 500 hours and cooling to room temperature by water quench or air. There are three types of twins depending on the formation process: nucleation and growth twin (solidification from vapor or liquid, annealing, or recrystallization), transformation twin (similar to twin forms during martensitic transformation), and deformation twinning. First, it is not the first case because twins do not exist in as-reflowed sample nor slow cooled sample which means they are formed during reflow process or thermal annealing process. Besides, twins formed in the first case are quite large and relatively perfect, but the twins here are narrow and thin. Second, transformation twins are highly organized and the alternate twin lamellae of fixed thickness ratios form regular arrays. In contrast, deformation twins are usually thin and in ellipsoid shape. Based on the thin and imperfect shape of the twins seen in Figure 4.9 and figure 4.10, it is believed that they are more likely deformation twins. In addition, because the temperature is above the cryogenic temperature, phase transformation from white tin to grey tin, also known as tin-cry, is not possible. Furthermore, if it is growth twin, then even at slow cooling rate, twins should also be presented in the matrix. Therefore, based on the shape and the possible formation process, these twins are believed to be deformation twins.

In the other hand, in order to further confirm the twin formation mechanism, a simple experiment was carried out. The sample with SAC105 solder joints was polished and the microstructure without any thermal exposure was taken, showing classical grain structure with no twins in the matrix. Subsequently, the sample was put into the oven and heated up to 150 °C. After 24 hour, the sample was taken out and cooled to room temperature by water. Immediately the optical microstructure was taken after cooling shown in Figure 5.3. Macroscopic twins are seen in solder joints right after cooling which means that they are formed during cooling (deformation twinning) not after cooling (growth twin).

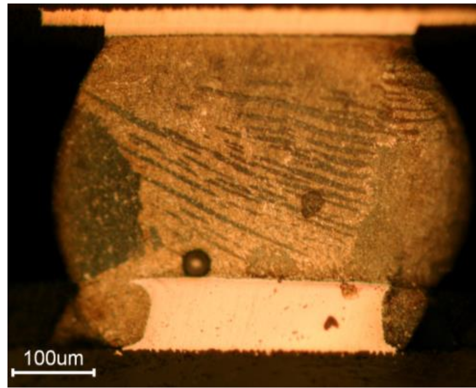

Figure 5.3 Optical images of solder joint after aging at 150 °C for 24 hours and water quenched.

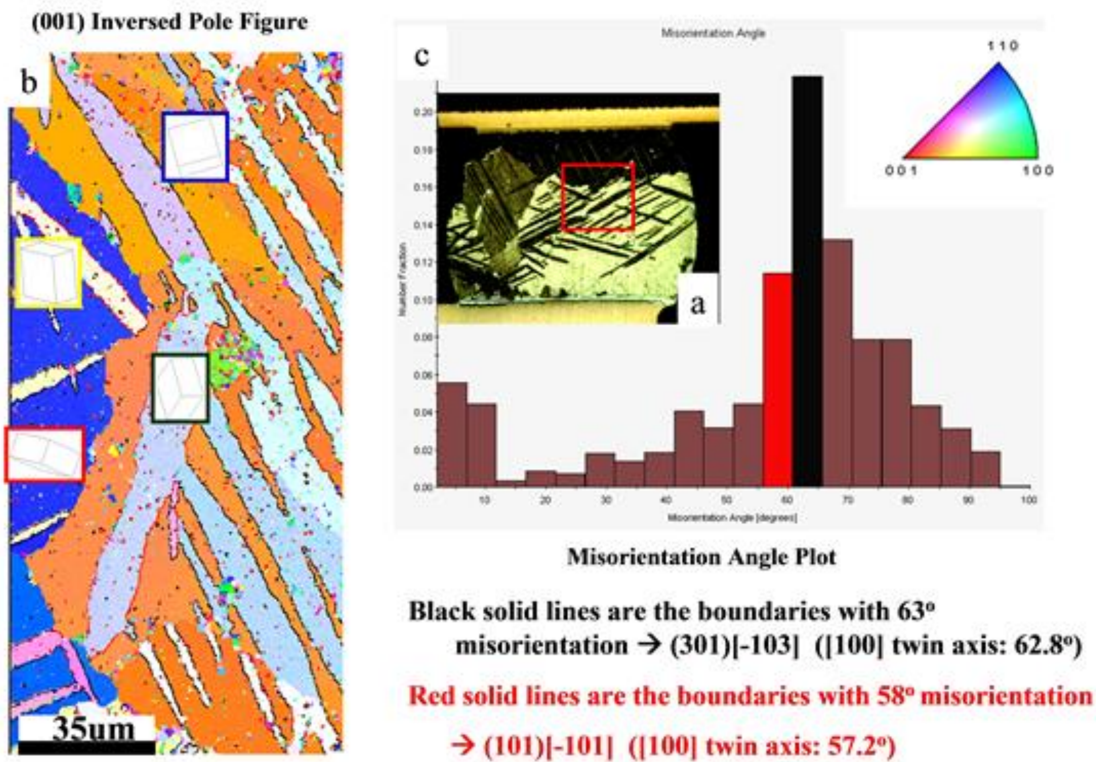

Figure 5.4. EBSD analysis of the twin (a) optical image of water quenched solder joints after 150 °C 500 hour thermal aging; (b) (001) inversed pole figure of the red rectangular area in (a); (c) misorientation angle plot.

Further analysis using EBSD was carried out to analyze the twin structure. Figure 5.4 (a) is the optical image of the 150°C 500 hours aged and water quenched sample. The red rectangular is the area where the EBSD image was taken. Figure 5.4 (b) is the (001) inversed

pole figure showing four major different orientations indicated by the cubes represent the unit cell in the twin area. There are some other colors refer to different orientations in Figure 5.4 (b), but they can be fake-signals because the quality of the EBSD image is highly depending on the sample surface condition and the resolution of the EBSD. Figure 5.4 (c) shows the misorientation angles between the boundaries shown in Figure 5.4 (b). The major misorientation angles are 63° and 58°, and they correspond to the boundaries in solid black lines and red lines in Figure 5.4 (b), which are close to the misorientation angle of (301)[-103] and (101)[-101] twin boundaries, respectively. It is found that (301)[-103] twin with [100] twin axis is the most possible twin found in Tin and the misorientation angle between the parent and the twin is 62.8°, while (101)[-101] twin with misorientation angle 57.3° can also occur. According to Figure 5.4 (b) and (c), it can be determined that the twins formed during cooling are mostly (301) [-103] twins which assigned as yellow and light blue in inversed pole figure and some are (101) [-101] twins assigned as blue and white.

As mentioned, deformation twinning as a plastic deformation mode in Tin is very difficult unless the strain rate is super high or temperature is very low. While the observation of deformation twins simply induced by cooling from 150 °C to room temperature at intermediate strain rate indicates that deformation twinning in Tin or Tin alloy is easier. The possible mechanism of deformation twinning and affecting factors need to be understood.

5.3.2 Factors Affect the Deformation Twinning Behavior During Cooling

Chapter 4 has described the grain structure evolution of the solder joint by one-time thermal exposure in detail. The grain structure map is shown in Figure 4.11 which describes how grain structure distributes in the BGA assembly with respecting to the joint position, cooling rate and thermal history. Same as recrystallization, deformation twinning also depends on the on the cooling rate, joint position and thermal history. It is found that deformation twinning occurs more readily with the cooling rate increasing. It makes sense because deformation twinning is known to occur at high strain rate where dislocation does not have enough time to

move. Moreover, deformation twinning happens more often in the corner and edge position than in the inner solder joints. As discussed in chapter four, the plastic deformation in the assembly increases from the inner to the corner position, so that the deformation twinning as the major plastic deformation mode increases from the inner position to the corner position. Meanwhile, as seen in the map, the twinning dependency on the thermal history is not as much as recrystallization. Deformation twinning can occur by simply increase the solder to elevated temperature and then cool to the room temperature without thermal aging, while certain thermal aging is required to reduce the strength of the solder before recrystallization could occur for recrystallization due to the difference in driving force. In the case of deformation twinning, the resolved shear stress should exceed the critical resolved shear stress for twinning; in the other hand, the driving force for recrystallization is the stored strain energy resulted from the plastic deformation.

One thing needs to be mentioned here is that in Figure 4.11, for water quenched 150°C thermal aged samples, no twins are found in the solder matrix which seems contradictory to the overall theory. Deformation twinning should be more ready to occur as cooling rate increases so that if it shows in solder joints with medium cooling rate it should also present in the joint with fast cooling rate. It is believed that the absence of twins in fast cooled corner joint matrix is due to the recrystallization. In order to reduce the stored strain energy after plastic deformation, recrystallization happens by removing the dislocations including the twin boundaries and creating new grains. Therefore, unless taking the microstructure image right after cooling before recrystallization occurs, no twins can be found in these samples. Therefore, it is believed that deformation twinning does occur in recrystallized solder joints but the twin boundaries disappear after recrystallization.

5.3.3 Proposed Deformation Twinning Mechanism

The twins seen in the SAC105 solder joints in the BGA packaging assembly was identified and confirmed to be deformation twins, though it is hard to believe. This poses new

challenges in terms of understanding the mechanism. Deformation twinning in tin and tin-alloy is so difficult to occur due to the high stacking fault energy and low melting temperature, unless it is under high strain rate impact, ultrasonic vibration and low temperature. Deformation twinning and dislocation slip are two major and competing plastic deformation modes in metals and alloys. At normal circumstance, dislocations in Tin and Tin-alloys should be free to move while dislocation slip should be the major plastic deformation mode. Therefore, to understand the mechanism, it is critical to answer what causes the dislocation difficult to slip while promotes the deformation by twinning. One of the possible explanations is hydrostatic pressure stress. It is known that shear stress induces dislocation glide and twinning, but how hydrostatic pressure stress can affect the dislocation glide and twinning is not fully understood. According to the conventional critical resolved shear stress for twinning theory, deformation twinning activates when the resolved shear stress exceeds the critical resolved shear stress for twinning. Similar theory applies to dislocation slip as well. When the resolved shear stress exceeds the critical resolved shear stress for slip in the slip plane, dislocation slip activates. Subsequent question is: how hydrostatic pressure stress influences the resolved shear stress for twinning and slip.

In one hand, it is found in some metal and alloy systems, such as BCC Mo and Cu alloys, the tension/compression stress can either prevent or promote mechanical twinning. [158-160] It is said that the critical resolved shear stress for twinning in Mo decreases with increasing tension stress, while under compression a dislocation loop of (011)[-1-11] nucleates instead of (112)[-1-11] twinning in Mo [158-159]. In the other hand, in Cu-4.9% Sn (atomic percentage) alloy with mixture grain orientations of [111] and [100], twinning volume fraction is higher under compression than under tension because the Schmid Factor for twinning is larger under compression (0.48) than under tension (0.32) [160]. At the same time, since dislocation glide is a diffusion process, hydrostatic pressure stress will affect the dislocation glide more than deformation twinning. Under hydrostatic pressure stress, the space between dislocations is tighter thus diffusion is slower. However, no report showing the impact of hydrostatic pressure

tress on the deformation twinning behavior in Tin is found, it is believed that the hydrostatic pressure stress plays an important role in the deformation twin formation seen in Tin-based solder alloy here.

In the other hand, in Figure 4.11, deformation twinning occurs at the corners and edges while not at the inner positions indicating that dislocation slip is prevented at the corners and edges while not at the inner positions. This may due to the difference in hydrostatic pressure stress with respect to the position of the solder joint. Figure 5.5 is the simplified configuration of the solder joints in BGA assembly where the UBM (under bump metallization) is ignored. The solder joints were sandwiched between the Silicon die (top) and FR4 PCB board (bottom). During cooling/heating, due to the CTE mismatch, solder joints were under non-uniform thermal stress consists of shear stress and hydrostatic pressure stress. Both the hydrostatic pressure stress and shear depend on the solder position. If same as Mo and Cu-4.9%Sn alloy, the hydrostatic pressure stress causes a reduction in critical resolved shear stress for twinning and an increasing in critical resolved shear stress for dislocation slip in tin-based solder alloys, then as shown in Figure 5.6, there exists a critical hydrostatic pressure stress (σ_c) that if pressure stress exceeds the value, twinning is preferred, while smaller than the value, dislocation glide is dominant. The hydrostatic pressure stress in the corner and edge is larger than in the inner joints that it exceeds the critical hydrostatic pressure stress (σ_c), so that when the corner and edge solder joints are able to undergo twinning when plastic deformation occurs, while the inner solder joints either does not deform plastically or deform by dislocation glide mode.

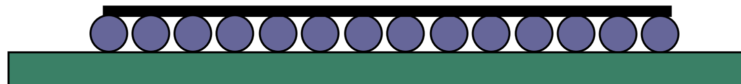

Figure 5.5 Simplified configuration of the solder joints in BGA assembly.

Based on observation and existing theory in other metal-alloy system, it is believed that hydrostatic pressure stress is critical for the deformation twinning seen in tin-based lead free

solder during cooling that it prevents the dislocation glide while promotes deformation by twinning in tin by lowering the critical resolved shear stress for twinning while increasing the critical resolved shear stress for dislocation glide.

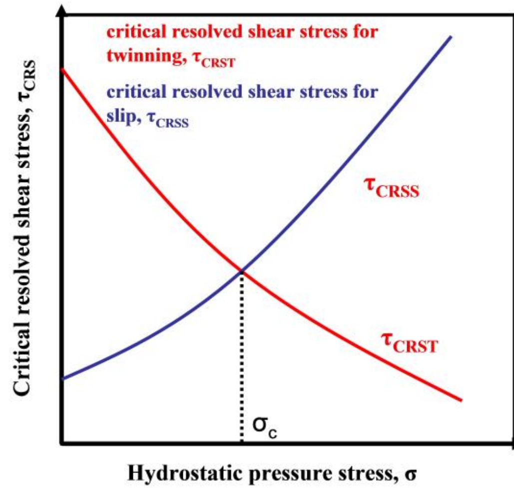

Figure 5.6. Change of Critical resolved shear stress for dislocation slip and twinning with hydrostatic pressure stress.

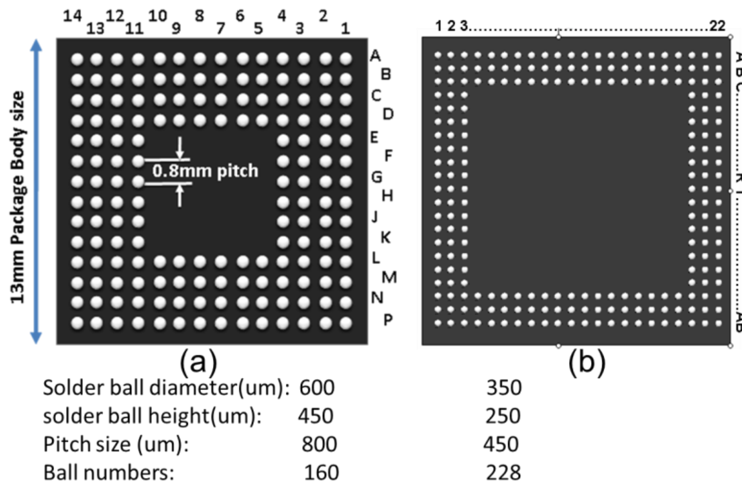

Figure 5.7 The schematic drawing of the solder joints layout in BGA packaging assembly.

5.3.3.1 FEM Analysis of the Hydrostatic Pressure Stress in Solder Joints under Cooling

To understand and confirm the mechanism, the hydrostatic pressure stress in the solder joints under cooling was calculated using ANASYS. Two BGA assemblies were investigated in this research, and the schematic drawings are shown in Figure 5.7. The 3-D configuration was constructed by Pro-Engineer as shown in Figure 5.8. Since the assembly is symmetric, quarter model (sometimes 1/8 model) is used to reduce the computation time. The stress free state is assumed at the maximum temperature before cooling. Details of the BGA features used in the thermal stress computation are summarized below:

- Chip size:1cm x 1 cm x 0.275 mm
- Packaging size: 1.3 cm x 1.3 cm x 0.1 cm
- BT substrate thickness: 0.25 mm
- Solder joints diameter:600 um/350 um
- Solder joints height:400 um/250 um
- Pitch size: 800 um/450 um

The material property parameters needed for analysis are listed in table 5.2. ANSYS and the Von-Mise criterion are used for analyzing the stress state.

Table 5.2. Material constants for FEM analysis

Materials	E(σPa)	CTE(ppm/^{o}C)	ν
Silicon	131	2.8	0.28
Copper	129	17	0.34
Substrate	16.8	16	0.3
PCB	26.2	18	0.3
EMC	20	9	0.3
solder	96.9	15.8	0.42

With the stress analysis, the hydrostatic pressure stress, which equals to $(\sigma_{xx}+\sigma_{yy}+\sigma_{zz})/3$, can be calculated for each solder joint in the BGA assembly in case of cooling from various

temperatures. The change of hydrostatic tension with position and cooling temperature can be calculated.

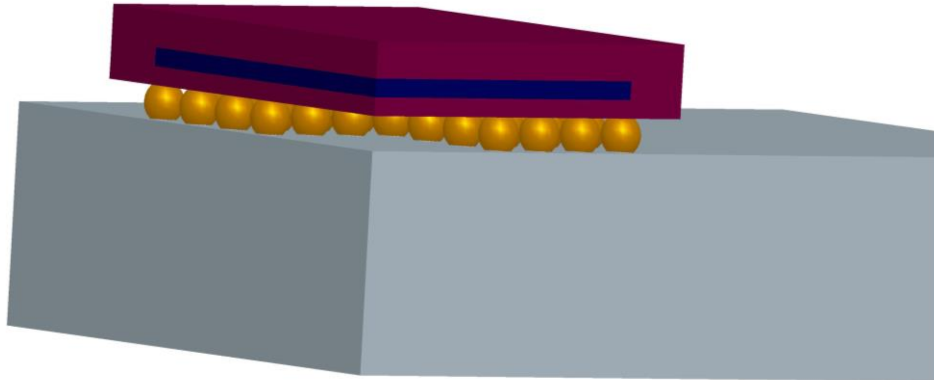

Figure 5.8. 3-D Quarter model of the BGA assembly

Figure 5.9 is the 1/8 model showing the hydrostatic pressure stress distribution in the BGA assembly when it was cooled from 150 $^{\circ}$C to room temperature for configuration 5.7(a). The result indicates that the solder joint is under asymmetric hydrostatic pressure stress. The middle of the solder joint is under tension while the outer is under compression, and this is displayed in figure 5.10 as well. Two important findings can be seen from Figure 5.10. First, the hydrostatic pressure decreases from the corner to the center and the maximum hydrostatic pressure stress exists in the corner joint. Second, volume fraction of compression to tension stress decreases from the corner position to the center. In other words, it is noticeable that almost the whole corner solder joint is under hydrostatic compressive stress, while for the center joint, the whole solder joint is under hydrostatic tension stress. Combining the simulation results with the microstructure observation, the deformation twinning is sensitive to the joint position that corner joint is most prone to twinning, and it is believed that the hydrostatic pressure stress is very critical for the deformation twinning behavior in tin-base solder alloy. Since the hydrostatic pressure stress decreases from the corner to the center, according to Figure 5.6, the critical resolved shear stress for twinning should increase from the corner to the center; while at the same time the shear stress in the solder joint also decreases from corner to

the center. As a result, the corner joint is easier to twin than the joint in the corner. In conclusion, the hydrostatic compression stress decreases the critical resolved shear stress for twinning and favors deformation twinning. At the same time, hydrostatic compression stress increases the critical resolved shear stress for dislocation glide and dislocation movement is confined.

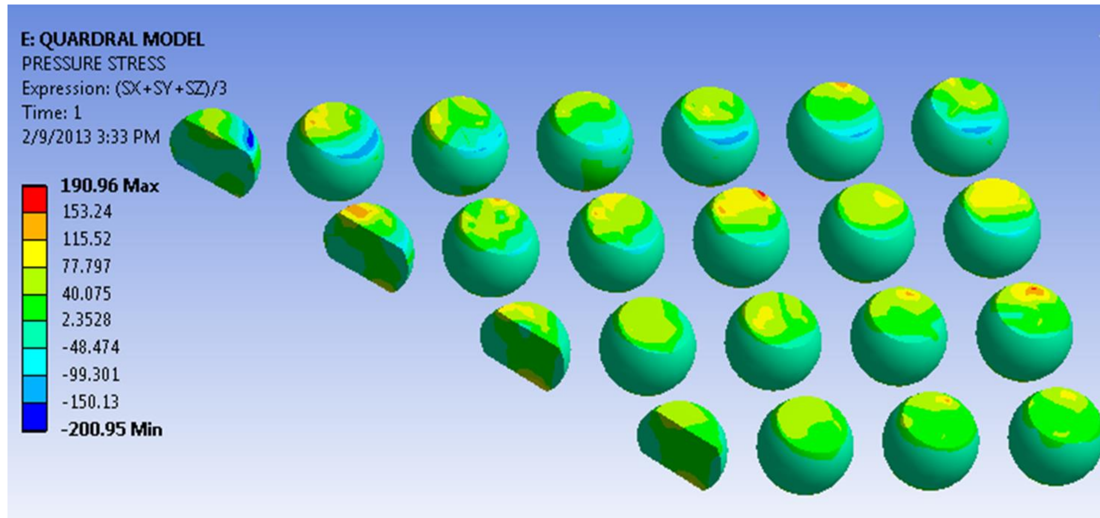

Figure 5.9. 1/8 model showing the hydrostatic pressure distribution in the solder joint in BGA assembly after cooling from 150 °C to room temperature.

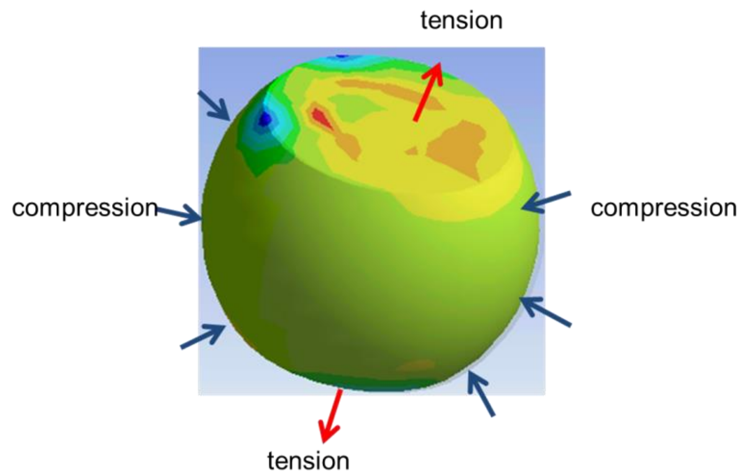

Figure 5.10 Hydrostatic pressure stress distribution in the solder joint after cooling.

Moreover, from this simulation, the critical hydrostatic compression stress for deformation twinning to occur is estimated to be 200MPa. Also, it is obvious that the deformation twinning is preferred when hydrostatic compression stress exists within the solder joint. Moreover, according to the deformation twinning theory, deformation twin forms by two stages, nucleation and growth. It says that the shear stress required for twin growth is lower than the force needed for twin nucleation. It is highly possible that the hydrostatic compression stress promotes not only the nucleation but also the growth of the twin.

5.3.3.2 Deformation Twinning vs. Cooling Temperature

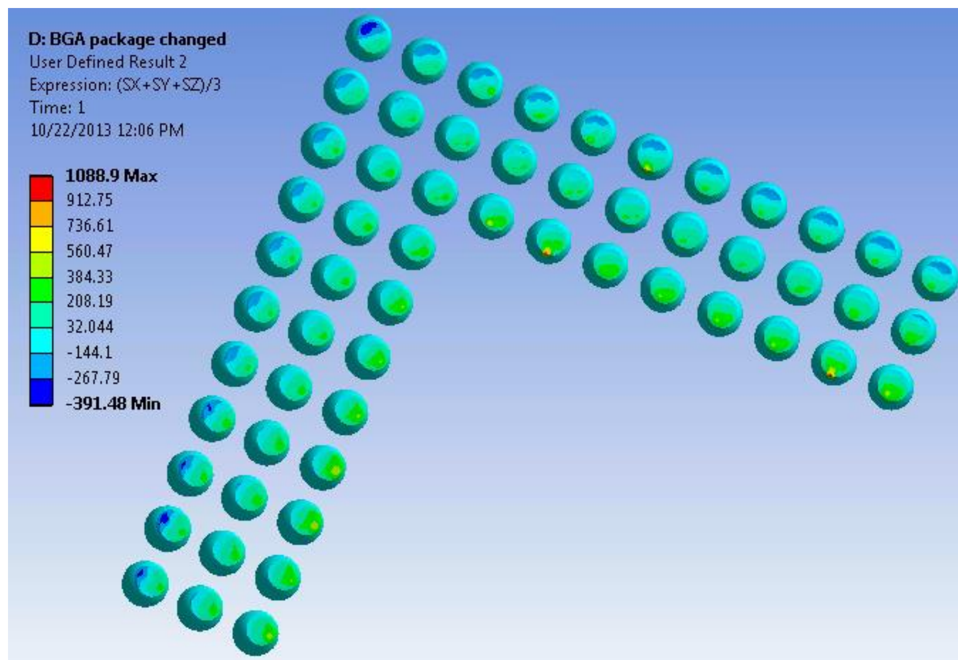

Figure 5.11 The hydrostatic pressure distribution in solder joints in BGA assembly when cooling from 180 °C.

In order to find out how hydrostatic pressure stress influences the deformation twinning behavior of the tin-based solder alloy, different cooling temperatures is introduced. It is expected to see that as cooling temperature increases the hydrostatic compression stress as well as shear stress in the twin plane would increase, thus deformation by twinning would be

more aggressive. Simulation was carried out to find out the hydrostatic pressure stress changes with temperature and the results are shown in Figure 5.11. As revealed by the simulation, both hydrostatic tension and compression in the solder joints increase with cooling temperature. As the cooling temperature increases from 150 °C to 180 °C, the maximum hydrostatic compression stress increases from 315 MPa to 391 MPa.

At the same time, microstructures for assembly shown in Figure 5.7(b) cooled from various temperatures are investigated and shown in Figure 5.12. One important point to be mentioned here is that the joint with polygranular structure goes through deformation twinning yet twins are not shown in the microstructure just because they are removed by the subsequent recrystallization process. As a result, revealed in Figure 5.12(b), when cooling the solder from 180 °C to room temperature with fast cooling rate, all the solder joints in the assembly deforms by twinning and then recrystallizes due to the increased plastic deformation and hydrostatic pressure stress. Meanwhile, in case of sample fast cooled from 165 °C, shown in Figure 5.12(c) and (d), all solder joints twins but only some of them show recrystallized Polygrained structure. In case of fast cooling from 150°C, indicated in Figure 5.12 (a), deformation twinning is found to be also prevalent in all the solder joints but recrystallization does not occur.

To summarize the microstructure dependency on cooling temperature and solder joint position: all the solder joints plastically deformed by mechanical twining regardless of joint position and cooling temperature. Then the question is why the dependence contradicts with the previous result shown in Figure 4.11. This is due to the difference in assembly layout. Figure 4.11 corresponds to the configuration shown in Figure 5.7(a), and Figure 5.12 corresponds to configuration (b). Because there are only three rows of solder joints in the latter layout that the solder joints distances to the center are further and also the solder joints are smaller in size, the hydrostatic compression stress and shear stress at the inner solder joints are larger compared to the ones in configuration (a). It is found that the maximum compression stress in (a) is 550MPa at the corner joint and 150MPa at the inner joint, while in the second one it is 315MPa

in the corner joint and 200MPa in the inner solder joint. In configuration (b), even the innermost row solder joints, compression stress is high enough to trigger deformation twinning, but in configuration (a), the inner rows are much closer to the center that the compression stress is not high enough for deformation twinning to occur. Alternatively, when configuration (a) is cooled from 100°C to room temperature, only corner joint exhibit deformation twins due to the reduced hydrostatic compression stress and plastic deformation. At the same time, it is noticed that recrystallization in solder joints in configuration (a) is easier than in the configuration (b) that no polygrains are observed in solder joints in configuration (b) when they are fast cooled from 150°C to room temperature. This is due to the reduction in plastic deformation and thus the stored strain energy for recrystallization in configuration (b) compared to (a).

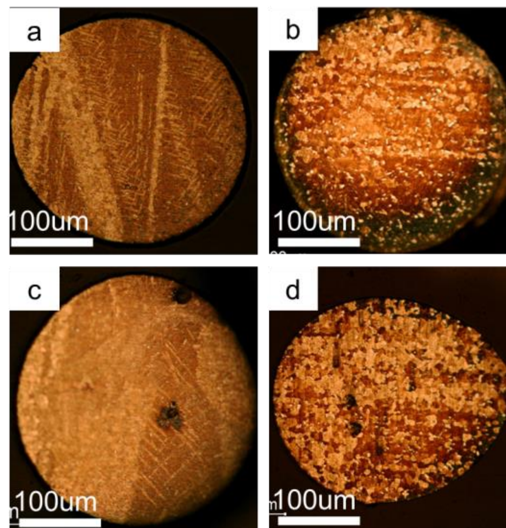

Figure 5.12 optical image showing the grain structure of SAC105 solder joint after cooling from (a)150 $^{\circ}$C, (b)180 $^{\circ}$C, and (c)and (d)165 $^{\circ}$C.

The above results show the change of deformation twinning behavior with cooling temperature and it suggests that the hydrostatic pressure stress is very critical for twinning to occur. As long as hydrostatic compression stress is high enough (about 200MPa) and plastic deformation occurs, deformation twinning activates in the tin-based lead-free solder.

5.3.3.3 Deformation Twinning vs. Cooling Rate

Besides cooling temperature and joint position, mechanical twinning in tin-based solder alloy also exhibits cooling rate dependency that it increases with increasing cooling rate. It is found that twinning occurs when cooling the samples by fast water quench or medium air cool. If slowly cooling the samples in the furnace, then regardless of the cooling temperature and geometry of the assembly, no twinning will occur. The cooling rate sensitivity, in other words strain rate sensitivity, is very common phenomenon seen in other materials as well. To explain the strain rate sensitivity, energy model instead of critical resolved shear stress theory is applied which states that the stored energy has to exceed critical energy for twinning. The challenge here is the strain rate even with fast cooling rate is low compared to the conventional strain rate needed for twinning to occur in tin-based alloy. It is found that mechanical twinning in tin is very sensitive to impact load when the strain rate is as high as 2.8 /s, and the critical resolved shear stress for twinning is found to vary between 12.4 MPa to 44.13 MPa. In this study, the strain rate ranges from 0.008 /s to $5X10^{-7}$ /s, which is very low compared to the strain rate in impact load. Therefore, it is believed that hydrostatic compression stress which confines dislocation movement by gliding is the key for deformation twinning to occur at such low strain rate.

5.4 Conclusions and Implications

The deformation twinning seen in tin-based solder alloy, specifically SAC105 solder, poses a big challenge in understanding the deformation twinning mechanism. However, our observation and analysis suggests that hydrostatic compression stress coming from the surrounding confine components is very critical for this phenomenon. It is believed that the hydrostatic compression stress reduces the critical resolved shear stress for twinning while increases the critical resolved shear stress for dislocation slip. According to the stress analysis, the hydrostatic compression stress increases from the center to the corner which makes the twining in the corner solder joint easier than the solder in the other positions. Therefore, deformation twinning in the packaging assembly shows position sensitivity. Also, due to the

increase of hydrostatic compression stress and plastic deformation with increasing temperature, as cooling temperature increases, deformation twinning occurs more readily.

The impact of the hydrostatic compression stress on the deformation twinning behavior in tin is very surprising and possesses scientific as well as industrial importance. First, it suggests new twinning mechanism that mechanical twinning is not necessary to occur at super high strain rate or low temperature, and the hydrostatic compression stress could promote twinning. Second, it suggests a way to introduce twins if it is needed, because some researches indicate that twins could enhance the strength of the material. Third, it implies that twinning in tin-based solder is much easier than expected that it has to be really careful when handling the sample to avoid applying hydrostatic compression stress in the solder which may cause plastic deformation by twinning.

As a summary, this chapter introduces a new mechanism associates to the deformation twinning in tin and tin-based alloy together with experimental, simulated and theoretical explanations.

CHAPTER 6

SENSITIVITY OF FATIGUE RELIABILITY ON GRAIN STRUCTURE

6.1 Background

Up to now, the grain structure evolution of tin-based lead-free solder in electronic packaging during one time thermal exposure and the mechanism related to the grain structure change was discussed. It is found that by one-time thermal exposure and cooling, poly-grain, twin and classical beach-ball structure can be developed in the Sn-Ag-Cu solder joint in BGA assembly. This suggests an ideal way of studying the grain structure impact on the reliability of the solder joints, specifically how fine grain structure and twin affect the fatigue failure. At the same time, a shear fatigue test was introduced and proved to be a good way of evaluating the fatigue reliability of the solder joint in packaging. It is a good way to extract the fatigue properties, specifically fatigue ductility coefficient, ductility exponent and frequency exponent for the solder. With these information ready, the following step is to study how the fatigue behavior changes with grain structure. The scope of this chapter is to evaluate the grain structure influence on the fatigue reliability of the tin-based solder joint in electronic packaging.

6.2 Experiment

The as received SAC105 and SAC305 samples were stored in the furnace at 150 $^{\circ}$C for 500 hours and then cooled to room temperature with different cooling rates to produce various grain structures: poly-grain, twins, or classic beach-ball structure. Subsequently, shear fatigue tests were carried out for these samples at room temperature, 1Hz, 100mA and various shear displacements (strains). The resistance was tracked to record the failure lifetime and location. The microstructures were investigated by optical microscope and SEM.

6.3 Results and Discussion

6.3.1 Fatigue Reliability vs. Cooling Rate

Fatigue test of SAC105 and SAC305 were carried out by the cyclic shear fatigue tester described in the previous chapters. The shear strain was set to 2%, frequency was 1HZ, and testing temperature was 25 $^{\circ}$C. SAC105 sample were aged at 150 $^{\circ}$C for 500 hours. Figure 6.1 shows the fatigue lifetime of the solder joints at fast, medium and slow cooling rates. It indicates that the fatigue lifetime of the solder joint decreases with increasing cooling rate: slow cool>medium cool>fast cool. Specifically, the fast cooling makes the fatigue life decrease by 47%. As discussed in chapter four and chapter five, fast cooled sample composed of Polygrained structure, medium cooled sample has twins, and slow cooled sample preserved classical beach ball structure. Therefore, the shear fatigue results may appear to suggest that the polygranular joint structure is most susceptible to the fatigue while beach ball structure is the best in terms of resisting fatigue induced fracture. However, the observation is the opposite. Tracking of the failure location reveals that the failure in fast cooled sample does not occur at the most fatigue prone position of the assembly. This behavior is shown in Figure 6.2 where resistance tracking data for 1st row and 2nd row of assembly is shown. Note that fast cooled samples fail first at the 2nd row not at the 1st row. The same is found from the samples with medium cooling rate. In the case of slow cooling, the failure location is found to be fixed at the corner joint. It was mentioned in chapter two and three that the most fatigue prone joint in the assembly is the corner (or near to the corner) joint. It is most fatigue prone because the joint has the highest residual stress unless released by some other mechanisms. However, in the case of fast cooling and medium cooling, the failure location is not fixed at the 1st row but at the 2nd row of the assembly. This result contradicts the results tested from all other samples cannot be explained without accepting the existence of strengthening mechanism of the joints in the 1st and 2nd rows. These 1st /2nd row joints are either recrystallized (corner) or heavily twinned. It is

therefore reasonable to conclude that the joint with polygranular structure or heavily twinned structure is much more resistant to fatigue than the joint with beach ball structure.

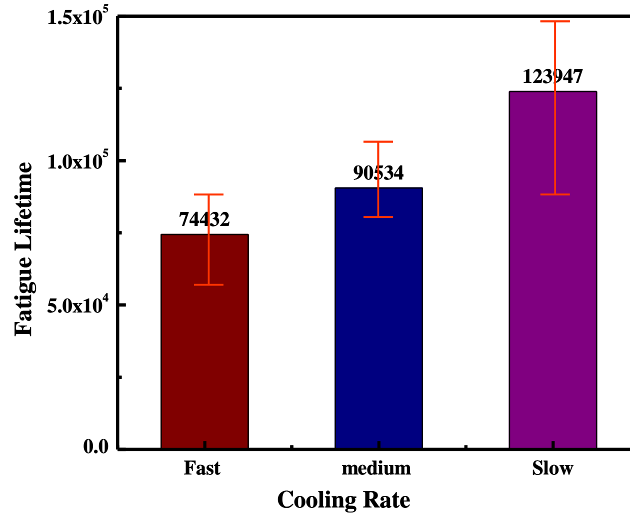

Figure 6.1 Fatigue lifetime of 150 °C 500 hour aged SAC105 cooling with fast, medium and slow rate, at strain 2%, 1Hz, room temperature.

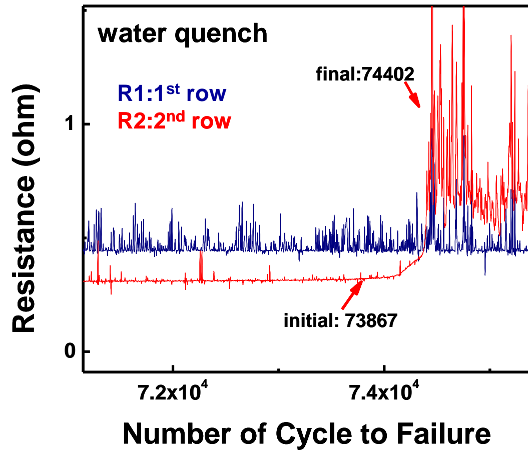

(a)

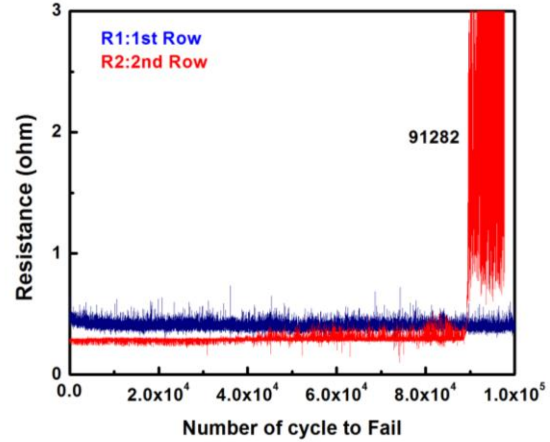

(b)

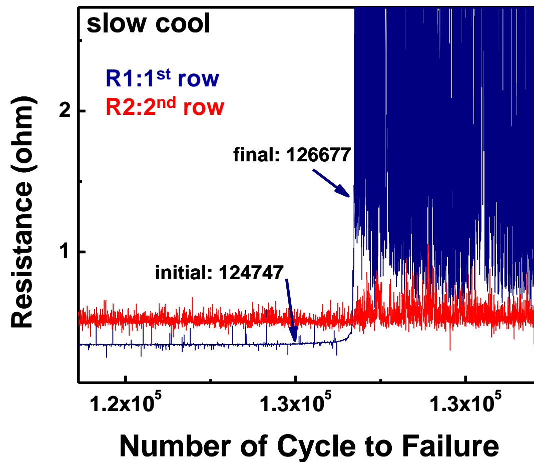

(c)

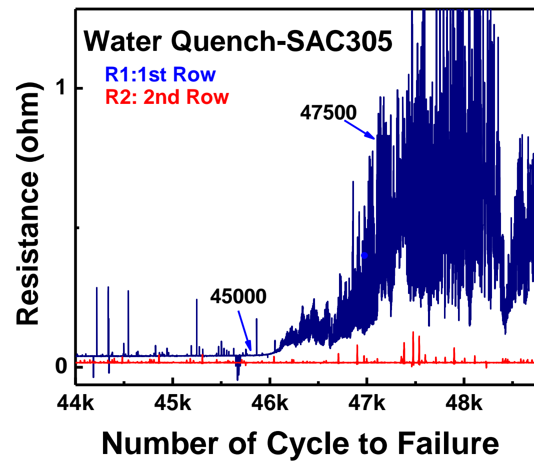

(d)

Figure 6.2. Resistance change with number of cycle for (a) fast cool, (b) medium cool and (c) slow cool for SAC105 150 °C, 500 hour aged samples, and (d) SAC305 fast cool sample, at strain 2%, 1Hz, room temperature.

Then the other question here is why there exists a reduction in the fatigue life with increasing cooling rate. It is believed that it is due to the level of residual thermal stress after cooling. As mentioned in chapter four, the total deformation field increases as the distance of joint increases from the center of the assembly. Thus, the corner joint is likely to contain most residual stress which increases susceptibility of fatigue failure. This view is also consistent with the fatigue result obtained from SAC 305 assembly. Cyclic shear fatigue testing on the SAC305

assembly after the same aging and cooling treatment reveals that the failure location is always fixed at the 1st row irrespective of cooling rate (Figure 6.2 (d)). Moreover, as shown in Figure 6.3, the fatigue lifetime of SAC305 tested at 8% strain, room temperature and 1Hz decreases with increasing cooling rate. Also the fact that fatigue life is reduced by ~50% using a fast cooling treatment. As mentioned in the grain structure section, the grain structure of SAC305 does not change with joint location or cooling rate. Therefore, the fatigue life reduction by fast cooling can be a measure of residual stress impacting fatigue life. The fact that the fast cooled SAC105 fails at the 2nd row while life is reduced by roughly 50% presents clear evidence that the joint with polygranular structure (or mechanical twins) is far more resistant to the fatigue failure than the beach ball joint.

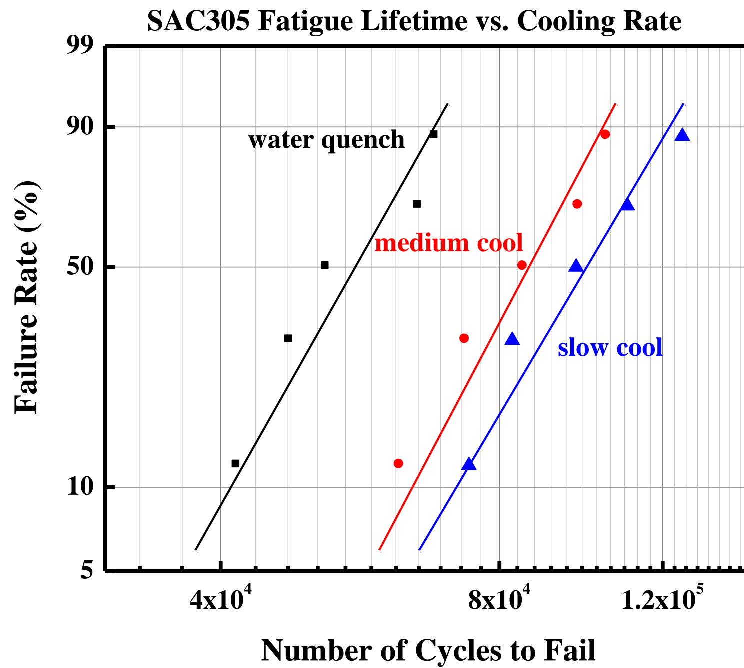

Figure 6.3 Fatigue lifetime of 150 °C 500 hour aged SAC305 cooling with fast, medium and slow cooling rate, at strain 8%, 1Hz, room temperature, first row solder joints lifetime.

In order to identify the effect of cooling rate and grain structure on the fatigue reliability, residual thermal stress has to be removed or minimized in the solder joints. To achieve this goal, 24 hour thermal aging of SAC105 at 100 °C was applied after cooling. Then the samples were

cooled from 100 °C to room temperature in the furnace at slow cooling rate. In this way, the residual thermal stress due to cooling from 150 °C can be partially relaxed, and the residual thermal stress remained in the solder joints are in the same level for all the samples after cooling from 100 °C to room temperature. After removing residual thermal stress, shear tests were executed and the fatigue lifetimes of the first row solder joints are shown in Figure 6.4. It indicates that after minimizing the residual thermal effect on the fatigue reliability, the fatigue lifetime increases with increasing cooling rate: N_f fast cool > N_f medium cool > N_f slow cool. This result suggests that the Polygrained and twinned structure are more resistant to fatigue failure.

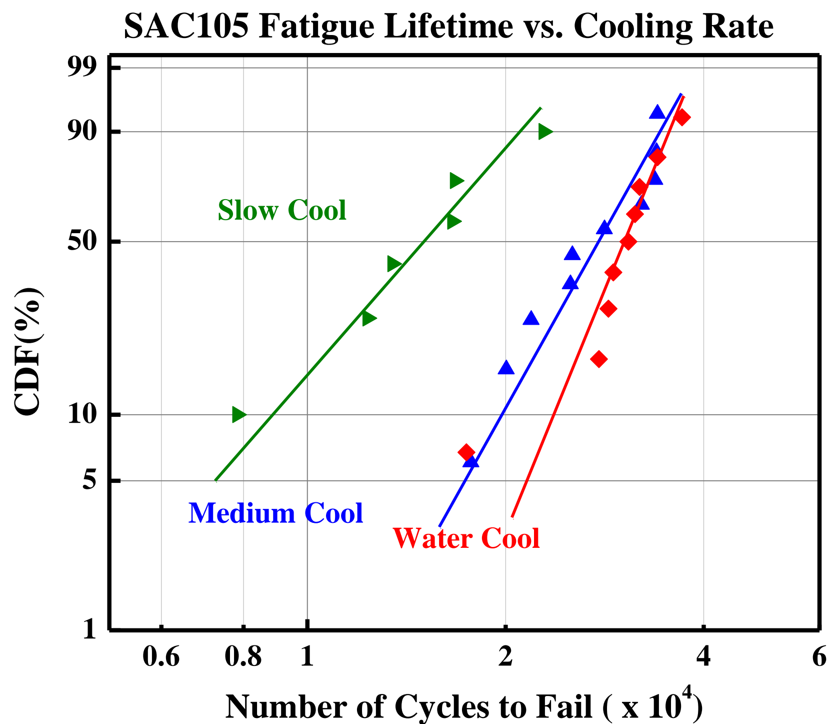

Figure 6.4. Fatigue lifetime of 150 °C 500 hour aged SAC105 cooling with fast, medium and slow cooling rate after stored in 100 °C for 24 hour. Shear test at strain 8%, 1Hz, room temperature, first row solder joints fatigue life.

6.3.2 Crack Path vs. Cooling Rate

To further understand the grain structure sensitivity, the crack path of the sample after shear fatigue failure was investigated using optical and SEM microscope and the images are

displayed in Figure 6.5 (a) showing the crack path for slow cooled solder joint with two grains in the solder matrix. It can be seen that part of crack follows the grain boundaries and part of it is trans-granular. In the case of medium cooling, twins are observed in the joint and the crack is trans- -granular since only one grain is viewed in this image. In the case of fast cooling, it composes of many fine grains and most of the crack follows grain boundaries unless it encounters big grains. It is known that the smaller grain size increases the ductility and the strength of the solder joint. In fact, grain refinement is the only mechanism that increases both parameters. With an increase in both ductility and strength, the joint becomes more resistant to fatigue inducing deformation and fracture inducing crack growth. At the same time, some researches revealed that twins can also enhance the strength of the material. Therefore, it is believed that the fatigue resistance increases with increasing cooling rate because the strength and ductility of the solder joint are improved by recrystallization and deformation twinning.

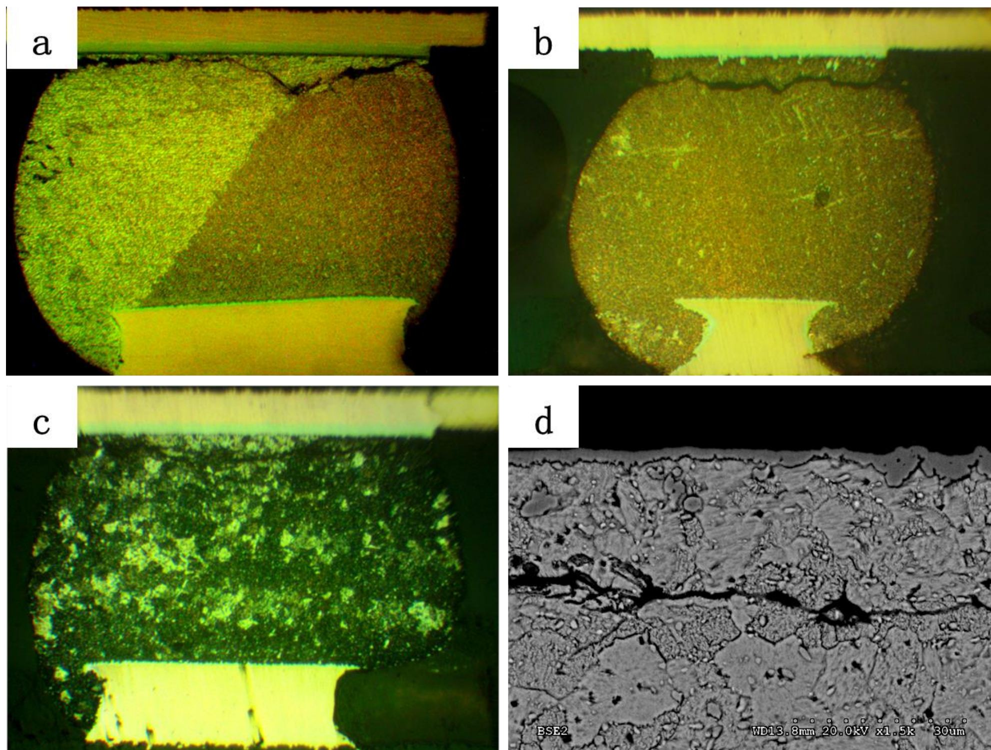

Figure 6.5 crack path of the solder joint after shear fatigue test at room temperature, 8% strain, 1Hz for (a) slow cool, (b) medium cool, (c) (d) fast cool.

6.4 Conclusions and Implications

In this chapter, it is found that the fatigue lifetime of the solder joints is very sensitivity to the cooling rate and the grain structure. The fast cooled solder joints with polygrain structure or medium cooled sample with twinned structure show better fatigue performance than the solder joint with classical beach ball structure. This finding has a very practical application in the industry. It indicates that the fatigue resistance can be improved by producing finer grain structure or introducing twins in the solder matrix. The other important finding in this chapter is that residual thermal stress can affect the fatigue reliability. Careful consideration on the residual thermal stress has to be taken when evaluating the fatigue behavior of a given solder joints in the packaging assembly.

CHAPTER 7

CONCLUSIONS AND FUTURE WORK

7.1 Conclusions

The fatigue reliability of lead-free solder in BGA packaging assembly and its controlling factors especially the microstructure impact are investigated by the shear fatigue test. In this study, the evolution of grain structure in tin-based solder joint by thermal stress and its possible mechanism are studied.

7.1.1 Shear Fatigue Mechanism and Mechanics

With the trend of miniaturization and mobilization of electronic devices, the reliability concerns are not limited to the conventional thermal cycling or power cycling due to CTE mismatch but also isothermal fatigue coming from vibration, shock and bending. To understand the isothermal fatigue behavior of the tin-based lead-free solder joints in BGA packaging assembly, isothermal shear fatigue tester was designed and was found to be an effective and efficient way to evaluate the fatigue reliability of the BGA assembly.

It is found that solder joints fail by crack opening mode under cyclic shear load and the crack always initiates at the solder neck area in the package side regardless of the testing conditions. This is due to the asymmetric stress/strain distribution in solder joint resulted from the geometry of the solder ball. The four corners especially the solder neck areas in the packaging side are under the highest compression/tension stress. The fixation of failure site in the solder matrix indicates that the fatigue behavior of the solder joint is controlled by the solder fatigue property itself which means the shear fatigue can be a good way of evaluating the fatigue property of the solder joint in the assembly. Also the fast crack opening mode makes the shear fatigue test an efficient method for fatigue reliability characterization.

7.1.2 Fatigue Property Parameters and Fatigue Lifetime Prediction

Shear Fatigue tests were carried out to investigate the factors that affect the fatigue behavior of the solder joints: solder alloy composition, thermal aging, frequency, strain range and testing temperatures. It is found that the fatigue failure of the solder joint under shear follows the Coffin-Manson model and frequency-modified Coffin-Manson Model is developed for fatigue lifetime prediction. The importance of this model is that the most critical fatigue property parameters that dictate the fatigue behavior of the solder joints are extracted. These parameters are determined to be fatigue ductility coefficient, cyclic strain hardening exponent/cyclic ductility exponent, and frequency exponent. They are all temperature dependent. Fatigue ductility coefficient represents the ductility of the material and it increases with increasing temperature. Strain hardening exponent which is inversely proportional to the cyclic ductility exponent represents the strength and strain hardening behavior of the material, and it decreases with increasing temperature. The third parameter frequency exponent is related to the creep and viscous property of the solder material, which affects the fatigue more as temperature increases.

SAC305 has the highest strain hardening exponent leading to a better fatigue performance at low strain range. SAC105 has the highest fatigue ductility coefficient means that at high strain range the fatigue resistance is better than SAC305 and SnPb. Because strength and ductility dominant the fatigue behavior of the solder material, it is predicted that SAC305 will have a better performance in terms of resist vibration load, while SAC105 may be better in the case of shock resistance.

Moreover, the fatigue lifetime seems to decrease with thermal aging time and aging temperature. Also the failure site after thermal aging is more complex while cracks are found not only at the solder matrix of the chip side but also in the solder/IMC interface of the board side. The failure site shifting and lifetime decreasing are due to the IMC growth in the interface especially in the board side interface and IMC coarsening in the solder matrix. Thermal aging makes the solder matrix weaker because the IMC strengthening effect is weaker.

Meanwhile, the fatigue resistance also shows strain rate/frequency sensitivity that it decreases with increasing strain rate/frequency. This is due to increasing of the strain energy with increasing strain rate.

The temperature has a negative effect on the fatigue reliability probably due to decrease of strain hardening exponent with temperature increasing. However, shear fatigue at elevated temperature has to consider thermal strain effect that in addition to the shear displacement the thermal shear strain need to be included. As a result, the thermal strain and frequency modified Coffin-Manson equation is developed for fatigue lifetime prediction at elevated temperature.

By known the fatigue property parameters namely fatigue ductility coefficient, ductility exponent and frequency exponent, and their dependency on the temperature, the fatigue lifetime of the solder joint under mechanic load can be predicted using the frequency-modified coffin-Manson equation at any given condition.

7.1.3 Grain Structure Evolution and Its Impact on the Fatigue Reliability

Recrystallization and deformation twinning are observed in SAC105 solder joint by one-time thermal exposure. This suggests that the recrystallization and deformation twinning are much easier than expected. It indicates that stored strain energy required for recrystallization to occur in tin is much less than normal that thermal strain resulted from one-time thermal exposure only is enough to trigger recrystallization. In addition, the deformation twinning is even more surprising due to the high stacking fault energy and low melting temperature of tin which makes the deformation twinning to be very difficult at normal circumstance. However, our investigation finds that deformation twinning can be promoted if hydrostatic compression stress exists. The hydrostatic compression is able to reduce the critical resolved shear stress required for twinning and makes twinning to be easier than expected.

In addition, grain structure evolution of the tin-based lead-free solder joint in BGA assembly is found to be highly sensitive to the cooling temperature and joint location in the

assembly. The plastic deformation in solder joint is found to increase from the center to the corner solder joint resulting in the increased stored strain energy from the center to the corner. The cooling rate sensitivity is due to the competition between the dynamic recovery process and recrystallization process. At high cooling rate, dynamic recovery which reduces the stored strain energy is less happening in the solder resulting in high stored strain energy for recrystallization to occur， while at low cooling rate, stored strain energy is relaxed by the dynamic recovery process and recrystallization does not happen.

The grain structure evolution with cooling provides an ideal way of investigating the microstructure effect on the fatigue reliability. The recrystallized polygrain structure and twin structure are found to enhance the fatigue resistance more than 50%.

7.1.4 Deformation Twinning in Tin-based Solder Alloy

Deformation twinning instead of dislocation glide was observed in SAC105 solder joint in BGA packaging assembly during simply cooling, though mechanical twinning in tin is only seen when the strain rate is super high such as impact and ultrasonic load or the temperature is below cryogenic temperature. The twins are identified to be (301) [-103] and (101) [-101] twins. The mechanism of this deformation twinning was investigated and found that hydrostatic compression which reduces the critical resolved shear stress for twinning is the key for deformation twinning to occur. Also the hydrostatic compression stress decreases from the corner to the center that makes the deformation twinning more prevalent in corner and edge solder joint. Hydrostatic compression stress makes tin able to twinning at moderate strain rate and relative high temperature. This finding is scientifically and technically significant for tin-based solder alloy.

7.2 Future Work

7.2.1 Fatigue Parameters and Fatigue Reliability of Solder Joints

7.2.1.1 Shear Fatigue Test of Solder Joints with Polygrain and Twin Structure

The fatigue parameters, specifically fatigue ductility coefficient, ductility exponent and frequency exponent can be extracted from the shear fatigue test for solder joints with polygrain structure and twin structure at various strain ranges, temperatures and frequencies. With these parameters known, the fatigue behavior of the solder joint with twins and fine grains can be predicted and the fatigue strengthening mechanism can be understood better. I expected that solder joint with fine grain structure would have a higher strength and strain hardening exponent while the ductility my decrease. The same for solder joint with twins the strength would increase as well.

However, one difficulty of carrying out this test is that the effect of residual thermal stress on the fatigue behavior. Due to residual thermal stress failure in the shear test tends to occur at the corner side which makes the direct assessment of grain structure impact on fatigue difficult. There are several ways of solving this problem. First, measure the residual thermal stress in the solder joints after reflow and thermal treatment. This can be carried out by Finite Element Analysis using ANSYS. Alternatively, to get rid of the effect of residual thermal stress on the fatigue, a longer storing time in a proper environment without deteriorating the solder microstructure may be needed. In this way, the fatigue reliability solely related to the grain structure can be evaluated.

7.2.1.2 Isothermal Shear Fatigue Test with Thermal Cycle

As mentioned. Thermal cycling is the conventional reliability concern in solder joint while usual thermal cycling test is time consuming and instrument requirement is high. In order to understand the linkage between the isothermal fatigue and thermal cycling, besides all the tests have been carried out, the shear test with thermal cycling can be conducted. Instead of the complicated thermal cycling, a heater that can be switched on and off can be placed on top of

the sample. In this way, shear test with temperature cycling can be conducted. Comparison between these results and isothermal shear fatigue can be made so that the temperature cycling effect on the fatigue reliability can be concluded.

7.2.2 Deformation Twinning in Tin and Its Mechanism

To further study the deformation twinning mechanism in tin, a single solder joint in packaging can be specially designed to find out the level of hydrostatic compression stress needed to trigger the plastic deformation by twinning.

Moreover, the strain rate sensitivity needs to be studied in more detail and systematically. Drop shock tests can be an ideal way of this study.

REFERENCES

1. M. Abtew, G. Selvaduray, "Lead-free Solders in Microelectronics", Materials Science and Engineering, 27(2000), pp. 95-141.
2. Haleh Ardebili, Michael G.Pecht, "Encapsulation technologies for electronic application", William Andrew Applied Science Publisher, 2009.
3. H.M. Tong, Y.S. Lai, C.P. Wong, "Advanced flip chip packaging", Springer, 2013.
4. Y. Zhang, "Tin and Tin alloys for lead-free solder", Modern Electroplating, John Wiley & Sons, Inc. 2010.
5. P. T. Vianco and D. R. Frear, "Issues in the Replacement of Lead-Bearing Solders," Journal of Materials, 23(7)(1993), pp.14-19.
6. W. Hampshire., "Solders in Electronic Materials Handbook", Volume 1, Packaging, ASM International, Metals Park, OH, 1989, pp. 633–642.
7. K.J. Puttlitz, K.A. Stalter ," Handbook of Lead-Free Solder Technology for Microelectronic Assemblies", Technology & Engineering, 2004.
8. J,W. Evans, "A guide to lead-free solder", Springer London, 2007, pp.1-27
9. M. Abtew, G.Selvaduray, , "Lead Free Solders in Microelectronics", Material Science and Engineering, 27(2000), pp.95–141
10. D.Shangguan, "Leading the Lead-free transition", Circuits Assem., March, 2004
11. D.Shangguan, "Understanding compatibility and clarifying issues in Lead-free transition", Electronics Manufacturing China, April, 2004, pp.20-24.
12. D.Shangguan, A. Achari, "Evaluation of Lead-free eutectic Sn-Ag solder for automotive electronics packaging applications", Proceedings of the International Electronics Manufacturing Technology Symposium, September, 1994, pp.25-37.
13. D.Shangguan, A. Achari, "Lead-free solder development for automotive electronics

packaging applications", Proceedings of the Surface Mount International Conference, September, 1994, pp.25-37.

14. J.S. Hwang, "environment-friendly electronics: Lead-free technology", Electrochemical Publications Ltd., 2001.
15. J. Lau, C.P. Wong, N.C. Lee, S.W.R. Lee, "Electronics manufacturing with Lead-free, halogen-free and Conductive Adhesive Materials", McGraw-Hill, 2003.
16. S. ganesan, M. Pecht, "Lead-free electronics", Calce Epsc Press, 2003.
17. B.P. Richards, C. L. Levoguer, C. P. Hunt, K. Nimmo, S. Peters, P. Cusack ,"An Analysis of the current status of the lead-free soldering", https://www.itri.co.uk/index.php?option=com_mtree&task=att_download&link_id=49445&cf_id=24P.
18. Y. Kariya, M. Otsuka, "Effect of Bismuth on the Isothermal Fatigue Properties of Sn-3.5 mass%Ag Alloy", Journal of Electronic Materials, 27(1998), pp.866-870.
19. J.S. Hwang, "An Overview of Lead-Free Solders for Electronic and Microelectronics", Proc. of Surface Mount International, IPC, 1994, pp. 405–421.
20. C.M. Miller, I.E. Anderson, J.F. Smith, "A viable Sn-Pb solder substitute: Sn-Ag-Cu", Journal of Electronic Materials, 23(7)(1994), pp.595-601.
21. M.E. Loomans, M.E. Fine, "Tin-Silver-Copper Eutectic Temperature and Composition", Metall. Mater. Trans. A, 31(2000), pp.1155-1162.
22. I.E. Anderson, "Development of Sn-Ag-Cu and Sn-Ag-Cu-X alloys for Pb-free electronic solder applications", Lead-free electronic Solders, Spring US., 2007, pp.55-76.
23. I.E. Anderson, J.C. Foley, B.A. Cook, J. Harringa, R.L. Terpstra, and O. Unal, "Alloying Effects in Near-Eutectic Sn-Ag-Cu Solder Alloys for Improved Microstructural Stability", Journal of ELECTRONIC MATERIALS, 30(9)(2001), pp.1050-1059.

24. C.Y. Yu, T.K. Lee, M. Tsai, K.C. Liu, J. G. Duh, "Effects of Minor Ni Doping on Microstructural Variations and Interfacial Reactions in Cu/Sn-3.0Ag-0.5Cu-xNi/Au/Ni Sandwich Structures", Journal of Electronics Materials, 39(12)(2010), pp.12544-2552.
25. T. Laurila, J. Hurtig, V. Vuorinen, J.K. Kivilahti, "Effect of Ag, Fe, Au and Ni on the growth kinetics of Sn–Cu intermetallic compound layers", Microelectronics Reliability, 49(2009), pp. 242–247.
26. K.S. Kim, S.H. Huh, K. Suganuma, "Effects of fourth alloying additive on microstructures and tensile properties of Sn–Ag–Cu alloy and joints with Cu", Microelectronics Reliability, 43(2003), pp. 259–267.
27. L.L. Gao, S. B. Xue, L. Zhang, Z. Sheng, F. Ji, W. Dai, S.L. Yu, G. Zeng, "Effect of alloying elements on properties and microstructures of SnAgCu solders", Microelectronic Engineering, 87(2010), pp. 2025–2034.
28. J.Y. Park, R. Kabade, C.U. Kim, T. Carper, S. Dunford, V. Puligandla, "Influence of Au Addition on the Phase Equilibria of Near-Eutectic Sn-3.8Ag-0.7Cu Pb-Free Solder Alloy", Journal of Electronic Materials, 32(12)(2003), pp.1474-1482.
29. C.M. Chuang， K.L. Lin, "Effect of Microelements Addition on the Interfacial Reaction between Sn-Ag-Cu Solders and the Cu Substrate", Journal of Electronic Materials, 32(12)(2003), pp.1426-1431.
30. H.X. Xie, L. Jiang, N. Chawla, "Effect of cerium addition on wetting, undercooling, and mechanical properties of Sn-3.9Ag-0.7Cu Pb-free solder alloys", Journal of Materials Science: Materials Electron, 24(2013), pp.3456–3466.
31. D.H. Kim, M.G. Cho, H.M. Lee, S.K. Seo, "Effects of Co Addition on Bulk Properties of Sn-3.5Ag Solder and Interfacial Reactions with Ni-P UBM", Journal of Electronic Materials, 38(1)(2009), pp.39-45.

32. C.E. Ho, W. Gierlotka, S.W. Lin, “Strong effect of Pd concentration on the soldering reaction between Ni and Sn–Pd alloys”, Journal of Materials Research, 25(11)(2010), pp. 2078-2081.

33. C.M.L. Wu, D.Q. Yu, C.M.T. Law, L. Wang, “Properties of lead-free solder alloys with rare earth element additions”, Materials Science and Engineering R, 44(2004), pp.1–44.

34. M. McCormack, S. Jin, “New lead-free solders”, Journal of Electronic Materials, 23 (7)(1994), pp.635–640

35. J. Bath, “Lead-free Soldering”, Springer, 2007, pp.28

36. J. Bath, “Lead-free Soldering”, Springer, 2007, pp.190

37. C.M.L. Wu, M.L. Huang, J.K.L. Lai, and Y.C. Chan, “Developing a Lead-free Solder Alloy Sn-Bi-Ag-Cu by Mechanical Alloying”, Journal of Electronic Materials, 29(8)(2000), pp.1015–1020.

38. R. K. Shiue, L.W. Tsay, C.L. Lin, J.L. Ou, “A study of Sn-Bi-Ag-(In) lead-free solders”, Journal of Material Science, 38(6)(2003), pp.1269-1279 .

39. G. Izuta, T. Tanabe, “Dissolution of copper on Sn-Ag-Cu system lead free solder”, Soldering & Surface Mount Technology, 19(2)(2007), pp. 4–11

40. M.O. Alam, Y.C. Chan, K.N. Tu, “Effect of 0.5 wt % Cu addition in Sn–3.5%Ag solder on the dissolution rate of Cu metallization”, Journal of Applied Physics, 94(12)(2003), pp.7904-7909.

41. M.L. Huang, T. Loeher, A. Ostmann, H. Reichl, “Role of Cu in dissolution kinetics of Cu metallization in molten Sn-based solders”, Applied Physics Letter, 86(18)(2005), pp.181908-3.

42. L. Xu, J.H.L. Pang, F. Che, “Impact of Thermal Cycling on Sn-Ag-Cu Solder Joints and Board-Level Drop Reliability”, Journal of Electronic Materials, 37(6)(2008) pp.880-886.

43. I. Ohnuma, M. Miyashita, K. Anzai, X. J. Liu, H. Ohtani, R. Kainuma, K. Ishida, “Phase equilibria and the related properties of Sn-Ag-Cu based Pb-free solder alloys”, Journal of Electronic Materials, 29(10)(2000), pp.1137-1144.

44. K.W. Moon, W.J. Boettinger, U.R. Kattner, F.S. Biancaniello, C.A. Handwerker, “Experimental and thermodynamic assessment of Sn-Ag-Cu solder alloys”, Journal of Electronic Materials, 29(10)(2000), pp.1122-1136.

45. J.W. Yoon, S.W. Kim, S.B. Jung, “IMC morphology, interfacial reaction and joint reliability of Pb-free Sn–Ag–Cu solder on electrolytic Ni BGA substrate”, Journal of Alloys and Compounds, 392(1-2)(2005) pp. 247–252.

46. C.M. Miller, I.E. Anderson, J.F. Smith, “A viable tin-lead solder substitute: Sn-Ag-Cu”, Journal of Electronic Materials, 23(7)(1994) pp.595-601.

47. K.S.Kim, K. Suganuma, “Development of new Sn-Ag-Cu lead-free solders containing fourth elements”, Proceealngs of EmDesqn 2003: Third Internatinal Symposium on Environmentally Conscious Design and Inverse Manufacturing, Japan, 2003.

48. F.J. Wang, Z.S. Yu, Kai Qi,” Intermetallic compound formation at Sn–3.0Ag–0.5Cu–1.0Zn lead-free solder alloy/Cu interface during as-soldered and as-aged conditions”, Journal of Alloys and Compounds, 438(1-2)(2007) pp.110–115.

49. K.K. Xiang, A.S.M.A. Haseeb, M.M. Arafat, G. Yingxin, “Effects of Mn nanoparticles on wettability and intermetallic compounds in between Sn-3.8Ag-0.7Cu and Cu substrate during multiple reflow”, 4th Asia Symposium on Quality Electronic Design, 2012, pp.297-301.

50. K Suganuma, “Advances in lead-free electronics soldering”, Current Opinion in Solid State and Materials Science, 5(1)(2001) pp.55–64

51. CW. Hwang,K. Suganuma, “Joint reliability and high temperature stability of Sn–Ag–Bi

lead-free solder with Cu and Sn–Pb/Ni/Cu substrates", Materials Science and Engineering: A, 373(1–2)(2004), pp.187–194

52. Z. Moser,W. Gasior, J. Pstrus, "Surface tension measurements of the Bi-Sn and Sn-Bi-Ag liquid alloys", Journal of Electronic Materials, 30(9)(2001), pp.1104-1111.
53. H. Takao, H. Hasegawa, "Influence of alloy composition on fillet-lifting phenomenon in Sn-Ag-Bi alloys", Journal of Electronic Materials, 30(9)(2001), pp.1060-1067.
54. C.W. Hwang, K. Suganuma, "Joint reliability and high temperature stability of Sn–Ag–Bi lead-free solder with Cu and Sn–Pb/Ni/Cu substrates", Materials Science and Engineering A, 373(2004), pp.187–194.
55. P. T. Vianco, J. A. Rejent, "Properties of ternary Sn-Ag-Bi solder alloys: Part II—Wettability and mechanical properties analyses", Journal of Electronic Materials, 28(10)(1999), pp.1138-1143
56. Y. Kariya, M. Otsuka, "Mechanical fatigue characteristics of Sn-3.5Ag-X (X=Bi, Cu, Zn and In) solder alloys", Journal of Electronic Materials, 27(11)(1998), pp.1229-1235.
57. Y. Kariya, M. Otsuka, "Effect of bismuth on the isothermal fatigue properties of Sn-3.5mass%Ag solder alloy", Journal of Electronic Materials, 27(7)(1998), pp.866-870.
58. J. K. Shang, Q. L. Zeng, L. Zhang, Q. S. Zhu, "Mechanical fatigue of Sn-rich Pb-free solder alloys", Journal of Materials Science: Materials in Electronics,18(1-3)(2007), pp.211-227.
59. K. N. Subramanian, "Reliability of Lead-Free Electronic Solder Interconnects: Roles of material and service parameters", "Lead-Free solders: materials reliability for electronics", Wiley online library, 2012, pp.1-8.
60. D. Wojciechowski, M. Chan, F. Martone, "Lead-free plastic area array BGAs and polymer stud grid arraysTM package reliability" Microelectronics Reliability, 41(11)(2001), pp. 1829–1839.

61. D. R. Frear, , W. B. Jones, K. R. Kinsman, , , “Solder Mechanics: A State of the Art Assessment”, The Minerals, Metals and Materials Society, EMPMD Monograph, 1991, pp. 155–189.

62. J.H. Lau, et al., "Design for lead-free solder joint reliability of high-density packages", Soldering and Surface Mount Technology, 16 (2004), pp.12-26.

63. K. Zeng, K.N.Tu, “Six cases of reliability study of Pb-free solder joints in electronic packaging technology”, Materials Science and Engineering R, 38(2002), pp.55-105.

64. J. Hokka, J. Li, T.T. Mattila, P.K. Mervi, “The reliability of component boards studied with different shock impact repetition frequencies” Microelectronics Reliability, 52(2012), pp.1445-1453.

65. L. Leicht et al., "Mechanical cycling fatigue of PBGA package interconnects", Microelectronics Reliability, 40 (2000), pp. 1129-1133.

66. H. Rhee, J.P. Lucas, K.N. Subramanian, “Micromechanical characterization of thermomechanically fatigued lead-free solder joints”, Journal of Materials Science: Materials in Electronics, 13(8)(2002), pp.477-484.

67. A. Schubert, H. Walter, R Dudek, B. Michel, “Thermo-mechanical properties and creep deformation of lead-containing and lead-free solders”, International Symposium on Advanced Packaging Materials, 2001, pp.129-134.

68. M.A. Matin, W.P. Vellinga∗, M.G.D. Geers , Thermomechanical fatigue damage evolution in SAC solder joints, Materials Science and Engineering A, 445–446(2007), pp.73–85.

69. T. Laurila, T. Mattila, V. Vuorinen, J. Karppinen, J. Li, M. Sippola, J.K. Kivilahti, “Evolution of microstructure and failure mechanism of lead-free solder interconnections in power cycling and thermal shock tests”, Microelectronics Reliability, 47 (2007), pp.1135–1144.

70. X. Li, Z. Wang, “Thermo-fatigue life evaluation of SnAgCu solder joints in flip chip

assemblies", Journal of Materials Processing Technology, 183 (2007), pp.6–12.

71. B. Vandevelde, M. Gonzalez, P. Limaye, P. Ratchev, E. Beyne ,"Thermal cycling reliability of SnAgCu and SnPb solder joints: A comparison for several IC-packages", Microelectronics Reliability, 47 (2007), pp.259–265.
72. J.W. Lee, Z. H. Lee and H.M. Lee, "Formation of Intermetallic Compounds in the Ni Bearing Lead Free Composite Solders", Materials Transactions, 46(11) (2005) 2344-2350.
73. A.Lee,, K.N. Subramanian, "Development of Nano-Composite Lead-Free Electronic Solders", Journal of Electronic Materials, 34(11)(2005), pp.1399-1407.
74. T.K. Lee, W.D. Xie, K.C., Liu,"Impact of Isothermal Aging on High G Mechanical Shock Performance Sn-Ag-Cu Solder Interconnect Board Level", 61st Electronic Components and Technology Conference, 2011, pp.547-552.
75. H.L. Xu, W.H. Bang , H.T. Ma, et al., "Fracture Mechanics of Lead-Free Solder Joints under Cyclic Shear Load", 60st Electronic Components and Technology Conference, 2010, pp.484-489.
76. H.L. Xu, W.H. Bang, , H.T. Ma, , et al., "Isothermal Shear Fatigue Mechanism of Lead Free Solder Joints", 62st Electronic Components and Technology Conference, 2010, pp.1299-1303.
77. C.R. Siviour, S.M. Walley, W.G. Proud, J.E. Field, "Mechanical properties of SnPb and lead-free solders at high rates of strain", Journal of Physics D: Applied Physics, 38 (2005), pp. 4131–4139.
78. Luan, T.Y. Tee, E. Pek, C.T. Lim, Z. Zhong, "Dynamic responses and solder joint reliability under board level drop test", Microelectronics Reliability, 47(2–3)(2007), pp.450–460.
79. T.Y. Tee, H.S. Ng, C.T. Lim, E. P., Z. Zhong, "Impact life prediction modeling of TFBGA packages under board level drop test", Microelectronics Reliability, 44(2004), pp.1131–

1142.

80. E.H. Wong, S.K.W. Seah, V.P.W. Shim, "A review of board level solder joints for mobile applications", Microelectronics Reliability, 48 (2008), pp.1747–1758.

81. E.H. Wong, S.K.W. Seah, W.D. van Driel, J.F.J.M. Caers, N. Owens, Y.-S. Lai, "Advances in the drop-impact reliability of solder joints for mobile applications", Microelectronics Reliability, 49(2)(2009), pp.139–149.

82. J. Gong, C. Liu, P.P. Conway, V.V. Silberschmidt, "Micromechanical modelling of SnAgCu solder joint under cyclic loading: Effect of grain orientation", Computational Materials Science, 39 (2007), pp. 187–197.

83. B. Wang, J. J. Li, A. Gallagher, J. Wrezel, P. Towashirporn, N.Q. Zhao, " Drop impact reliability of Sn–1.0Ag–0.5Cu BGA interconnects with different mounting methods", Microelectronics reliability, 52(2012), pp.1475-1482.

84. J. Karppinen, J. Li, J. Pakarinen, T.T. Mattila, M. P. Kröckel, "Shock impact reliability characterization of a handheld product in accelerated tests and use environment", Microelectronics Reliability, 52(2012), pp.190–198.

85. S. J. Jeon, J. W. Kim, B. Lee, H. J. Lee, S. B. Jung, S. Hyun, H. J. Lee, "Evaluation of drop reliability of Sn–37Pb solder/Cu joints using a high speed lap-shear test", Microelectronic Engineering, 91(2012), pp.147-153.

86. Y.Yao, L.M. Keer, "Cohesive fracture mechanics based numerical analysis to BGA packaging and lead free solders under drop impact", Microelectronics reliability, 53(2013), pp.629-637.

87. H. Yu, D. K. Shangguan, "Solidification and reliability of lead-free solder interconnection", Soldering & Surface Mount Technology, 25(1)(2013), pp.31–38.

88. Y. Li, K. S. Moon, C. P. Wong, "Electronics without lead", Science, 308(2005), pp.1419-

1420.

89. H. T. Lee, H. S. Lin, C. S. Lee, P. W. Chen, “ Reliability of Sn–Ag–Sb lead-free solder joints ”, Materials Science and Engineering A, 407(2005), pp.36-44.
90. J. Li, H. Xu, T.T. Mattila, J.K. Kivilahti, T. Laurila, M. Paulasto-Krokel, “Simulation of dynamic recrystallization in solder interconnections during thermal cycling”, Computational Materials Science, 50(2010), pp.690–697.
91. M. Berthou, P. Retailleau, H. Frémont, A. Guédon-Gracia, C.Jéphos-Davennel, “Microstructure evolution observation for SAC solder joint: Comparison between thermal cycling and thermal storage”, Microelectronics Reliability, 49 (2009), pp.1267–1272.
92. T. H. Ho, J.Y. Lee, “Linear finite Element Stress Simulation of Solder Joints on 225 I/O Plastic BGA Package Under Thermal Cycling”, 45th ECTC, 1995, pp.930-936.
93. W. H. Bang, C. U. Kim, H. T. Ma, and T.K. Lee, “Rate Dependence of Bending Fatigue Failure Characteristics of Lead-Free Solder Joint”, Electronic Components and Technology Conference, 2009, pp.2070-2074.
94. H. L. Xu, W. H. Bang, C. U. Kim, T. K. Lee, “Fracture Mechanics of Lead-Free Solder Joints under Cyclic Shear Load”, Electronic Components and Technology Conference, pp. 484-489.
95. Y. Zhao, C. Basaran, A. N. Cartwright, T. Dishongh, "Thermomechanical behavior of micron scale solder joints under dynamic loads," Mechanics of Materials, 32(3) (2000), pp.161-173.
96. T. K. Lee, H. T. Ma, K. C. Liu, J. Xue, “Impact of Isothermal Aging on Long-Term Reliability of Fine-Pitch Ball Grid Array Packages with Sn-Ag-Cu Solder Interconnects: Surface Finish Effects”, Journal of Electronic Materials, 39(2010), pp. 2564-2573.

97. W.W. Lee, et al., “Solder joint fatigue models: review and applicability to chip scale packages”, Microelectronics reliability, 40(2000), pp. 231-244.

98. H.L. Zhu, L. Weng , Y. Can , Y. Li, “Fatigue life prediction of electronic chips based on singular edge field”, Applied Mechanics and Materials, 390(2013), pp.601-605.

99. C.-U. Kim, W.-H. BangH., Xu , T.-K. Lee, “Characterization of solder joint reliability using cyclic mechanical fatigue testing “, Journal of Materials, 65 (10)(2013), pp.1362-1373.

100. H. Xie , Q. Tan , Y.C. Lee, “Electronic Packaging: Thermal, Mechanical, and Environmental Durability”, Encyclopedia of Materials: Science and Technology (Second Edition), 2001, pp. 2715–2725

101. C. Kanchanomai, et al., “Effect of temperature on isothermal low cycle fatigue properties of Sn-Ag eutectic solder”, Materials Science and Engineering A, 381(2004), pp.113-120.

102. X.Q. Shi., et al., “low cycle fatigue analysis of temperature and frequency effects in eutectic solder alloy”, International Journal of Fatigue, 22(2000), pp. 217-228.

103. H.L. John, et al., “Low cycle fatigue study of lead free 99.3Sn-0.7Cu solder alloy”, International Journal of Fatigue, 26(2004), pp. 865-872.

104. L.F. Coffin., “A study of the effects of cyclic thermal stress on a ductile material”, ASME Transactions, 76(1954), pp.931-950.

105. S.S. Manson, “Fatigue: a complex subject — some simple approximations”, Experimental Mechanics, 5 (1965), pp.193-226.

106. J.D. Morrow, “Internal Friction, Damping and Cyclic Plasticity”, ASTM-STP, 378(1965), pp. 45-52.

107. A. Dasgupta, “Failure mechanism models for cyclic fatigue”, IEEE Transactions on Reliability, 42(4)(1993), pp.548-555.

108. D. Yu, A.A. Yafawi, S. Park, and S. Chung, “Finite element based fatigue life prediction for

electronic components under random vibration loading," in Proc. 60th Electron. Components Technol. Conf., 2010, pp.188–193.

109. S. Knecht and L. Fox, "Constitutive relation and creep-fatigue life model for eutectic tin-lead solder", IEEE Transactions Components, Hybrids and manufacturing technology, 13(2)(1990), pp.424-433.

110. A.Syed, "Accumulated creep strain and energy density based thermal fatigue life prediction models for SnAgCu solder joints", 54th Electronic Components and technology Conference, 2004, pp.737-746

111. A.R., Fix, et al., "Microstructural changes of lead free solder joints during long-term aging, thermal cycling and vibration fatigue", Soldering & Surface Mount Technology, 20(2008), pp. 13-21.

112. W. Peng , E. Monlevade, M. E. Marques, "Effect of thermal aging on the interfacial structure of SnAgCu solder joints on Cu", Microelectronics Reliability, 47(12)(2007), pp.2161–2168.

113. John H.L. Pang, T.H. Low, B.S. Xiong, L. Xu , C.C. Neo, "Thermal cycling aging effects on Sn–Ag–Cu solder joint microstructure, IMC and strength", Thin Solid Films, 462–463(2004), pp.370–375

114. L. Xu, J.H.L. Pang, ; K.H. Prakash, ; T.H. Low, , "Isothermal and thermal cycling aging on IMC growth rate in lead-free and lead-based solder interface", IEEE Transactions on Components and Packaging Technologies, 28(3)(2005), pp. 408-414.

115. X. Ma, F. Wang, Y. Qian, F. Yoshida, "Development of Cu–Sn intermetallic compound at Pb-free solder/Cu joint interface", Materials Letters, 57(22–23)(2003), pp.3361–3365.

116. J.H. L. Pang, L. Xu, X. Q. Shi, W. Zhou, S. L. Ngoh, "Intermetallic growth studies on Sn-Ag-Cu lead-free solder joints", Journal of Electronic Materials, 33(10)(2004), pp.1219-1226.

117. D. Li, C. Liu, P. P. Conway, “Characteristics of intermetallics and micromechanical properties during thermal ageing of Sn–Ag–Cu flip-chip solder interconnects”, Materials Science and Engineering: A, 391(1–2)(2005), pp.95–103.

118. M. T. Sheen, C. M. Chang, H. C. Teng, J. H. Kuang, K. C. Hsieh, W. H. Cheng, “The influence of thermal aging on joint strength and fracture surface of Pb/Sn and Au/Sn solders in laser diode packages, Journal of Electronic Materials, 31(8)(2002), pp.895-902.

119. Y. Kanda, et al., “Influrence of cyclic strain hardening exponent on fatigue ductility exponent for a Sn-Ag-Cu micro-solder joint”, Journal of Electronic Materials, 41(2012), pp. 580-587.

120. C. Kanchanomai, Y. Mutoh, “Effect of temperature on isothermal low cycle fatigue properties of Sn-Ag eutectic solder”, Mater. Sci. Eng. A, 381(2004), pp. 113-120.

121. Kariya, Y., et al., “Effect of bismuth on the isothermal fatigue properties of Sn-3.5 mass% Ag solder alloy”, Materials Science and Engineering: A, 27(1998), pp. 866-870.

122. A.U. Telang, T.R. Bieler, “Characterization of microstructure and crystal orientation of the tin phase in single shear lap Sn–3.5Ag solder joint specimens”, Scripta Materialia, 52 (2005), pp. 1027–1031.

123. D.A.A. Shnawah, S.B.M. Said, M.F.M. Sabri, I.A. Badruddin, F.X. Che, “Microstructure, mechanical, and thermal properties of the Sn–1Ag–0.5Cu solder alloy bearing Fe for electronics applications ”Materials Science and Engineering: A, 551(2012), pp. 160–168.

124. M.A. Matin, W.P.Vellinga, M.G.D.Geers, “Microstructure evolution in a Pb-free solder alloy during mechanical fatigue”, Materials Science and Engineering A, 431 (2006), pp. 166–174.

125. S. K. Kang, P. A. Lauro, D.-Y. Shih, D. W. Henderson, K. J. uttlitz, “Microstructure and mechanical properties of lead-free solders and solder joints used in microelectronic applications”, IBM Journal of Research and Development, 49 (4)(2005), pp.607-620.

126. Q.P. Peng, et al., “Microstructural and Performance Implications of Gold in Sn-Ag-Cu-Sb Interconnections’, 53rd Electronic Components and Technology Conference, New Orleans, LA, May, 2003, pp. 809-815.

127. W. Yang, R.W. Messler, “Microstructure evolution of eutectic Sn-Ag Solder joints”, Journal of Electronic Materials, 23(8)(1994), pp.765-772.

128. A.U. Telang, T.R. Bieler, “The Orientation Imaging Microscopy of Lead-Free Sn-Ag Solder Joints”, Journal of Materials, 6(2005), pp. 44-49.

129. A.U. Telang, T.R. Bieler, A. Zamiri, F. Pourboghrat, “Incremental recrystallization/grain growth driven by elastic strain energy release in a thermomechanically fatigued lead-free solder joint”, Acta Materialia, 55(7)(2007), pp.2265–2277.

130. A.U. Telang, T.R. Bieler, M.A.Crimp, “Grain boundary sliding on near-7◦, 14◦, and 22◦ special boundaries during thermomechanical cycling in surface-mount lead-free solder joint specimens, Materials Science and Engineering, A, 421(2006), pp. 22–34.

131. S.K.W. Seah, E.H. Wong, V.P.W. Shim, “Fatigue crack propagation behavior of lead-free solder joints under high-strain-rate cyclic loading”, Scripta Materialia, 59(2008), pp.1239–1242.

132. J. J. Sundelin, S.T. Nurmib, T.K. Lepist, Recrystallization behaviour of SnAgCu solder joints, Materials Science and Engineering A , 474(2008), pp.201–207.

133. R.D. Doherty , D.A. Hughes, F.J. Humphreys, J.J. Jonas, D. Juul Jensen, M.E. Kassner, W.E. King, T.R. McNelley, H.J. McQueen, A.D. Rollett, ‘Current issues in recrystallization: a review”, Materials Science and Engineering A, 238(1997), pp.219–274.

134. M. Erinc, et al. “Intergranular thermal fatigue damage evolution in SnAgCu lead-free solder”, Mechanics of Materials, 40(2008), pp.780–791.

135. U. R. Kattner, “Phase Diagrams for Lead-Free Solder Alloys”, Journal of Materials,

54(2002), pp.45-51.

136. J.W. Elmer, E.D. Specht, M. Kumar, “Microstructure and In Situ Observations of Undercooling for Nucleation of b-Sn Relevant to Lead-Free Solder Alloys”, Journal of Electronic Materials, 39(3)(2010), pp.273-283.

137. J.Y. Park, C.U Kim, T. Carper, V. Puligandla, “Phase Equilibria Studies of Sn-Ag-Cu Eutectic Solder Using Differential Cooling of Sn-3.8Ag-0.7Cu Alloys”, Journal of Electronic Materials, 32(11)(2003), pp.1297-1302.

138. I. Ohnuma, M. Miyashita, X.J. Liu, H. Ohtani, and K. Ishida, “Phase Equilibria and the Related Properties of Sn-Ag-Cu Based Pb-free Solder Alloys”, Journal of Electronic Materials, 29(10)(2000), pp.1137-1144.

139. I. Ohnuma, M. Miyashita, X. J. Liu, H.S. Ohtani, and K. Ishida, “Phase Equilibria and Thermodynamic Properties of Sn-Ag Based Pb-Free Solder Alloys”, IEEE Tansactions on Electronics Packaging Manufacturing, 26(1)(2003), pp.84-89.

140. S.K. Kang, W.K. Choi, D.Y. Shih, D.W. Henderson, T.Gosselin, A. Sarkhel, C. Goldsmith, K.J. Puttlitz, “Ag_3Sn Plate Formation in the Solidification of Near-Ternary Eutectic Sn-Ag-Cu”, Journal of Materials, 55(2003), pp.61-65.

141. D.W. Henderson, T. Gosselin, A. Sarkhel, S.K. Kang, W.K.Choi, D.Y. Shih, C. Goldsmith K. J. Puttlitz, “Ag_3Sn plate formation in the solidification of near ternary eutectic Sn–Ag–Cu alloys”, Journal of Materials Research Society, 17(11)(2002), pp.2775-2778.

142. L. Snugovsky, P. Snugovsky, D. D. Perovic and J. W. Rutter, “Effect of cooling rate on microstructure of Ag–Cu–Sn solder alloys”, Materials Science and Technology, 21(1)(2005), pp.61-68

143. K.S. Kim, S.H. Huh , K. Suganuma , “Effects of cooling speed on microstructure and tensile properties of Sn–Ag–Cu alloys”, Materials Science and Engineering A, 333(2002),

pp.106–114

144. F.Y. Hung, et al., “The recrystallization of microelectronic lead free solders”, Materials Transactions, 49(2008), pp.2298-2302.

145. J.W. Christian and S. Mahajan, “Deformation Twinning”, Progress in Materials Science, 39(1995), pp.1-157.

146. K.N. Tu and D. Turnbull, “Direct observation of twinning in tin lamellar ”, Acta Mettellurgica., 18(1970), pp.915-929.

147. F.Q. Yang, J. C. M. Li, “Deformation behavior of tin and some tin alloys”, Journal of Materials Science: Materials in Electronics, 18(2007).191–210.

148. M. Mueller, S. Wiese, K.J .Wolter, “the twinning phenomenon in SnAgCu Solder Balls”, 59th Electronic Components and Technology Conference, 2009, pp.1027-1036.

149. B. Chalmers, “the twinning of single crystals of Tin”, Proceedings of the Physical Society, 47(1935), pp.733-746.

150. D. R. Overcash, E.P. Stillwell, M.J. Skov, “Deformation twinning in Zn, Sn, and Bi single crystals whiskers”, Philosophical Magazine,25(6)(1972), pp.1481-1488.

151. K. Ishii, “deformation twinning of Tin single crystals under impact loading”, Journal of the Physical Society of Japan, 14(1959), pp.1351-1321.

152. K. Ishii, “Incorpration of slip dislocations in mechanical twins of tin crystals Journal of the Physical Society of Japan n, 18(1963), pp.1122-1132.

153. S. Maruyama, , “Dynamic behavior of twinning in Tin crystals at various temperatures and strain rates”, Journal of the Physical Society of Japan, 15(1960), pp.1243-1251.

154. W.P. Mason, H.J. Mcskimin, W. Shockley, “ultrasonic observation of twinning in Tin”, Physical Review B, 73(1948), pp.1213

155. M.C .Jon, D.N. Beshers, W.P. Mason, “Twinning of Zn and Sn during ultrasonic

deformation", Journal of Applied Physics, 45(1974), pp.3716-3719.

156. S. Ogata., J. Li, S. Yip, "Energy landscape of deformation twinning in bcc and fcc metals", Physical Review B, 224(102)(2005), pp.1-11.

157. A. Rohatgi, K.S. Vecchio, G.T. Gray III, "The influence of stacking fault on the mechanical behavior of Cu and Cu-Al alloys: deformation twinning, work hardening, and dynamic recovery", Metallurgical and Materials Transactions A, 32(2001), pp.135-145.

158. D.S. Xu, J.P. Chang, J. Li, et al., "Dislocation slip or deformation twinning: confining pressure makes a difference", Materials science and Engineering A, 387-389(2004), pp. 840-844.

159. C.N. Reid, A. Gilbert, G.T. Hahn, Transactions of the Metallurgical Society of AIME, 236 (1966), pp.1024-1030.

160. S. Krishnamurthy, R.E. Reed-Hill, "Concerning the role of the mechanical twinning on the stress-strain behavior of Cu-4.9At.pct Sn alloy", Metallurgical Transactions A, 11A (1980), pp.565-572.

BIOGRAPHICAL INFORMATION

Huili Xu received her B. Sc. in Applied Chemistry in Xi'dian University in China in 2005 and later a Master of Science degree in Chemistry from Zhejiang University, Hangzhou, P. R. China in 2007. She joined the University of Texas at Arlington and pursued her Ph. D. in Materials Science and Engineering in 2008. During her Ph. D. study in the University of Texas at Arlington, she worked on the areas related to modern microelectronic technology, specifically focusing on the quality and reliability assessment of advanced microelectronics ranging from back-end of line (BEOL) to package level, and the development of practical methods for evaluating the reliability behavior of Lead-free solder in packaging.